PERMAFROST ORGANIC MATTER QUALITY AND BIOLABILITY IN THE VAULT LAKE THERMOKARST ENVIRONMENT, INTERIOR ALASKA, USA

By

Joanne K. Heslop, B.S.

A Dissertation Submitted in Partial Fulfillment of the Requirements

for the Degree of

Doctor of Philosophy

in

Geophysics

University of Alaska Fairbanks

May 2017

APPROVED:

Katey Walter Anthony, Committee Chair
Guido Grosse, Committee Member
Vladimir Romanovsky, Committee Member
Mingchu Zhang, Committee Member
Paul McCarthy, Chair
Department of Geosciences
Paul Layer, Dean
College of Natural Science and Mathematics
Michael Castellini, Dean of the Graduate School

Abstract

Warming and thawing of permafrost soils removes a major barrier to soil organic carbon (SOC) mineralization, leading to the mobilization and microbial degradation of previously frozen, inactive permafrost organic carbon (OC) into the greenhouse gases carbon dioxide (CO_2) and methane (CH_4). Many thermokarst (thaw) lakes formed in permafrost-dominated landscapes have high rates of CO_2 and CH_4 emission; however, the composition and biodegradability of the thawed permafrost OC as they relate to the relative magnitudes of anaerobic OC mineralization at different depths throughout the vertical profile of a thermokarst-lake talik system have, to my knowledge, never been measured. My research examined OC composition and mineralization potentials at the Vault Creek (VC) permafrost tunnel and Vault Lake, located 20 km north of Fairbanks, Alaska, USA, to better constrain these uncertainties. I found that, in a 590-cm long sediment core collected from the center of Vault Lake, whole-column CH_4 production is dominated by methanogenesis in the organic-rich mud facies, which occurred in the surface 0 to 152 cm. CH_4 production potential rates positively associated with substrate availability (carbon and nitrogen concentrations) and the relative abundances of terrestrially-derived organic matter compounds (alkanes, alkenes, lignin products, and phenols and phenolic precursors), measured using pyrolysis-gas chromatography-mass spectrometry. Temperature sensitivity analyses conducted on a subset of samples from the Vault Lake sediment core suggest century-scale time since permafrost thaw affects temperature sensitivities of CH_4 production. Freshly-thawed taberite sediments at the base of the talik (thaw bulb) were most sensitive to warming at lower incubation temperatures (0 °C to 3 °C), while the overlying taberite sediments thawed *in situ* longer periods of time (up to 400 years based on radiocarbon dating) did not experience statistically significant increases in CH_4 production until higher incubation temperatures (10 °C

to 25 °C). Finally, using anaerobic incubations and ultrahigh-resolution mass spectrometry of water-extractable organic matter along a 12-m yedoma profile in the VC permafrost tunnel, I show that yedoma OC biolability increases with depth as indicated by increasing proportions of aliphatics and peptides (reduced, high H/C compounds). These compounds also positively correlated with anaerobic CO_2 and CH_4 production, and corresponded to high proportions (5.6% to 118%) of OC mineralization rates in incubations. This suggests that as yedoma permafrost thaws beneath a thermokarst lake greenhouse gas production potentials may increase with thaw depth.

Table of Contents

List of Figures

Page

List of Tables

Page

Acknowledgements

I would like to express my gratitude to my adviser Katey Walter Anthony for the guidance, support, and knowledge she has shared. Additional, invaluable guidance, assistance, and feedback have been imparted by my committee members: Guido Grosse, Vladimir Romanovsky, and Mingchu Zhang. I thank my adviser and committee members for their time and support during my graduate studies.

I would also like to thank P. Anthony, N. Bigelow, S. Billings, A. Bondurant, J. Chanton, M. Engram, J. Guerard, N. Haubenstock, T. Howe, M. Jones, A. Kholodov, C. Knoblauch, K. Martinez-Cruz, L. Oliver, D. Podgorski, C. Schädel, A. Sepulveda-Jauregui, M. Short, R. Spencer, A. Soria, B. Van Veldhuizen, M. Winkel, M. Wooller, and P. Zito for assistance in data collection and/or analysis. I thank Sam Skidmore for granting access to Vault Lake and the Vault Creek permafrost tunnel. Additional, instrumental feedback in manuscript preparation was provided by: my coauthors at both UAF and collaborating laboratories; the Spring 2014 BIOL F604, the Fall 2015 GEOS F640, and the Spring ENVE F693 classes at UAF; and anonymous reviewers at Biogeosciences and Organic Geochemistry. Last, but not least, I would like to thank my family and friends for their encouragement and support.

Funding for my dissertation research has been provided by: DOE DE-SC0006920, NSF OPP-1107892, ARC-1304823, the UAF Graduate School, and a UAF Center for Global Climate Change Student Research Award with funding from the Center for Global Change. This dissertation was completed in part under STAR Fellowship Assistance agreement no. FP-91762901-0 awarded by the US Environmental Protection Agency (EPA). It has not been formally reviewed by EPA. The views expressed in this dissertation are solely those of J. Heslop,

and the EPA does not endorse any products or commercial services mentioned in this dissertation.

Introduction

I.1. The permafrost carbon feedback

Permafrost, defined as ground at or below 0 °C for at least two consecutive years, covers ~25% of the Northern Hemisphere (Ping et al., 2015). Air temperature records suggest high latitudes (>60 °N) are warming twice as fast as the remainder of the Northern Hemisphere (Bekryaev et al., 2010; Schuur et al., 2015), and amplified Arctic warming is projected to continue into the coming century (IPCC, 2013). In this warming climate, both models and observations indicate that permafrost is warming and thawing in many regions (Romanovsky et al., 2010).

Under climate warming, permafrost is considered a vulnerable carbon (C) pool (Schaefer et al., 2014; Schuur and Abbott, 2011). Permafrost contains an estimated 1330-1580 Pg of soil organic carbon (SOC), representing about one-third of the total global SOC stocks (Hugelius et al., 2014; Schuur et al., 2015). Warming and thawing of permafrost soils removes a major barrier to SOC mineralization, leading to the mobilization and microbial degradation of previously frozen, inactive permafrost SOC (Davidson and Janssens, 2006; Olefeldt et al., 2013; Schuur et al., 2015; Yang et al., 2016). Microbial degradation converts permafrost SOC into the greenhouse gases carbon dioxide (CO_2) and methane (CH_4), which, when released to the atmosphere, cause a positive feedback to climate warming (Schuur et al., 2015; Walter et al., 2006). Large uncertainties remain about the magnitude, timing, and form of C loss to the atmosphere from thawing permafrost. Some studies suggest thawing permafrost will release 19–208 Pg C by 2050 (Schuur et al., 2013; Harden et al., 2012); however, permafrost thaw is expected to be a long-term, accelerating occurrence with over 60% of total permafrost thaw and

subsequent SOC mobilization and mineralization expected to occur after 2100 (Grosse et al., 2016).

Permafrost thaw also changes local and regional hydrology, leading to fragmented wetting and drying of the landscape (Jorgenson et al., 2013). Landscape wetting and drying determines the fate of thawed SOC by affecting whether it will be mineralized aerobically as CO_2 or anaerobically as CO_2 and CH_4. While it has been suggested that permafrost SOC mineralization in aerobic conditions releases an average of 3.4 times more C than SOC mineralization in anaerobic conditions (Schädel et al., 2016), CH_4 has 34 times more global warming potential than CO_2 over a century time scale (Myhre et al., 2013). Therefore, it is important to increase our understanding of CH_4 production from permafrost SOC thawed under anaerobic conditions to fully estimate the potential strength of the permafrost C feedback.

I.2. Yedoma and thermokarst lakes

A substantial portion (~450 Pg) of the deep permafrost C pool is stored in permafrost soils of the yedoma region (Walter Anthony et al., 2014; Schuur et al., 2015). Yedoma refers to the icy late-Pleistocene loess-dominated permafrost soil type that occurs predominantly in previously unglaciated lowland regions of Beringia (NE Siberia, Alaska, and NW Canada; Grosse et al., 2013b; Zimov et al., 2006). With climate warming, or when subjected to ground-surface disturbance, ice-rich yedoma is prone to thermokarst formation, a process by which the melting of excess ground ice forms depressions that fill with thermokarst ponds (Soloviev, 1973). Once formed, thermokarst ponds enlarge to lakes by strongly altering the local thermal balance of the land surface and transfer heat from the water body into the underlying ground more effectively than other land cover types (Grosse et al., 2013a; Burn, 2005). The enhanced heat flux triggers rapid permafrost thaw and talik (thaw bulb) formation underneath the lake

(Plug and West, 2009) and thermal erosion around the lake shores (Jones et al., 2011), which can lead to the mobilization of freshly thawed OC from yedoma (Kessler et al., 2012).

Many thermokarst lakes formed in permafrost-dominated landscapes have high rates of CO_2 and CH_4 emission (Walter et al., 2007; Sepulveda-Jauregui et al., 2015; Wik et al., 2016). In rare cases, C emissions from these lakes originate from ancient geologic sources (Walter Anthony et al., 2012). More commonly, the C emissions are the result of modern microbial C mineralization. The C utilized for greenhouse gas production primarily originates from permafrost SOC both thawing beneath and eroding from shores into the lake (Brosius et al., 2012; Kling and Kipphut, 1991; Walter Anthony and Anthony, 2013; Walter et al., 2008; Zimov et al., 1997) and the decomposition of contemporary organic matter (OM) in the lakes (Walter Anthony et al., 2014). However, to my knowledge the composition and biodegradability of the OM and the relative magnitudes of anaerobic C mineralization at different depths throughout the entire vertical profile of a thermokarst-lake talik system have never been investigated. Research presented in this dissertation seeks to improve scientific understanding of anaerobic SOC mineralization in thermokarst-lake sediments and taliks.

I.3. Study site

The Vault Creek (VC) permafrost tunnel and Vault Lake (informal name; 65°01'46.3" N, 147°42'22.4" W) are located in the Chatanika River Valley 20 km north of Fairbanks, Alaska, USA. The region experiences a continental climate with a mean annual air temperature of -2.39°C and 274.6 mm mean annual precipitation (Fairbanks International Airport 1981-2010, National Climate Data Center). The yedoma-type permafrost in this region is discontinuous (Jorgenson et al., 2008) and relatively warm (mean annual temperature -0.7 °C at the tunnel site; Schirrmeister et al., 2016).

The VC permafrost tunnel was excavated in 1990 by a local private gold miner and extends through a 25-m thick yedoma sequence and a 15-m thick gravel horizon down to bedrock. It is thought to be the longest and deepest permafrost tunnel accessible for permafrost research in Alaska; sediment characteristics and paleoenvironmental records from the VC permafrost tunnel have been previously studied by Meyer et al. (2008) and Schirrmeister et al. (2016). Vault Lake (3200 m^2, 4.6 m maximum depth, 3.7 m average depth; Walter Anthony, unpublished data), located within 60 m of the subsurface tunnel, is a first-generation thermokarst lake formed by the melting of permafrost ground ice, including massive ice wedges. Based on radiocarbon dating of macrofossils in lake sediments, the lake is estimated to have formed within the last 400 years (Heslop et al., 2015). Steep, eroding bluffs, tilted spruce trees along the margins, and numerous CH_4 bubbling seeps across the lake surface indicate that Vault Lake is still actively deepening and laterally expanding.

During March 2013, a 590-cm long sediment core was collected by Arctic Drilling Inc. on behalf of a team of researchers led by Katey Walter Anthony from the center of Vault Lake. Concurrently, I collected permafrost soil samples from the walls of the VC permafrost tunnel. My research presented in this dissertation focuses on the analyses of these samples to investigate the following uncertainties concerning permafrost C cycling in thermokarst-lake environments:

Chapter 1: Thermokarst-lake methanogenesis along a complete talik profile

Thermokarst lakes emit CH_4 to the atmosphere formed from thawed permafrost organic matter (OM), but the relative magnitude of CH_4 production in surface lake sediments vs. deeper thawed permafrost horizons is not well understood. Research presented in this chapter helps fill this knowledge gap by quantifying CH_4 production potentials for two profiles in the Vault Lake

system: a 590-cm long lake sediment core beneath the center of Vault Lake and the adjacent 40-m deep Vault Creek permafrost tunnel.

Chapter 2: Utilizing pyrolysis GC-MS to characterize organic matter quality in relation to methane production in a thermokarst lake sediment core

Despite thermokarst lakes being an important source of atmospheric CH_4, few studies have examined the composition and biodegradability of their sediment organic matter (OM). Improving knowledge of the quality of permafrost OM will reduce uncertainty in estimating how thawed permafrost OC would behave in the global C cycle. Using the Vault Lake sediment core, research presented in this chapter assesses the molecular composition of bulk sediment OM using pyrolysis GC-MS and determines statistical relationships between OM properties and CH_4 production.

Chapter 3: Century-scale time since permafrost thaw affects temperature sensitivity of methane production in thermokarst-lake sediments

Two major uncertainties in estimating the strength of the permafrost C feedback are: (i) how permafrost SOC thawed and mineralized in saturated anaerobic conditions responds to changes in temperature and (ii) how temperature sensitivities change over century-scale time since thaw. Research presented in this chapter uses sediments from the Vault Lake core to help fill in these knowledge gaps for CH_4 production in saturated anaerobic conditions.

Chapter 4: Organic carbon biolabilty increases with depth in a yedoma permafrost profile

Once formed, thermokarst lakes and their taliks provide a direct conduit for CO_2 and CH_4 produced with deep, old yedoma OC to be emitted directly into the atmosphere. It has been suggested that OC from yedoma-type permafrost, which surrounds Vault Lake, is more biolabile upon thaw than OC from other permafrost types because it contains higher proportions of low

molecular weight compounds. This chapter presents research examining samples from the VC permafrost tunnel to determine how yedoma water-extractable OC molecular composition, biodegradability, and potentials for CO_2 and CH_4 emissions change with depth in anaerobic conditions consistent with a thermokarst-lake talik environment.

References

Bekryaev R, Polyakov I, Alexeev V (2010) Role of Polar Amplification in Long-Term Surface Air Temperature Variations and Modern Arctic Warming. Journal of Climate, 23, 3888–3906.

Brosius L, Walter Anthony KM, Grosse G, et al. (2012) Using the deuterium isotope composition of permafrost meltwater to constrain thermokarst lake contributions to atmospheric CH_4 during the last deglaciation. Journal of Geophysical Research Biogeosciences 117, G01022.

Burn C (2005) Lake-bottom thermal regimes, western Arctic coast, Canada. Permafrost and Periglacial Processes, 16, 355–367.

Davidson EA, Janssens IA (2006) Temperature sensitivity of soil carbon decomposition and feedbacks to climate change. Nature, 440, 165-173.

Grosse G, Jones B, Arp C (2013a) Thermokarst Lakes, Drainage, and Drained Basins, in: Treatise on Geomorphology, edited by: Shroder, J. F., Academic Press, San Diego, 325-353.

Grosse G, Robinson J, Bryant R, Taylor M, et al. (2013b) Distribution of late Pleistocene ice-rich syngenetic permafrost of the Yedoma Suite in east and central Siberia, Russia. USGS, Reston, VA, 31.

Grosse G, Goetz S, McGuire D, Romanovsky V, Schuur E (2016) Changing permafrost in a warming world and feedbacks to the Earth system. Environmental Research Letters, 11, 040201.

Harden J, Koven C, Ping CL, et al. (2012) Field information links permafrost carbon to physical vulnerabilities of thawing. Geophysical Research Letters, 39, L15704.

Heslop JK, Walter Anthony WK, Sepulveda-Jauregui A, Martinez-Cruz K, Bondurant A, Grosse G, Jones MC (2015) Thermokarst lake methanogenesis along a complete talik profile. Biogeosciences, 12, 4317–4331.

Hugelius G, Strauss J, Zubrzycki S, et al. (2014) Estimated stocks of circumpolar permafrost carbon with quantified uncertainty ranges and identified data gaps. Biogeosciences, 11, 6573–6593.

IPCC in Climate Change 2013: The Physical Science Basis. Contribution of Working Group I to the Fifth Assessment Report of the Intergovernmental Panel on Climate Change. Eds Stocker, T. F. et al., 1535, Cambridge Univ. Press, 2013.

Jones B, Grosse G, Arp C, Jones M, Anthony W, Romanovsky V (2011) Modern thermokarst lake dynamics in the continuous permafrost zone, northern Seward Peninsula, Alaska. Journal of Geophysical Research: Biogeosciences, 116, G00M03.

Jorgenson M, Yoshikawa K, Kanevskiy M, et al. (2008) Permafrost characteristics of Alaska. In: Kane, D., Hinkel, K. (Eds.), Proceedings of the Ninth International Conference on Permafrost. University of Alaska, Fairbanks, AK, 121-122.

Jorgenson T, Harden J, Kanevskiy M et al. (2013) Reorganization of vegetation, hydrology and soil carbon after permafrost degradation across heterogeneous boreal landscapes. Environmental Research Letters, 8, 035017.

Kessler MA, Plug LJ, Walter Anthony KM (2012) Simulating the decadal- to millennial-scale dynamics of morphology and sequestered carbon mobilization of two thermokarst lakes in NW Alaska. Journal of Geophysical Research: Biogeosciences, 117.

Kling G, Kipphut G (1991) Arctic lakes and streams as gas conduits to the atmosphere: implications for tundra carbon budgets. Science, 251, 298-301.

Meyer H, Yoshikawa K, Schirrmeister L, Andreev A (2008) The Vault Creek Tunnel (Fairbanks Region, Alaska): A Late Quaternary Palaeoenvironmental Permafrost Record. Ninth International Conference on Permafrost, 1191–1196, University of Alaska Fairbanks, Fairbanks, Alaska, USA, 29 June to 03 July, 2008.

Myhre G, Shindell D, Breon FM, et al. (2013) Anthropogenic and Natural Radiative Forcing. In: Climate Change 2013: The Physical Science Basis. Contribution of Working Group I to the Fifth Assessment Report of the Intergovernmental Panel on Climate Change. Intergovernmental Panel on Climate Change, New York, USA.

Olefeldt D, Turetsky M, Crill P, McGuire D (2013) Environmental and physical controls on northern terrestrial methane emissions across permafrost zones. Global Change Biology,19, 589–603.

Ping CL, Jastrow J, Jorgenson M, Michaelson G, Shur Y (2015) Permafrost soils and carbon cycling. SOIL, 1, 147–171.

Plug L, West J (2009) Thaw lake expansion in a two-dimensional coupled model of heat transfer, thaw subsidence, and mass movement. Journal of Geophysical Research, 114.

Romanovsky, V., Smith, S., and Christiansen, H (2010) Permafrost thermal state in the polar Northern Hemisphere during the International Polar Year 2007-2009: a synthesis. Permafrost and Periglacial Processes, 11, 137-152.

Schädel C, Bader M, Schuur E et al. (2016) Potential carbon emissions dominated by carbon dioxide from thawed permafrost soils. Nature Climate Change, advance online publication.

Schaefer K, Lantuit H, Romanovsky V, Schuur E, Witt R (2014) The impact of the permafrost carbon feedback on global climate. Environmental Research Letters, 9, 085003.

Schirrmeister L, Meyer H, Andreev A et al. (2016) Late Quaternary paleoenvironmental records from the Chatanika River valley near Fairbanks (Alaska). Quaternary Science Reviews.

Schuur E, and Abbott B (2011) High risk of permafrost thaw. Nature, 480, 32-33.

Schuur E, Abbott B, Bowden W, et al. (2013) Expert assessment of vulnerability of permafrost carbon to climate change. Climatic Change, 119, 359–374.

Schuur E, McGuire A, Schädel C, et al. (2015) Climate change and the permafrost carbon feedback. Nature, 520, 171–179.

Sepulveda-Jauregui A, Walter Anthony KM, Martinez-Cruz, Greene S, Thalasso F (2015) Methane and carbon dioxide emissions from 40 lakes along a north south latitudinal transect in Alaska. Biogeosciences, 12, 3197–3223.

Soloviev P (1973) Thermokarst phenomena and landforms due to frostheaving in central Yakutia. Biuletyn Peryglacjalny, 135-155.

Walter K, Zimov S, Chanton J, Verbyla D, Chapin F (2006) Methane bubbling from Siberian thaw lakes as a positive feedback to climate warming. Nature, 443, 71–75.

Walter K, Edwards M, Grosse G, Zimov S, Chapin F (2007) Thermokarst Lakes as a Source of Atmospheric CH4 During the Last Deglaciation. Science, 318, 633–636.

Walter K, Chanton J, Chapin F, Schuur E, Zimov S (2008) Methane production and bubble emissions from arctic lakes: Isotopic implications for source pathways and ages. Journal of Geophysical Research: Biogeosciences (2005–2012), 113.

Walter Anthony K, Anthony P, Grosse G, Chanton J (2012) Geologic methane seeps along boundaries of Arctic permafrost thaw and melting glaciers. Nature Geoscience.

Walter Anthony KM, Anthony P (2013) Constraining spatial variability of methane ebullition seeps in thermokarst lakes using point process models. Journal of Geophysical Research: Biogeosciences,118, 1015–1034.

Walter Anthony KM, Zimov SA, Grosse G et al. (2014) A shift of thermokarst lakes from carbon sources to sinks during the Holocene epoch. Nature, 511, 452–456.

Wik M, Varner R, Anthony K, MacIntyre S, Bastviken D (2016) Climate-sensitive northern lakes and ponds are critical components of methane release. Nature Geoscience.

Yang Z, Wullschleger S, Liang L, Graham D, Gu B (2016) Effects of warming on the degradation and production of low-molecular-weight labile organic carbon in an Arctic tundra soil. Soil Biology and Biochemistry, 95, 202–211.

Zimov SA, et al. (1997) North Siberian lakes: A methane source fueled by Pleistocene carbon. Science, 277, 800-802.

Zimov SA, et al. (2006) Permafrost and the Global Carbon Budget. Science, 312, 1612–1613.

Chapter 1: Thermokarst-lake methanogenesis along a complete talik profile[1]

Abstract

Thermokarst (thaw) lakes emit methane (CH_4) to the atmosphere formed from thawed permafrost organic matter (OM), but the relative magnitude of CH_4 production in surface lake sediments vs. deeper thawed permafrost horizons is not well understood. We assessed anaerobic CH_4 production potentials from various depths along a 590 cm long lake sediment core that captured the entire sediment package of the talik (thaw bulb) beneath the center of an interior Alaska thermokarst lake, Vault Lake, and the top 40 cm of thawing permafrost beneath the talik. We also studied the adjacent Vault Creek permafrost tunnel that extends through ice-rich yedoma permafrost soils surrounding the lake and into underlying gravel. Our results showed CH_4 production potentials were highest in the organic-rich surface lake sediments, which were 151 cm thick (mean ± SD 5.95 ± 1.67 μg C-CH_4 g dw^{-1} d^{-1}; 125.9 ± 36.2 μg C-CH_4 g C_{org}^{-1} d^{-1}). High CH_4 production potentials were also observed in recently-thawed permafrost (1.18 ± 0.61 μg C-CH_4 g dw^{-1} d^{-1}; 59.60 ± 51.5 μg C-CH_4 g C_{org}^{-1} d^{-1}) at the bottom of the talik, but the narrow thicknesses (43 cm) of this horizon limited its overall contribution to total sediment column CH_4 production in the core. Lower rates of CH_4 production were observed in sediment horizons representing permafrost that has been thawed in the talik for longer periods of time. No CH_4 production was observed in samples obtained from the permafrost tunnel, a non-lake environment. Our findings imply that CH_4 production is highly variable in thermokarst-lake

---

[1] Heslop, J. K., Walter Anthony, K. M., Sepulveda-Jauregui, A., Martinez-Cruz, K., Bondurant, A., Grosse, G., and Jones, M. C.: Thermokarst lake methanogenesis along a complete talik profile, Biogeosciences, 12, 4317-4331, doi:10.5194/bg-12-4317-2015, 2015.

systems and that both modern OM supplied to surface sediments and ancient OM supplied to both surface and deep lake sediments by in situ thaw as well as shore erosion of yedoma permafrost are important to lake CH_4 production.

1.1. Introduction

Permafrost contains an estimated 1140–1476 Pg of soil organic carbon (OC; Hugelius et al., 2014). It is considered to be a vulnerable carbon (C) pool in a warming climate (Schaefer et al., 2014; Schuur and Abbott, 2011), as both models and observations indicate that permafrost is warming and thawing in many regions (Romanovsky et al., 2010). Large uncertainties remain about the magnitude, timing, and form of C loss to the atmosphere from thawing permafrost; however, some studies suggest thawing permafrost will release 19–208 Pg C by 2050 (Schuur et al., 2013; Harden et al., 2012). A substantial portion (~450 Pg) of the deep permafrost C pool is stored in permafrost soils of the yedoma region, both in undisturbed yedoma and in the organic-rich sediments of thermokarst lake basins in the yedoma region (Walter Anthony et al., 2014). Yedoma refers to the icy late- Pleistocene loess-dominated permafrost soil type that occurs predominantly in previously unglaciated lowland regions of Beringia (NE Siberia, Alaska, and NW Canada; Grosse et al., 2013b; Zimov et al., 2006). Typical yedoma deposits in Alaska are 10–30m thick, but can reach local thicknesses greater than 60 m (Pewe, 1975). Late Pleistocene yedoma ice wedges range from 2 to 6 m in width and can extend tens of meters below the ground surface (Kanevskiy et al., 2011). In addition to being ice-rich, the OC content of yedoma is high (2–5%) for mineral soils (Walter Anthony et al., 2014; Strauss et al., 2013; Schirrmeister et al., 2011; Kholodov et al., 2003), and yedoma soils typically contain OC contents 10–30 times higher than that of similar loess-dominated non-permafrost soils (Zimov et al., 2006).

In a warming climate, or when subjected to ground-surface disturbance, ice-rich yedoma is prone to thermokarst lake formation, a process by which the melting of massive ground ice forms depressions that fill with water (Soloviev, 1973). In yedoma-dominated regions, up to 90% of all lakes are thermokarst lakes (Pienitz et al., 2008). Thermokarst lakes strongly alter the local thermal balance of the land surface and transfer heat from the water body into the underlying ground more effectively than other land cover types (Grosse et al., 2013a; Burn, 2005), especially when the depth of a lake exceeds the thickness of the winter lake ice. The enhanced heat flux triggers rapid permafrost thaw and talik (thaw bulb) formation underneath the lake (Plug and West, 2009), which can lead to the mobilization of freshly thawed OC from yedoma (Kessler et al., 2012).

As permafrost thaws, it releases previously frozen OC, which can subsequently be processed by microorganisms that produce methane (CH_4) and carbon dioxide (CO_2). It is estimated that arctic systems annually emit 15–50 Tg of CH_4 (McGuire et al., 2009), a potent greenhouse gas which has 34 times more global warming potential than CO_2 over a 100-year time period (Myhre et al., 2013). Many lakes formed in permafrost-dominated landscapes, particularly yedoma-type thermokarst lakes, have high rates of CH_4 emission (Sepulveda-Jauregui et al., 2015; Walter et al., 2007). The CH_4 emitted from arctic lakes largely originates in terrestrial sources such as the Holocene soils of the lakes' watersheds (Kling and Kipphut, 1991), the thaw of Holocene- and Pleistocene-aged permafrost soil beneath and surrounding the lakes (Walter Anthony and Anthony, 2013; Brosius et al., 2012; Walter et al., 2008; Zimov et al., 1997), and decomposition of contemporary organic matter (OM) in the lakes (Walter Anthony et al., 2014).

The location of CH_4 production in thermokarst lake systems is not well understood. Using radiocarbon dating, stable isotopes, and spatial mapping of CH_4 emissions within lakes, Walter et al. (2006) concluded that the highest rates of CH_4 emission occur along thermokarst margins, originating from actively expanding taliks. Numerical modeling of CH_4 production in thermokarst lakes confirmed field-based observations that CH_4 production is concentrated along permafrost thaw margins of lakes (Kessler et al., 2012). Surface lake sediments contain contemporary OM as well as re-deposited, thawed permafrost OM. Both sources may fuel CH_4 production. At greater sediment depths, permafrost thaw in taliks under thermokarst lakes also supplies substrate for methanogenesis. However, the labile fraction of thawed permafrost OM is in limited supply so, given enough time, CH_4 production in thawed permafrost sediments can diminish (Walter Anthony et al., 2014; Kessler et al., 2012).

The objective of this study was to constrain the location and magnitude of CH_4 production in a thermokarst lake environment. We conducted long-term anaerobic incubations using sediment samples collected from a deep thermokarst lake core in the center of the lake that extended from the sediment surface, through the talik, and into the yedoma permafrost underlying the talik. We compared CH_4 production rates from the lake core to those of samples collected from an adjacent permafrost tunnel, which extended through yedoma deposits into the underlying gravel. We also measured the thickness of the talik at various locations in the lake to help constrain the spatial variability of CH_4 production in the lake.

1.2. Methods

1.2.1. Study site

The Vault Creek permafrost tunnel and Vault Lake (informal name; 65.0293 ºN, 147.6987 ºW) are located approximately 40 km north of Fairbanks, Alaska, USA, in a region

characterized by discontinuous permafrost (Fig. 1.1). The region experiences a continental climate with a mean annual air temperature of -2.39 °C and 274.6 mm mean annual precipitation (Fairbanks International Airport 1981–2010, National Climate Data Center). The 220 m long Vault Creek permafrost tunnel, previously described by Meyer et al. (2008), extends through a 25 m thick yedoma sequence and a 15 m thick gravel horizon down to bedrock. The tunnel entrance is secured by a steel tube, making the top 8 m of the profile inaccessible to sampling. Vault Lake (3200 m^2, 4.6 m maximum depth, 3.7 m average depth; Walter Anthony, unpublished data), located within 60 m of the subsurface tunnel, is a first-generation thermokarst lake formed by the melting of permafrost ground ice, including massive ice wedges. Steep, eroding bluffs, tilted spruce trees along the margins, and numerous CH_4 bubbling seeps across the lake surface indicate that the lake is still actively deepening and laterally expanding.

We measured lake and talik depth in March 2013 by drilling boreholes through thawed sediments to the permafrost table at six points along a transect spanning the long axis of the lake and at eight additional points distributed across the lake. Lake area and thermokarst bank height were measured by differential GPS (Leica Viva GS15, Leica Geosystems, Norcross, Georgia, USA) in November 2013. Talik temperatures were measured in galvanized steel tubes placed in two boreholes, one near the center of the lake (borehole (BH) 13) and the other 6.1 m from an actively expanding thermokarst margin (BH10). We installed temperature sensors (Onset TMCx-HD, accuracy ±0.21 °C, Onset Corporation, Bourne, Massachusetts, USA) at four depths below the sediment–water interface within the talik (BH10: 0.5, 1.0, 6.2, and 8.85 m; BH13: 0.5, 1.0, 5.7, and 6.2 m). With the exception of a missing-data period between 25 July 2014 and 11 November 2014, temperatures were recorded hourly from May 2013 through December 2014.

1.2.2. Sediment sample collection, preparation, and characterization

During March 2013, a 590 cm long sediment core was collected from the center of Vault Lake (BH14, 4.0 m water depth). Using a Boart Longyear diamond core drilling system, continuous sediment cores were retrieved by percussion coring with a split spoon sampler. Sediment core sections were retrieved in 6 cm diameter clear plastic liners inside of core barrels in approximately 60 cm intervals from the same hole. Casing inside the hole ensured that adjacent sediments did not slough. The sediment core captured nearly the entire sequence of thawed lake sediments in the talik (550 cm) and the top 40 cm of permafrost beneath the talik, though several short sections of core were lost from tubes during retrieval (Fig. 1.2). Thawed core sections were sealed and stored in the laboratory at 3 °C. The permafrost section was sealed and stored in the laboratory at -10 °C.

We measured magnetic susceptibility on the intact Vault Lake core using a loop sensor on an automated core logger (Geotek MSCL-X, Geotek Limited, Daventry, Northamptonshire, United Kingdom) at the Limnological Research Center Core (LacCore) Facility in the University of Minnesota, Minneapolis, Minnesota, USA. Then we split the core lengthwise and immediately sealed and archived one half of the core at 3 °C for later use in anaerobic incubations. This first half of the core was sealed with four layers of oxygen- (O_2) and moisture-barrier film (Krehalon PC101, Filcon, Clare, Michigan, USA).

On the second half of the core, we conducted initial core descriptions and made the following measurements at LacCore. We imaged the core using a line scan camera (Geotek Geoscan-III, Geotek Limited, Daventry, Northamptonshire, United Kingdom). High-resolution magnetic susceptibility was measured in 0.5 cm intervals using a point sensor on an automated core logger (Geotek MSCL-XYZ, Geotek Limited, Daventry, Northamptonshire, United

Kingdom). We sampled sediments in 10 cm intervals along the core at a known volume (3 cm^3). We weighed samples at field moisture, then dried them at 105 °C for 48 h and reweighed them to determine the weight loss compared to the total weight of the wet sample (gravimetric water content) and dry sediment weight per unit volume (dry bulk density). Smear slides were created from samples taken every 10 cm along the core and analyzed under a microscope to quantify the relative abundance of organic and mineral matter, sponge spicules, and diatoms.

We quantified plant macrofossils in a subset of lake sediment core samples (Table 1.A-1). Macrofossil samples were sieved using a 250 μm sieve, and the remaining plant material was examined in a petri dish in a slurry with deionized water using a binocular microscope. Relative percentages of each macrofossil type were calculated for each sample. Any macrofossils worth noting (seeds, leaves, needles, etc.) that did not comprise a large enough fraction of the sample were counted separately and simply noted as present.

In addition to the lake sediment core, triplicate samples of permafrost soils exposed in the Vault Creek tunnel adjacent to the lake were collected using a 75 cm^3 hole saw mounted on a hand-held hammer drill from 16 distributed depths along the tunnel walls. The sediment samples represented the accessible profile from 9 to 40 m vertical depth beneath the ground surface. Permafrost samples were collected from both the yedoma horizon and the silty matrix of the underlying gravel horizon. Permafrost samples were stored in the laboratory at -10 °C until further analyses.

1.2.3. Sediment facies classification

Using the imagery, smear slides, macrofossil data, and our knowledge of thermokarst lake sediment facies classification based on Murton (1996), Walter Anthony et al. (2014), and Farquharson et al. (2016), we classified the Vault Lake core into five facies for subsampling:

Organic-rich mud, Lacustrine silt, Taberite, Recently thawed taberite, and Transitional permafrost (Fig. 1.2).

Organic-rich mud consisted of the top 152 cm thick section of the lake core containing alternating layers of dark, organic-rich sediments, some peaty layers with variable sized plant debris, and lighter, mineral silt dominated layers. Smear slides and macrofossil analyses revealed relatively higher abundances of aquatic and terrestrial macrofossils indicative of the thermokarst-affected late-Holocene black spruce ecosystem with peaty, organic rich soil that is still observed around the lake today. Aquatic indicators included spicules, diatoms, *Daphnia ephippia*, and benthic mosses. Terrestrial macrofossils included mosses (*Aulacomnium palustre*, *Sphagnum* spp., *Tomenthypnum nitens*, *Polytrichum* spp.), and roots and leaves of ericaceous shrubs, and spruce (*Picea* spp.) needles (Table 1.A-1).

The Lacustrine silt facies, 178 cm thick (153–330 cm) and underlying the Organic-rich mud, consisted of massive mineral sediment with occasional peat balls, representing material that sloughed off exposed thermokarst margins of the lake. Since sediments of Lacustrine silt were exposed to the lake water column during erosion and re-deposition, they contained some, albeit fewer, aquatic indicators (spicules, diatoms, and *Daphnia ephippia*). Few other macrofossils were found in the silt-dominated matrix. These were primarily un-differentiated organic detritus with a few fragments of terrestrial mosses, bark, and ericaceous rootlets.

Taberite sediments (331–550 cm), representing yedoma sediment which thawed in situ and remained underneath the lake (Walter Anthony et al., 2014; Schirrmeister et al., 2011), were identified as massive, mostly mineral (silt)-dominated sediments. We did not find diatoms or any other aquatic indicators in this facies. The little OM that was present was dominated by fine,

indistinguishable detritus. The bottom 43 cm of the taberite (508–550 cm), representing the most recently thawed sediments, was designated as Recently thawed taberite.

Beneath the thawed portion of the lake core, we sampled 40 cm of transitional permafrost (551–590 cm), which is close to the thaw transition with a large amount of unfrozen water in the inter-pore space but with numerous small lenses of bulk ice still present (Williams and Smith, 1989). The Transitional permafrost section of our core was ice-bearing, silt-dominated soil with few organic remains, identified as graminoid detritus indicative of the cold, dry Pleistocene steppe ecosystem.

1.2.4. Lake age

We estimated the age of Vault Lake by obtaining accelerator mass spectrometry (AMS) radiocarbon dates on terrestrial plant macrofossils picked from the lake center sediment core. Samples were analyzed at the National Ocean Sciences AMS (NOSAMS) facility (Table 1.1). All radiocarbon ages were calibrated to calendar 2σ years before present (BP) using Calib 7.0 (Reimer et al., 2013).

1.2.5. Geochemical analyses

Sediment samples (3 cm^3) from both the core and tunnel were oven-dried (105 °C for 48 h), homogenized using a mortar and pestle, and analyzed for total C (C_{tot}) and nitrogen (N_{tot}), C_{tot}:N_{tot} ratios, and isotope ratios $\delta^{15}N_{tot}$ using an elemental analyzer (Finnigan DeltaPlus XP, Thermo Scientific) coupled to a Costech ECS4010 Elemental Analyzer (Costech Scientific, Valencia, California, USA) at the University of Alaska Stable Isotope Facility, Fairbanks, Alaska, USA. A subsample of the homogenized oven-dried sediments was acidified using muriatic acid (31.45 % HCl), rinsed five times with deionized (DI) water, and used to measure total organic carbon (C_{org}) and $\delta^{13}C_{org}$ on the same elemental analyzer. Measurement of an

internal laboratory standard (peptone, n = 7) indicated measurement precision of ≤0.4 ‰ for both sets of C and N isotopes. Sediment C_{tot}, C_{org}, and N_{tot} contents are reported in weight percentage (wt %). $\delta^{13}C_{org}$ and $\delta^{15}N_{tot}$ contents are reported in parts per mil (‰). All $\delta^{13}C_{org}$ and $\delta^{15}N_{tot}$ values are expressed relative to Vienna Pe Dee Belemnite (VPDB) and ambient air, respectively. We report all results in mean ± standard deviation (SD).

1.2.6. Anaerobic laboratory incubations

Sediment slurries were prepared and incubated in triplicate for 21 depths along the Vault Lake core and 16 depths along the Vault Creek permafrost tunnel (Figs. 1.1 and 1.2; Table 1.2). We homogenized sediment samples under anaerobic conditions with O_2-free, sterilized DI water while flushing the slurry with ultra high purity (UHP) N_2 gas (Air Liquide, Houston, Texas, USA) in a solution container. Subsamples of slurry were oven-dried (105 °C for 48 h) and analyzed for dry sediment C_{tot}, C_{org}, N_{tot}, $\delta^{13}C_{org}$, and $\delta^{15}N_{tot}$ contents using the methods outlined above. Fifty milliliters of the anaerobic slurry was transferred to 100 mL glass serum bottles (Wheaton, Millville, New Jersey, USA) using a pipette. Serum bottles were degassed using a constant stream of UHP N_2 gas and sealed with butyl rubber stoppers (Bellco Glass, Vineland, New Jersey, USA). The slurry in each incubation bottle was reduced by injecting L-cysteine (Sigma-Aldrich, St. Louis, Missouri, USA) to a concentration of 0.025% (wt/v; Gorini, 1961). Anaerobic conditions in the bottles were subsequently verified by measuring O_2 concentrations in the headspace using gas chromatography (Shimadzu GC-2014, Shimadzu, Kyoto, Japan). We incubated the bottles at 3 °C until linear CH_4 production rates were achieved in all Vault Lake sediment core incubation bottles. The bottles remained sealed to maintain anaerobic conditions throughout the incubation period, which was 175 days for lake sediments and 220 days for permafrost tunnel samples.

We measured headspace CH_4 concentrations in each incubation bottle every 30 days using gas chromatography (Shimadzu GC-2014, Shimadzu, Kyoto, Japan). CH_4 production potential rates were calculated by the slope of the CH_4 concentration in headspace over time. We normalized CH_4 production rates across incubation bottles in two ways: dividing the CH_4 production rates by the mass of dry sediment and the mass of C_{org} in each bottle. CH_4 production rates are reported in units of μg C-CH_4 g dw^{-1} d^{-1} and μg C-CH g C_{org}^{-1} d^{-1}. We calculated whole sediment-column CH_4 production (μg C-CH_4 cm^{-2} d^{-1}) for the center lake core as the sum of facies' products of mean CH_4 production (μg C-CH_4 gdw^{-1} d^{-1}), dry bulk density (g cm^{-3}), and facies thickness (cm). Using a conversion factor of 0.01, we report whole sediment-column CH_4 production in units of g C-CH_4 m^{-2} d^{-1}.

1.2.7. Statistics

Sediment characteristics (dry bulk density, gravimetric water content, C_{tot}, C_{org}, N_{tot}, C_{tot}:N_{tot}, $\delta^{13}C_{org}$, and $\delta^{15}N_{tot}$) and CH_4 production rates (μg C-CH_4 gdw^{-1} d^{-1}, μg C-CH g C_{org}^{-1} d^{-1}) were tested for normal distribution using the Jarque-Bera test (MATLAB R2013a Student Version, MathWorks, Natick, Massachusetts, USA). All parameters except CH_4 production rate expressed as μg C-CH g C_{org}^{-1} d^{-1} were non-normally distributed ($\alpha = 0.05$); therefore, differences among facies were tested for statistical significance using Wilcoxon rank sum tests (MATLAB R2013a Student Version). Differences were considered statistically significant when $p \leq 0.05$. Spearman's rank correlation coefficients (MATLAB R2013a Student Version) were used to determine correlations between explanatory variables (C_{tot}, C_{org}, N_{tot}, and C_{tot}:N_{tot} ratios) and anaerobic CH_4 production (μg C-CH_4 gdw^{-1} d^{-1}) in our incubations.

1.3. Results

1.3.1. Lake age, morphology, and talik temperatures

Calibrated ages of macrofossils picked from the Organic-rich mud facies of the Vault Lake core ranged from 190 ± 20 to 405 ± 25 calendar years BP (Fig. 1.2; Table 1.1).

Lake water depths determined at the borehole locations ranged from 0.7 to 4.6 m (mean ± SD 2.9 ± 1.1 m, n = 14 boreholes). Talik depths below the sediment–water interface ranged from 0 to 8.8 m (mean ± SD 5.9 ± 2.1 m, n = 14 boreholes). Figure 1.1c shows borehole data for the long axis of the lake, including the lake center borehole (BH 14) from which our sediment core was taken. The talik was ~50 % thicker adjacent to the southern thermokarst margin than it was in the lake center.

Vertical profile temperatures measured along the bore hole in the center of Vault Lake, where water depth was 4.0 m and talik thickness was 5.7 m, ranged from -0.40 to 4.22 ºC (Fig. 1.3a). In the borehole adjacent to the southwest thermokarst margin (6.1m offshore), talik thickness was greater (8.6 m), lake water shallower (1.4 m), and sediment temperatures were warmer than in the lake center (-0.40 to 14.00 ºC; Fig. 1.3b). In both profiles, temperatures in the shallower sediment depths [-0.5 to -1.0 m (0 m = sediment/water interface), temperature range 0.14 to 14.00 ºC, mean annual temperature 3.57 ºC] were warmer and showed clear seasonal variations (Fig. 1.3a and b). Temperatures along the thaw boundary (-5.70 to -8.85 m, temperature range -0.40 to 2.07 ºC, mean annual temperature 0.13 ºC) were colder and relatively more consistent throughout the year.

The temperature data also indicated a strong thermal lag and lateral offset in the propagation of summer heat into deeper sediments and the lake center. The maximum temperature in the near-shore surface sediments (14.00 ºC at -0.5 m) occurred on 10 August

2013, while maximum temperature at -6.2 m (2.07 °C) and -8.9 m (-0.03 °C) depths in the same vertical profile occurred on 22 October 2013. In the lake center, where water depth was deeper, the maximum temperature of 4.22 °C occurred on 24 September 2013 at -0.5 m sediment depth, and also showed a thermal lag of heat propagation to greater depths in the same profile.

1.3.2. Sediment attributes

Sediment properties in the Vault Lake core and Vault Creek permafrost tunnel varied by facies and are summarized in Table 1.3. Magnetic susceptibility (MS) results indicate two points with low MS values at approximately 100 and 400 cm depth in the lake core (Fig. 1.4). These points are associated with diamagnetic materials in the core, potentially indicative of tephra. Tephra layers were observed in the Vault Creek permafrost tunnel, albeit at greater depths below the surface (Meyer et al., 2008). The Organic-rich mud facies had the lowest bulk density values in the lake core (Table 1.3). Differences in dry bulk density values between the remaining facies and between the silt and silty matrix of the gravel horizons of the permafrost tunnel were not statistically significant. Organic-rich mud had higher gravimetric water content values and Taberite had lower values than the remainder of the core (Table 1.3). High dry bulk density values had a strong linear correlation with low gravimetric water contents in samples ($R^2 = 0.74$).

Sediment geochemical parameters varied among the lake core and permafrost tunnel facies (Fig. 1.5) and are summarized in Table 1.4. The Organic-rich mud facies had the highest soil C concentrations (mean ± SD C_{tot} 6.01 ± 1.90; C_{org} 3.83 ± 1.66) in the core (Table 1.4), while the Taberite facies had the lowest C concentrations (mean ± SD C_{tot} 1.21 ± 0.44; C_{org} 0.84 ± 0.45). The remaining lake core facies grouped together had lower C concentrations (C_{tot} 1.24–2.52 %; C_{org} 0.84–1.52 %). Table 1.4 shows the C concentrations for individual facies, but C

concentrations among the Lacustrine silt, Recently thawed taberite, and Transitional permafrost were not significantly different from each other.

High levels of C_{tot} were observed in the permafrost tunnel (Table 1.4), and differences between relatively high levels of C_{tot} (mean 14.5 % wt) and lower levels of C_{org} (mean 1.9 % wt) indicate significant inorganic C content in the permafrost tunnel soils (mean ± SD 86.5 ± 8.4 % of total C). In contrast, inorganic C was 33.4 ± 17.8 % of total C in the lake sediment core samples.

Among the lake core facies, the highest N_{tot} concentrations occurred in the Organic-rich mud (0.40 ± 0.13 % wt). The permafrost tunnel horizons also had high N_{tot} concentrations (2.39 ± 2.37 % wt). The Taberite facies had the lowest C_{tot}:N_{tot} ratios among all facies and the Organic-rich mud had the highest C_{tot}:N_{tot} ratios, but there were no statistically significant differences among the other core facies. The Taberite facies had higher $\delta^{13}C_{org}$ values (-26.58 ± 0.44) than the remaining lake sediment core facies (Table 1.4).

1.3.3. CH_4 production potentials and depth-integrated CH_4 production

Mean CH_4 production potentials varied across the lake core facies (Table 1.5) and no CH_4 production was observed in the thawed permafrost tunnel samples. CH_4 production potentials in the lake core over the 175-day incubation period ranged from 0.002 to 8.08 μg C-CH_4 g dw^{-1} d^{-1} and 0.51 to 178.9 μg C-CH_4 g C_{org}^{-1} d^{-1} (Fig. 1.6). The highest production potentials were observed in the Organic-rich mud and the lowest rates occurred in Taberites and Transitional permafrost (Table 1.5). We found that C_{tot} ($r = 0.47$, $p = 0.043$) and C_{org} ($r = 0.47$, $p = 0.043$) were positively correlated with C-CH_4 production. Total N and C_{tot}:N_{tot} ratios were unrelated to CH_4 production potentials in our incubations.

The ratios (R) of facies' CH_4 production potentials to their thickness in the lake center sediment column revealed the highest CH_4 production per unit of sediment were in the Organic-rich mud (R = 2.6) and Recently thawed taberite (R = 1.2) facies, while R of the remaining facies was lower (R = 0.2 to 0.5; Table 1.5). Specifically, the Organic-rich mud facies, which represented 26% of the sediment column thickness, dominated (67%) whole-column CH_4 production in the lake center sediment core (5.2 g C-CH_4 m^{-2} d^{-1}; Table 1.5). The Lacustrine silt facies, which represented 30% of the sediment column thickness, had the second largest contribution (14%; 1.1 g C-CH_4 m^{-2} d^{-1}) to whole-column CH_4 production. Results for other facies are shown in Table 1.5.

1.4. Discussion

1.4.1. CH_4 production potentials

Our study indicates that, in the center of the lake, the Organic-rich mud facies contributed the most (67%) to whole-column CH_4 production despite occupying a lesser fraction (26 %) of sediment column thickness. This is consistent with findings from a study examining an 8 m deep Holocene permafrost core from the Lena Delta, in which the top (125 cm) section of permafrost sediments were also found to have the highest observed CH_4 production in the sediment column (Wagner et al., 2007).

A main reason for the Organic-rich mud facies in our study having high CH_4 production potentials is its relatively high OM content. Past studies have suggested that CH_4 production rates in natural ecosystems are controlled by environmental conditions, including substrate availability (Tranvik et al., 2009; Wallmann et al., 2006; Bergman et al., 1999; Valentine et al., 1994; Westermann, 1993). Correlation analyses showed that CH_4 production in our study was positively correlated to sediment C_{tot} and C_{org} contents ($p = 0.043$ for both). This indicates that

facies with higher C contents, such as the Organic-rich mud, would have higher CH_4 production potentials compared to other facies.

Following the Organic-rich mud facies, relatively high CH_4 production potentials were also observed in the Recently thawed taberite facies. However, the narrowness of the Recently thawed taberite in the center of the lake limited its overall contribution to total sediment column CH_4 production potentials. The thickest sequence, which consisted of combined Lacustrine silt and Taberite facies (60% of total core thickness), had low CH_4 production potentials, contributing only 21% of whole sediment column CH_4 production potential. Our results of higher CH_4 production in the Recently thawed taberite facies compared to the Lacustrine silt and Taberite facies are consistent with model simulations of CH_4 production in a thermokarst lake that showed CH_4 production among the thawed yedoma horizons to be highest along the talik's downward progressing thaw boundary (Kessler et al., 2012). Assuming homogenous C contents along the full yedoma profile in numerical modeling, the higher CH_4 production at the thaw boundary was explained by fresh OM made available to microbial decomposition by permafrost thaw. Conversely, lower CH_4 production in the overlying mineral-dominated sediments, which represent permafrost that thawed earlier, is explained by earlier microbial decomposition that previously exhausted a large fraction of the labile C pool of permafrost sediment OM.

Total soil OC consists of various OC pools with turnover times ranging from less than a year to up to thousands of years (Schädel et al., 2014). OC pool sizes and turnover times significantly impact how OC behaves in the global C cycle and remain a significant uncertainty in estimating how permafrost OC will be processed as it thaws (Schädel et al., 2014; Strauss et al., 2013). In our study, CH_4 production potential rates in the Recently thawed taberite facies, which we estimate thawed during approximately the previous decade based on downward talik

growth rates determined through numerical modeling of a similar yedoma thermokarst lake system (Kessler et al., 2012), were approximately 4.7 times higher than those in the overlying taberite, which we estimate thawed over longer periods of time (up to 400 years). This suggests that, upon thaw, labile fractions of OC in the talik are depleted over decadal to century timescales and the remaining OC pool is less susceptible to processing upon thaw. Prior studies of Siberian yedoma suggest that approximately 30% of the yedoma C pool is bioavailable upon thaw under anaerobic conditions in yedoma-lake taliks (Walter Anthony et al., 2014). Under aerobic conditions, 5–30 % of the total C pool in both organic and mineral circumpolar permafrost samples are estimated to have a rapid turnover time (mean 0.35 ± 0.6 years) upon thaw (Schädel et al., 2014; Shaver et al., 2006). Remaining permafrost C contains 10–90 % "slow" C (mean turnover time 7.21 ± 4.32 years) and 5–85 % "passive" C (mean turnover time > 2500 years; Schädel et al., 2014) under aerobic decomposition regimes. However, further research is necessary to determine the relative sizes of permafrost C pools and better assess what proportion of permafrost OC can be processed into CH_4 upon thaw in an anaerobic thermokarst lake environment.

Within the Organic-rich mud facies, we observed higher CH_4 production potentials (g C_{org}^{-1}) near the surface of the Vault Lake core and slightly decreasing CH_4 production potentials with depth through the facies. Surface lake sediments originate from both allochthonous (terrestrial soils and vegetation) and autochthonous (i.e., lake biota) sources (Tranvik et al., 2009; Cole et al., 2007; Wetzel, 2001). Surface sediments typically contain the most recently deposited materials while deeper sediments represent older deposited materials (Smol, 2008; Cohen, 2003). The higher CH_4 production near the surface of the Organic-rich mud facies may be explained by these more recently deposited surface sediments containing fresher, more labile substrates than

the older, underlying sediments. Another possibility is that autochthonous organic matter in the surface sediments provides a labile C substrate that may prime decomposition of more recalcitrant allochthonous C in the sediments, leading to higher total CH_4 production than in underlying sediments that do not receive the autochthonous C.

1.4.2. CH_4 production potentials versus observed emissions

Laboratory incubations measure maximum CH_4 production potentials, while CH_4 emissions observed in the field represent in situ production minus CH_4 consumption, dissolved CH_4, and trapped CH_4 accumulating in the system (Blazewicz et al., 2012; Wright et al., 2011; Westermann, 1993). Because of this, the CH_4 production potentials measured in our study may be higher than in situ CH_4 production in the Vault thermokarst lake system, possibly explaining the discrepancies among potential CH_4 production rates for the total lake center sediment core in our study (2819 g CH_4 m^{-2} yr^{-1}) and observed, lower CH_4 emission rates from across Vault Lake (41 g CH_4 m^{-2} yr^{-1}; Sepulveda-Jauregui et al., 2015) and observations in the literature for northern (> 54 N) lakes (~7 g CH_4 m^{-2} yr^{-1}; Bastviken et al., 2011). It is possible that CH_4 emissions at Vault Lake are underestimated due to lake sediments storing large quantities of CH_4 which are released during rare extreme-low pressure events and are unlikely to be captured by the ebullition ice-bubble surveys combined with bubble trap measurements utilized by Sepulveda-Jauregui et al. (2015). Other possible explanations for higher potential CH_4 production rates observed by laboratory incubations in this study compared to emissions observed through field measurements are poor representation of spatial heterogeneity in the lake by a single lake center core and CH_4 oxidation. Aerobic and anaerobic oxidation in sediments and the water column consumes a significant fraction of CH_4 produced in lakes (Lofton et al., 2014; Borrel et al., 2011; Deutzmann and Schink, 2011; Bastviken et al., 2008; Kankaala et al.,

2006). A simulated CH_4 production study found CH_4 production in a modeled thermokarst lake talik was up to 10 times higher than observed emissions in the field (Kessler et al., 2012). Produced CH_4 may also be oxidized in anaerobic environments (Gupta et al., 2013; Smemo and Yavitt, 2007; Valentine, 2002), but the magnitude of anaerobic CH_4 oxidation in lake environments is not well understood. The combined effects of aerobic and anaerobic CH_4 oxidation may also account for, in part, the higher talik CH_4 production potentials compared to lake emissions observed by Kessler et al. (2012).

Differences between our incubation temperature (3 °C) and actual temperatures in the talik environment may also lead to some differences between the CH_4 production potentials observed in our incubations and in situ CH_4 production at Vault Lake. Observed annual temperatures under Vault Lake ranged from -0.4 to 14.0 °C (mean ± SD 1.61 ± 2.80 °C). Microorganisms show increased methanogenesis with temperature increases (Yvon-Durocher et al., 2014; Yavitt et al., 2005; Schulz et al., 1997). Therefore, depending on the actual temperatures throughout the talik profile, CH_4 production rates at a given time at Vault Lake may be higher or lower than those measured at our reference incubation temperature of 3 °C.

1.4.3. Spatial patterns of CH_4 production and emission within lakes

Previous field and modeling studies found CH_4 emissions to be up to an order of magnitude higher along thermokarst margins of yedoma lakes than in lake centers (Kessler et al., 2012; Walter et al., 2006). While our sediment incubation study was limited to a single lake center core, other physical data measured along the thermokarst margin at Vault Lake lend support to the findings of previous studies. The talik was 50% deeper along the expanding thermokarst lake margin (measured 6.1 m offshore; Sect. 3.1) compared to the lake center core site. This suggests that the Recently thawed taberite facies would be substantially thicker along

the lake margin than in the lake center, though individual facies thicknesses were not measured. This would also be consistent with field measurements of ^{14}C-CH_4 ages being older (35,000 to 43,000 years old) along yedoma thermokarst lake margins compared to lake centers (Brosius et al., 2012; Kessler et al., 2012; Walter et al., 2006). Based on field observations of cross-basin sediment stratigraphy in other yedoma lakes (Walter Anthony et al., 2014; Farquharson et al., 2016), it is possible that the overlying lake sediment (Organic-rich mud facies) is thinner along the lake margin than in our lake center core; however, Walter Anthony et al. (2014) observed >2 m thick lake sediments within 15 m of the shore in much larger Siberian yedoma thermokarst lakes. Regardless of relative facies thicknesses, the thermokarst margin zone of the lake was more recently converted from permafrost-dominated terrestrial landscape into an open-water lake environment compared to the lake center core location. This suggests that sediments along the margin have had less time to decompose and, therefore, should have an overall higher fraction of labile OM remaining, consistent with higher total-column CH_4 production rates described in the literature.

1.4.4. CH_4 production in thermokarst, permafrost, and non-permafrost systems

Among long-term anaerobic incubations (>115 days), observed CH_4 production rates in the Vault Lake sediment core incubations at 3 ºC were comparable to rates observed in incubations of shallow (<1 m) permafrost from non-lake environments in Alaska (0.01 to 1.14 µg C-CH_4 g dw^{-1} d^{-1}; Lee et al., 2012). However, these soil samples were incubated at a significantly higher temperature (15 ºC), which would yield higher CH_4 production rates than incubations performed at 3 ºC. Terrestrial soils from other shallow (<1 m) permafrost and active layer sites in Alaska incubated at 5 ºC (Waldrop et al., 2010) produced CH_4 at rates approximately an order of magnitude lower than the Vault Lake sediments in our study. Some of the sampling locations of

Lee et al. (2012) and Waldrop et al. (2010) are underlain by yedoma-type permafrost; however, samples collected from shallow surface depths (≤ 1 m) were likely disturbed and thawed at some point during the Holocene, as indicated by the depth of Pleistocene ice-wedge surfaces (Jorgenson et al., 2013; Kanevskiy et al., 2011; Meyer et al., 2008). Deeper Pleistocene-aged yedoma soils (up to 5 m depth) from the Lena Delta region of Siberia incubated at 4 ºC had similar CH_4 production rates (approximately 0.1 to 1.3 μg C-CH_4 g dw^{-1} d^{-1}; Knoblauch et al., 2013) to the lake sediment facies dominated by thawed yedoma in our study; however, these high rates in the non-lake yedoma sediments in Siberia were only observed after a significant lag time (average 963 days). Comparisons across these studies suggest that undisturbed Pleistocene-aged yedoma permafrost may have more biolabile OM than younger or previously thawed yedoma permafrost soils. This conclusion is consistent with findings of Lee et al. (2012), in which yedoma samples had the highest anaerobic C release per gram soil C among a variety of mineral soil samples.

CH_4 production rates in high latitude, non-permafrost lake sediments (eight lakes in central Sweden) incubated at 4 ºC were generally much lower (0.002 to 0.06 μg C-CH_4 g dw^{-1} d^{-1}; Duc et al., 2010) than the rates we observed in the Organic-rich mud facies of the Vault Lake sediment core. These differences could be due to a combination of Vault Lake's yedoma environment containing more biolabile OM derived from yedoma permafrost thawing along lake margins as well as potentially higher rates of Holocene-aged organic matter loading to Vault Lake resulting from thermokarst expansion and high primary production in and around the lake enhanced by nutrients released from thawing yedoma (Walter Anthony et al., 2014).

It is interesting to note that studies of deep permafrost (non-lake) sediments found that (a) no CH_4 was produced (Wagner et al., 2007; this study), (b) CH_4 production rates were an order

of magnitude lower (Lee et al., 2012), or (c) CH_4 production was only observed after a significant lag time (Knoblauch et al., 2013). In contrast, in studies of shallow-permafrost sediments, CH_4 production potentials were observed in anaerobic incubations (Knoblauch et al., 2013; Lee et al., 2012; Waldrop et al., 2010; Wagner et al., 2007). We suggest a potential explanation for these observations in the following section.

1.4.5. Role of modern methanogens in CH_4 production from old C

The quantity of methanogens preexisting in soil samples can influence the rate of methanogenesis in laboratory experiments (Gutknecht et al., 2006; Yavitt et al., 2000). In our study, all samples collected from the Vault Lake core produced CH_4 within 60 days of incubation, including the Transitional permafrost samples at the bottom of the lake core. In contrast, no samples collected from the Vault Creek permafrost tunnel had detectable CH_4 production during the observed 220 days of incubation. A possible explanation for the lack of detectable CH_4 production in the permafrost tunnel could be a paucity of viable methanogens naturally present in deep permafrost soils (Wagner et al., 2007; Steven et al., 2006; Gilichinsky et al., 2003; Rivkina et al., 1998). In previous anaerobic incubations of deep permafrost, little or no CH_4 production has been observed and there was either no observed CH_4 production (non-yedoma permafrost; Wagner et al., 2007), a significant delay before detectable CH_4 production occurred (yedoma permafrost; Knoblauch et al., 2013), or no CH_4 production until samples were inoculated with modern lake sediments (yedoma permafrost; Walter et al., 2007; S. Zimov, personal communication, 2002). Since we observed CH_4 production in the Transitional permafrost (thawing yedoma) beneath Vault Lake but no CH_4 production in the permafrost tunnel samples (yedoma and underlying gravel horizons) it is possible that, in thermokarst lake environments, CH_4 produced from yedoma OM requires the reproduction of modern and/or

ancient microbes along a thermally expanding substrate source as permafrost thaws radially beneath lakes.

1.5. Conclusions

Our study suggests that in the center of a first-generation thermokarst lake, whole-column CH_4 production is dominated by methanogenesis in the Organic-rich mud facies; however, it is likely that other facies contribute significantly more to CH_4 production along laterally expanding thermokarst lake margins. Variability in permafrost C source, quality, and biodegradability remain significant uncertainties in estimating how thawing permafrost OC will be processed. Labile fractions of OC seem to be more absent in near-surface portions of the taberite, reducing CH_4 production rates compared to the underlying Recently thawed taberite along the permafrost thaw boundary. The rapid depletion of the most labile OC pools suggests OC quality may be a limiting factor in determining how thawing permafrost C is processed in a thermokarst lake environment. The knowledge as to where CH_4 originates and what proportion of produced CH_4 is emitted will aid in estimations of how C release and processing in a thermokarst lake environment differs from other thawing permafrost and non-permafrost environments.

Author contributions

K. M. Walter Anthony devised the study. J. K. Heslop and K. M. Walter Anthony were responsible for data analysis and writing the paper. K. M. Walter Anthony, J. K. Heslop, G. Grosse, and A. Bondurant conducted field work. J. K. Heslop, A. Sepulveda-Jauregui, K. Martinez-Cruz, and K. M. Walter Anthony performed lab work. M. C. Jones performed macrofossil analysis. All authors commented on data analyses and manuscript composition.

Acknowledgements

We would like to thank P. Anthony, N. Bigelow, S. Billings, N. Haubenstock, T. Howe, and L. Oliver for assistance in data collection and/or analysis and Sam Skidmore for granting access to Vault Lake and the Vault Creek permafrost tunnel. The Spring 2014 Biology 604 class at the University of Alaska, Fairbanks, Vladimir Romanovsky, and Mingchu Zhang provided invaluable guidance and feedback in the preparation of this manuscript. Funding for J. K. Heslop, K. M. Walter Anthony, A. Sepulveda-Jauregui, G. Grosse, and A. Bondurant was provided by DOE DE-SC0006920, NSF OPP-1107892, and ARC-1304823; funding for K. Martinez-Cruz was provided by Conacyt 330197/233369; and funding for M. C. Jones was provided by the USGS Climate and Land Use Research and Development program. This publication was developed under STAR Fellowship Assistance agreement no. FP-91762901-0 awarded by the US Environmental Protection Agency (EPA). It has not been formally reviewed by EPA. The views expressed in this publication are solely those of J. Heslop, and the EPA does not endorse any products or commercial services mentioned in this publication.

Figures

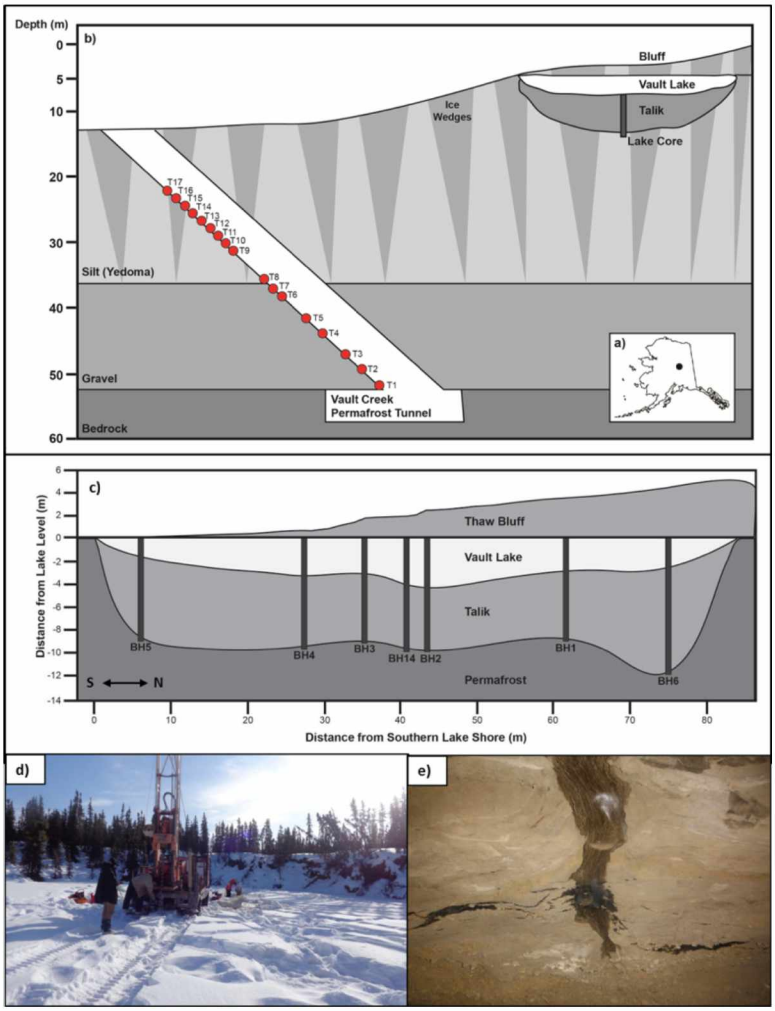

Figure 1.1. Location map (a), study site overview (b), and Vault Lake morphology shown in cross section along the long axis of the lake (c) for Vault Lake and Vault Creek permafrost tunnel, Alaska, USA (65.0293 ºN, 147.6987 ºW). Height of the thaw bluffs was measured using differential GPS (DGPS). Depth of the Vault Lake talik was measured using the delineated borehole transect (c). Thaw bluff heights, lake depth, talik depths, and distance between boreholes (b, c) are shown to scale. Vault Lake is a 3230 m^2, 3.7 m deep thermokarst lake with thermokarst bluffs (d) ranging from 0.2 to 4.5 m in height and a 5.9 m deep talik underneath. The Vault Lake core was collected from the center of the lake (BH14). The Vault Creek permafrost tunnel extends 220 to 40 m depth below the ground surface. Ice wedges (e) are present to 23 m depth. Tunnel sampling sites are marked as red dots; numbers adjacent to the dots represent incubation sample IDs. Photographs by K. M. Walter Anthony (d) and J. K. Heslop (e).

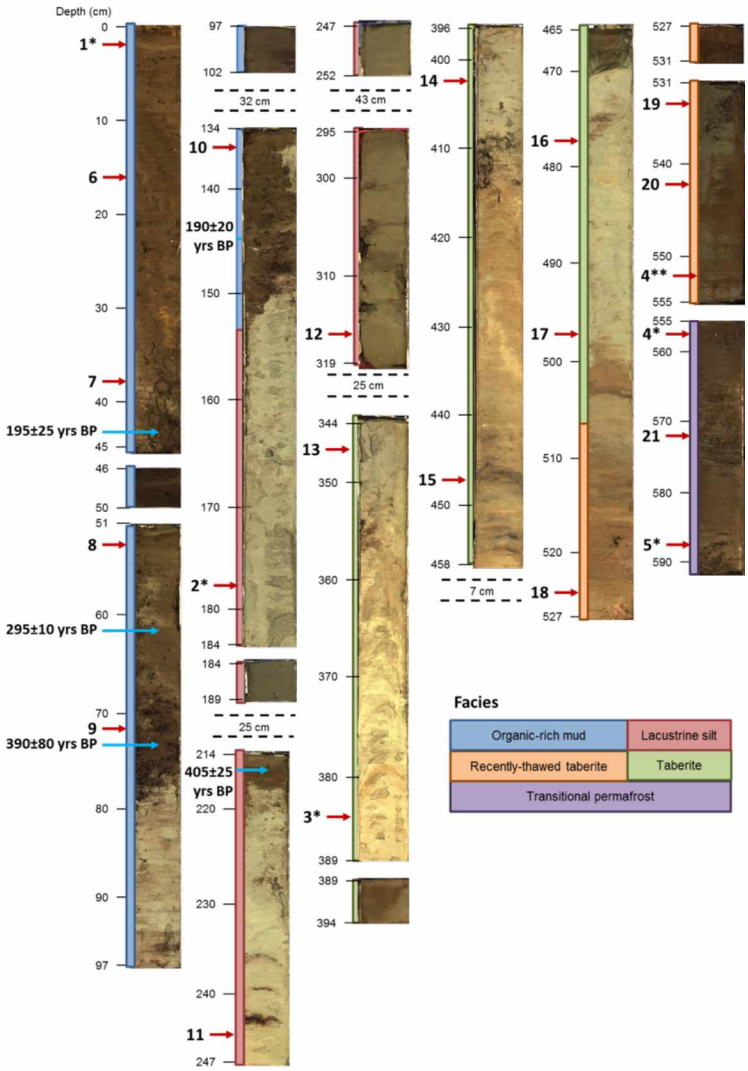

Figure 1.2. The Vault Lake core with the five facies (Organic-rich mud, Lacustrine silt, Taberite, Recently thawed taberite, and Transitional permafrost) delineated. Core depth values are indicated; core subsampling locations for incubations are marked using red arrows with bold numbers indicating incubation sample IDs; locations of picked and ^{14}C dated macrofossil are shown by blue arrows and calibrated ^{14}C ages (calendar years BP). Labeled breaks represent gaps in the sediment core.

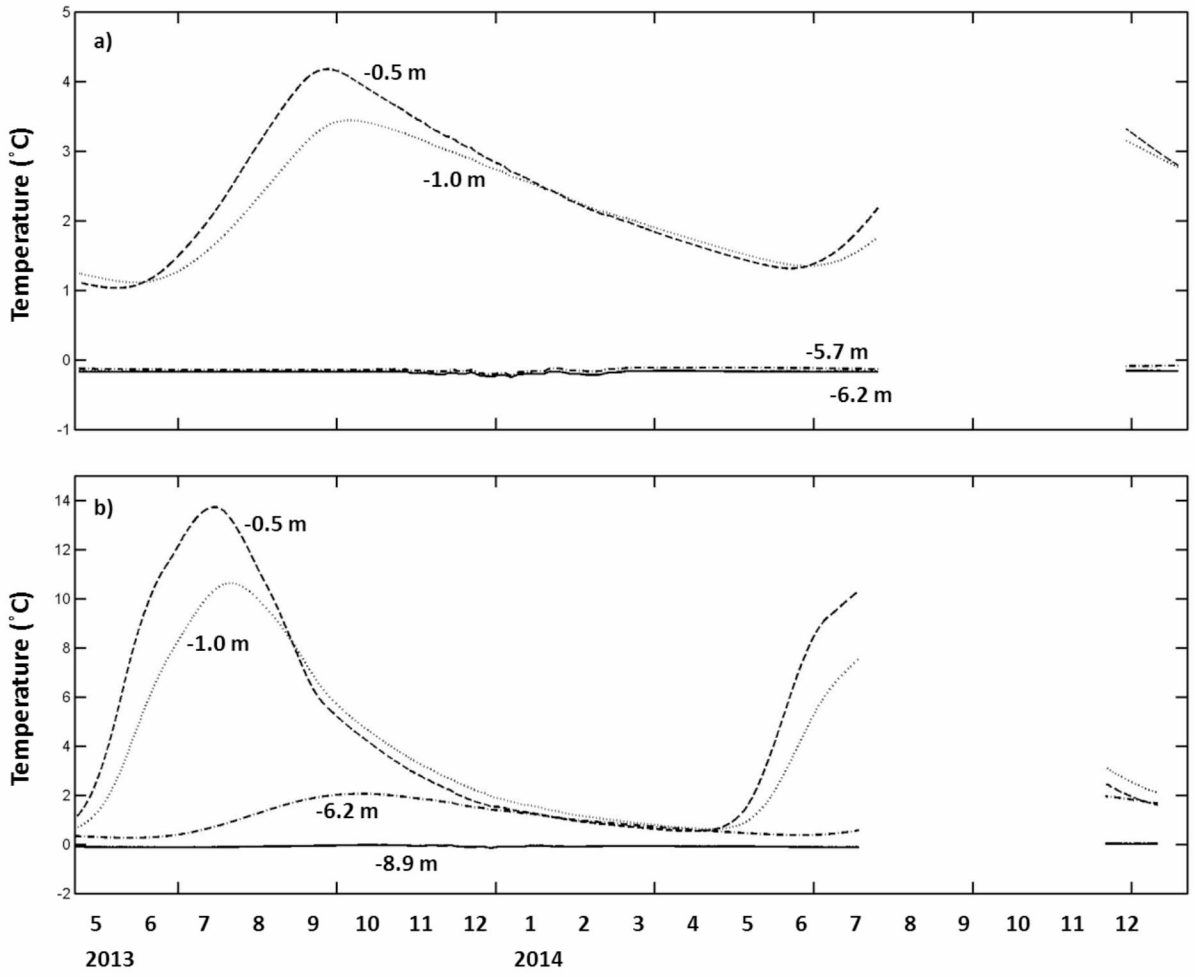

Figure 1.3. Vertical profile temperatures measured in the lake center (< 1 m from BH14; a) and 6.1 m offshore of the southwestern thermokarst margin (b). Negative depth values indicate depth from the sediment–water interface (0 m) at each of the examined boreholes. Loggers did not record temperature between 25 July and 11 November 2014.

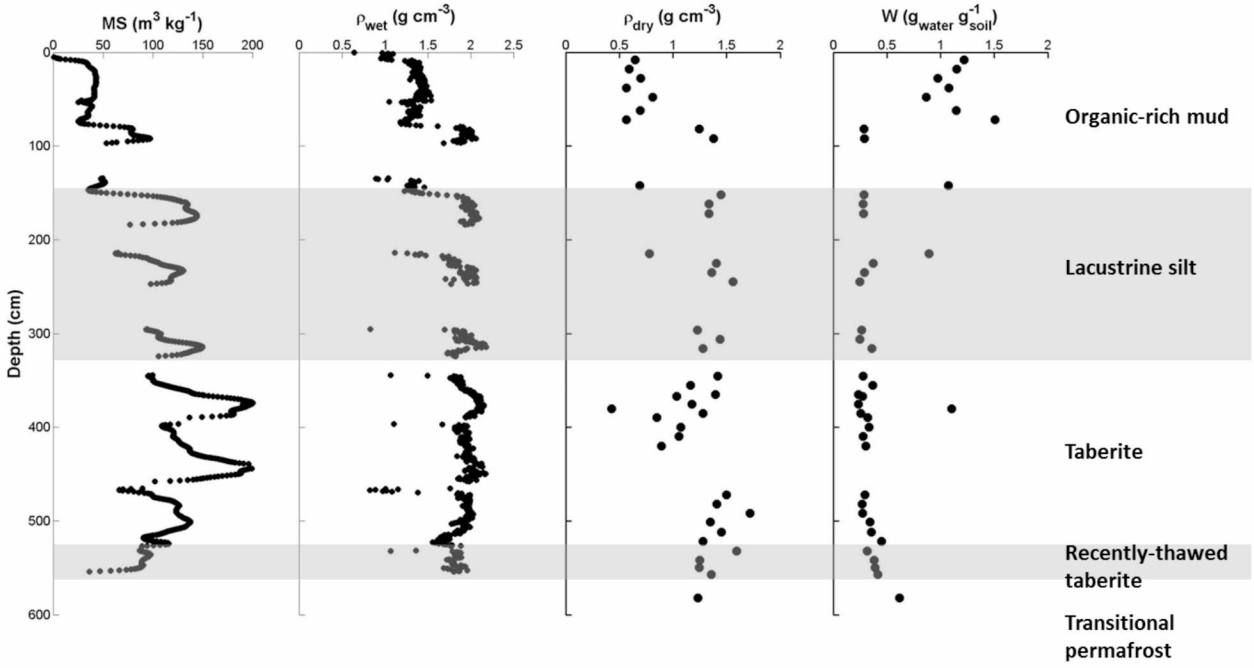

Figure 1.4. Depth profiles for magnetic susceptibility (MS), wet bulk density (ρ_{wet}), dry bulk density (ρ_{dry}), and gravimetric water content (W) in the Vault Lake sediment core. Two MS values at 95.4 and 405.4 cm were -493.1 and -488.0 m^3 kg^{-1}, respectively (not shown).

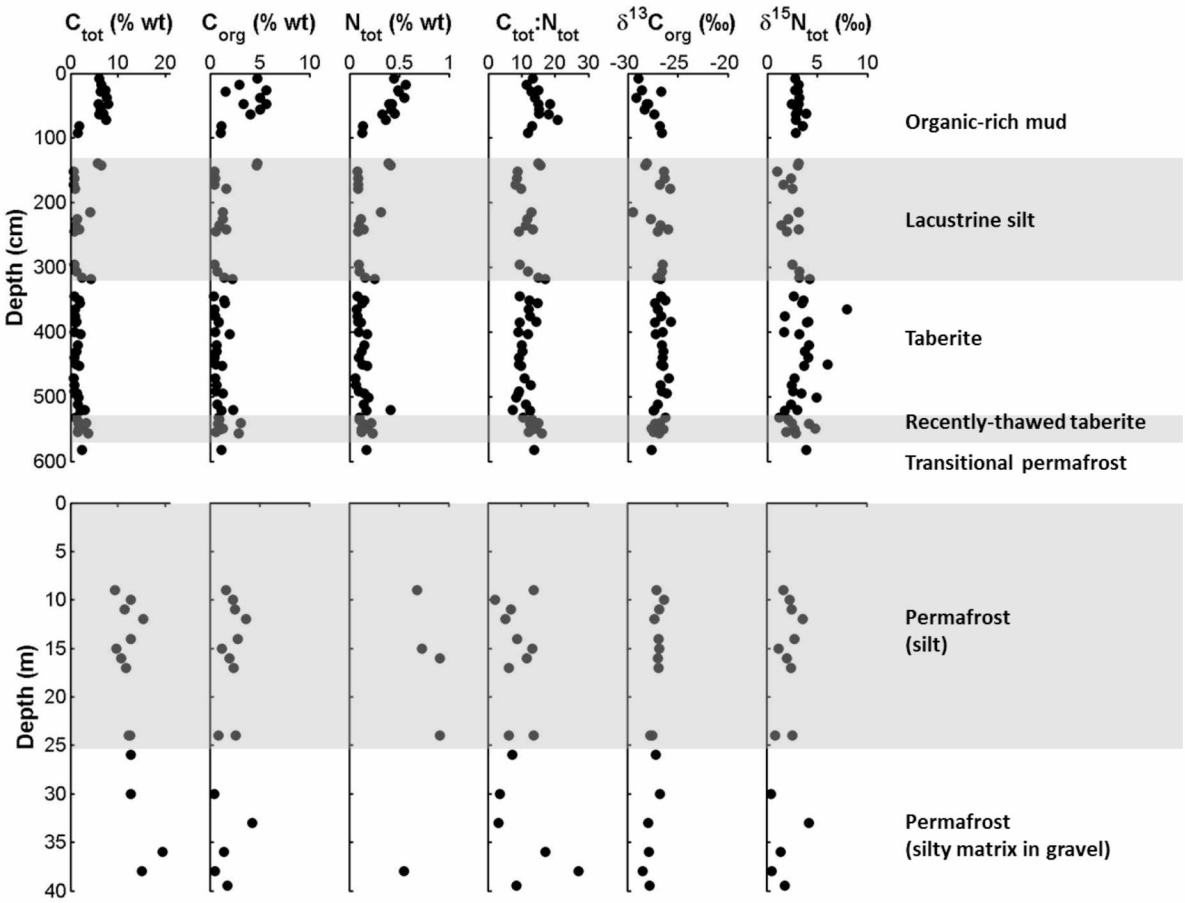

Figure 1.5. Depth profiles for sediment geochemical characteristics: total carbon (C_{tot}), organic carbon (C_{org}), total N (N_{tot}), C_{tot}:N_{tot} ratios, $\delta^{13}C_{org}$ and $\delta^{15}N_{tot}$. Values for the Vault Lake core are in the top panel; values for the Vault Creek permafrost tunnel are in the bottom panel.

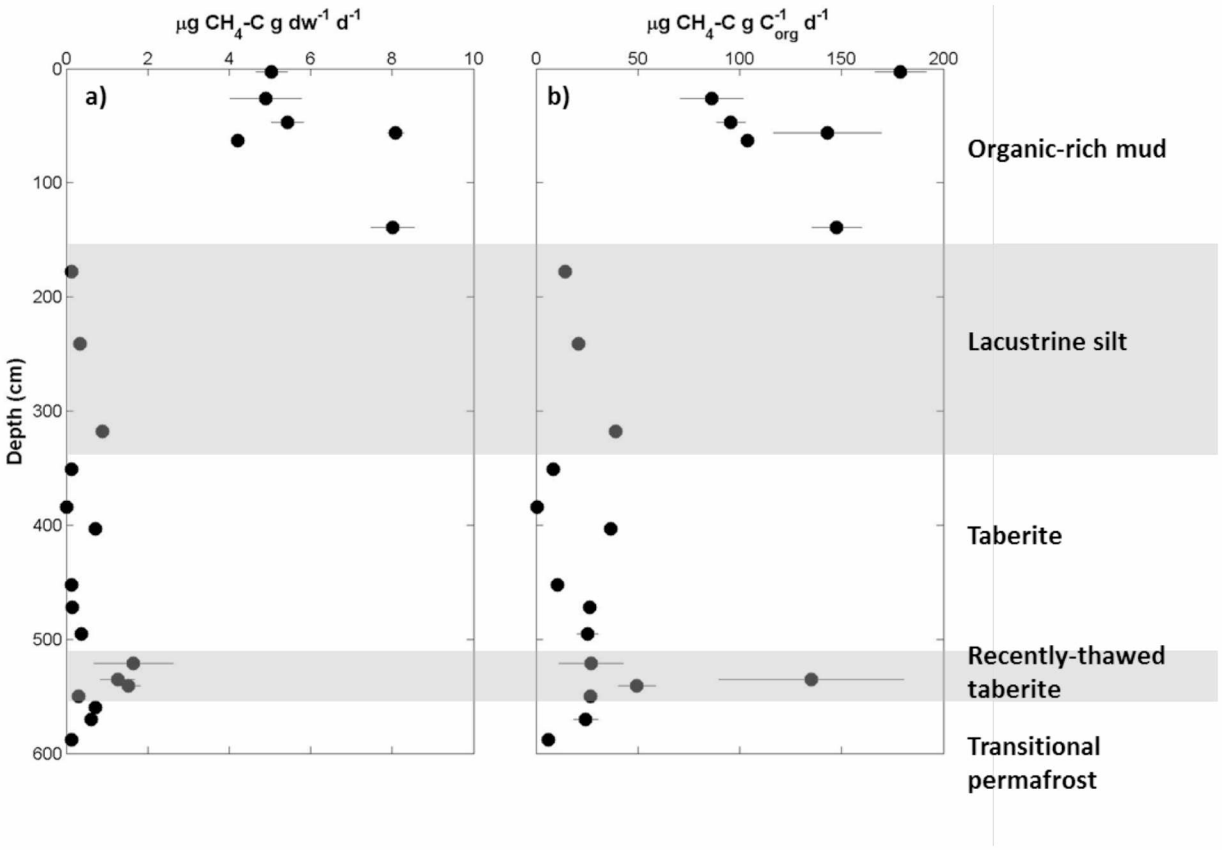

Figure 1.6. Depth profile for CH_4 production potentials in the Vault Lake core. Samples were anaerobically incubated at 3 ºC. Methane production potentials are represented as mean value ± SD among replicates and normalized per gram dry weight sediment (a) and per gram organic carbon (C_{org};b).

Tables

Table 1.1. Radiocarbon ages of macrofossils picked from the Vault Lake sediment core, calibrated to calendar 2σ years before present (BP) using Calib 7.0 (Reimer et al., 2013).

Depth in Core (cm)	Lab ID	NOSAMS ID	14C Age (Yrs. BP)	Calibrated Age (Cal. Yrs. BP)	Average Age (Cal. Yrs. BP)	Material Dated
45	VAULT13-14A-1G-1-W , 48-50CM	122576	150 ±25	172-223	195	Byrophyte (*Aulacomnium palustre*)
62	VAULT13-14A-3N-1-W , 10.5-12.5CM	122577	240 ±20	285-303	295	Byrophyte (*Aulacomnium palustre*), leaf fragments from ericaceous shrubs or *Betula nana*, *Picea* needles
72	VAULT13-14A-3N-1-W, 20.5-22.5	122578	320 ±30	356-432	394	Byrophyte (*Aulacomnium palustre*)
144	VAULT13-14A-4N-1-W, 8-19cm	122579	170 ±20	170-214	190	Byrophyte (*Aulacomnium palustre*), leaf fragments from ericaceous shrubs or *Betula nana*, *Picea* needles
214	VAULT13-6N-1-W, 1-3CM	122580	315 ±20	375-429	405	Leaf fragments from ericaceous shrubs or *Betula nana*

Table 1.2. Vault Lake core and Vault Creek permafrost tunnel facies, their depths and thicknesses, and the representative number of samples used in anaerobic laboratory incubations.

Profile	**Facies**	**Depth (cm)**	**Thickness (cm)**	**Incubation samples (n)**
Vault L. core	Organic-rich mud	0-152	152	6
	Lacustrine silt	153-330	178	3
	Taberite	331-507	177	6
	Recently-thawed taberite	508-550	43	4
	Transitional permafrost	551-590	40	3
Vault Cr. tunnel	Permafrost (Silt)	0-2,400	2,400	7
	Permafrost (Silty matrix of Gravel)	2,400-4,000	1,600	9

Table 1.3. Summary of dry bulk density (ρ) and gravimetric water content (W) data from the Vault Lake core and the Vault Creek permafrost tunnel. Data are presented as mean ± SD.

Sample		Sediment Properties	
Profile	**Facies**	**ρ ($g\ cm^{-3}$)**	**W ($g_{water}/g_{sediment}$)**
Vault L. core	Organic-rich mud	0.79 ±0.29[a]	0.96 ±0.39[a]
	Lacustrine silt	1.32 ±0.21	0.35 ±0.19
	Taberite	1.22 ±0.33	0.29 ±0.04[b]
	Recently-thawed taberite	1.36 ±0.15	0.38 ±0.05
	Transitional permafrost	1.29 ±0.06	0.52 ±0.10
Vault Cr. tunnel	Permafrost (Silt)	0.89 ±0.28	0.91 ±0.40
	Permafrost (Silty matrix of Gravel)	1.28 ±0.21	0.44 ±0.20

[a,b] Different letters indicate significant differences from other facies in the same profile at the α = 0.05 level. Vault L. core and Vault Cr. tunnel profiles were analyzed separately.

Table 1.4. Summary of geochemical properties and stable isotopes measured on sediment samples from the Vault Lake core and Vault Creek permafrost tunnel. Data are presented as mean ± SD.

Sample		Geochemistry					
Profile	**Facies**	**C_{tot} (% wt)**	**C_{org} (% wt)**	**N_{tot} (% wt)**	**C_{tot}:N_{tot}**	**$\delta^{13}C_{org}$ (‰)**	**$\delta^{15}N_{tot}$ (‰)**
Vault L. core	Organic-rich mud	6.01 ±1.90[a]	3.83 ±1.66[a]	0.40 ±0.13[a]	15.0 ±2.5[a]	-28.11 ±1.12	3.05 ±0.34[a]
	Lacustrine silt	1.60 ±1.24	1.04 ±0.58	0.13 ±0.07	11.3 ±2.7	-26.85 ±0.92	2.49 ±0.90
	Taberite	1.24 ±0.44[b]	0.84 ±0.45[b]	0.12 ±0.04[b]	10.8 ±1.9[b]	-26.58 ±0.44[a]	3.70 ±1.46[a]
	Recently-thawed taberite	2.04 ±0.79	1.36 ±0.80	0.18 ±0.10	12.2 ±2.4	-26.94 ±0.51	2.72 ±1.13
	Transitional permafrost	2.52 ±1.10	1.52 ±1.18	0.18 ±0.05	14.0 ±1.9	-27.28 ±0.39	2.88 ±0.98
Vault Cr. tunnel	Permafrost (Silt)	11.88 ±1.75[b]	2.21 ±0.80[a]	1.91 ±1.60	8.8 ±4.1	-27.02 ±0.40	2.21 ±0.80[a]
	Permafrost (Silty matrix of Gravel)	18.77 ±6.80[a]	1.31 ±1.66[b]	3.19 ±3.32	11.2 ±9.4	-27.63 ±0.60	1.40 ±1.55[b]

[a,b] Different letters indicate significant differences from other facies in the same profile at the $\alpha = 0.05$ level. Vault L. core and Vault Cr. tunnel profiles were analyzed separately.

Table 1.5. Summary of facies' CH_4 production potentials and depth-integrated CH_4 production for the total sediment column. Data are presented as mean ± SD. It should be noted that, based on optical properties (Fig. 1.2), dry bulk density (mean±SD, 1.31 ± 0.07g cm^{-3}), gravimetric moisture content (29 ± 0.00 %), and C_{org} (1.64%) values measured on two samples in the depth interval 77–97 cm of the core, which were similar to those of Lacustrine Silt and very different from the remainder of the Organic-rich mud facies segments, we applied CH_4 production rates measured on Lacustrine silt samples to this 21 cm interval of the Organic-rich mud section. This was done because no samples from this 21 cm thick, mineral-dominated segment of organic-rich mud were represented in the incubation.

Sample		**CH_4 Production Potentials (µg C-CH_4 d^{-1})**		**Sediment column CH_4 Production**			
Profile	**Facies**	**g dw^{-1}**	**g C_{org}^{-1}**	**g C-CH_4 m^{-2} d^{-1}**	**% Total C-CH_4 Production**	**% Total Column Thickness**	***R* (% production/ % thickness)**
Vault L. core	Organic-rich mud	5.95 ±1.67[a]	125.9 ±36.2[a]	5.2	67	26	2.6
	Lacustrine silt	0.45 ±0.39	24.6 ±12.8	1.1	14	30	0.5
	Taberite	0.25 ±0.26[b]	17.9 ±13.6	0.5	7	30	0.2
	Recently-thawed taberite	1.18 ±0.61	59.6 ±51.5	0.7	9	7	1.2
	Transitional permafrost	0.48 ±0.31	15.3 ±9.1[b]	0.2	3	7	0.5

[a,b] Different letters indicate significant differences from other facies in the same profile at the α = 0.05 level.

References

Bastviken, D., Cole, J.J., Pace, M.L., and Van de Bogert, M.C.: Fates of methane from different lake habitats: Connecting whole-lake budgets and CH$_4$ emissions, Journal of Geophysical Research, 113, 1-13, 2008.

Bastviken, D., Tranvik, L.J., Downing, J.A., Crill, P.M., and Enrich-Prast, A.: Freshwater Methane Emissions Offset the Continental Carbon Sink, Science, 331, 50-50, 2011.

Bergman, I., Lundberg, P., and Nilsson, M.: Microbial carbon mineralisation in an acid surface peat: effects of environmental factors in laboratory incubations, Soil Biology & Biochemistry, 31, 1867-1877, 1999.

Blazewicz, S.J., Petersen, D.G., Waldrop, M.P., and Firestone, M.K.: Anaerobic oxidation of methane in tropical and boreal soils: Ecological significance in terrestrial methane cycling, Journal of Geophysical Research: Biogeosciences, 117, G02033, 2012.

Borrel, G., Jézéquel, D., Biderre-Petit, C., Morel-Desrosiers, N., Moerl, J.P., Peyret, P., Fonty, G., and Lehours, A.C.: Production and Consumption of Methane in Freshwater Lake Ecosystems, Research in Microbiology, 162, 832-847, 2011.

Brosius, L.S., Walter Anthony, K.M., Grosse, G., Chanton, J.P., Farquharson, L.M., Overduin, P.P., and Meyer, H.: Using the deuterium isotope composition of permafrost meltwater to constrain thermokarst lake contributions to atmospheric CH$_4$ during the last deglaciation, Journal of Geophysical Research, 117, 2012.

Burn, C.R.: Lake-bottom thermal regimes, western arctic coast, Canada, Permafrost and Periglacial Processes, 16, 355–367, 2005.

Cohen, A.S.: Paleolimnology: the History and Evolution of Lake Systems, Oxford University Press, New York, USA, 2003.

Cole, J., Prairie, Y., Caraco, N., McDowell, W., Tranvik, L., Striegl, R., Duarte, C., Kortelainen, P., Downing, J., Middelburg, J., and Melack, J.: Plumbing the Global Carbon Cycle: Integrating Inland Waters into the Terrestrial Carbon Budget, Ecosystems, 10, 172-185, 2007.

Deutzmann, J.S., and Schink, B.: Anaerobic Oxidation of Methane in Sediments of Lake Constance, an Oligotrophic Freshwater Lake, Applied and Environmental Microbiology, 77, 4429-4436, 2011.

Duc, N.T., Crill, P., and Bastviken, D.: Implications of Temperature and Sediment Characteristics on Methane Formation and Oxidation in Lake Sediments, Biogeochemistry, 100, 185-196, 2010.

Farquharson, L., Anthony, K., Bigelow, N., Edwards, M. and Grosse, G.: Facies analysis of yedoma thermokarst lakes on the northern Seward Peninsula, Alaska, Sedimentary Geology, 340, 25-37, 2016.

Gilichinsky, D., Rivkina, E., Shcherbakova, V., Laurinavichuis, K., and Tiedje, J.: Supercooled Water Brines Within Permafrost—An Unknown Ecological Niche for Microorganisms: A Model for Astrobiology, Astrobiology, 3, 331-341, 2003.

Gorini, L.: Effect of L-Cysteine on Initiation of Anaerobic Growth of *E. Coli* and *A. Aerogenes*, Journal of Bacteriology, 82, 305-312, 1961.

Grosse, G., Jones, B., and Arp, C.: Thermokarst Lakes, Drainage, and Drained Basins, in: Treatise on Geomorphology, edited by: Shroder, J. F., Academic Press, San Diego, 325-353, 2013a.

Grosse, G., Robinson, J.E., Bryant, R., Taylor, M.D., Harper, W., DeMasi, A., Kyker-Snowman, E., Veremeeva, A., Schirrmeister, L., and Harden, J.: Distribution of late Pleistocene ice-

rich syngenetic permafrost of the Yedoma Suite in east and central Siberia, Russia, USGS, Reston, VA, 31, 2013b.

Gupta, V., Smemo, K., Yavitt, J., Fowle, D., Branfireun, B., and Basiliko, N.: Stable Isotopes Reveal Widespread Anaerobic Methane Oxidation Across Latitude and Peatland Type Environmental Science and Technology, 47, 8273-8279, 2013.

Gutknecht, J., Goodman, R., and Balser, T.: Linking soil process and microbial ecology in freshwater wetland ecosystems, Plant & Soil, 289, 17-34, 2006.

Harden, J.W., Koven, C.D., Ping, C.-L., Hugelius, G., David McGuire, A., Camill, P., Jorgenson, T., Kuhry, P., Michaelson, G.J., O'Donnell, J.A., Schuur, E.A.G., Tarnocai, C., Johnson, K., and Grosse, G.: Field information links permafrost carbon to physical vulnerabilities of thawing, Geophysical Research Letters, 39, L15704, 2012.

Hugelius, G., Strauss, J., Zubrzycki, S., Harden, J.W., Schuur, E.A.G., Ping, C.L., Schirrmeister, L., Grosse, G., Michaelson, G.J., Koven, C.D., O'Donnell, J.A., Elberling, B., Mishra, U., Camill, P., Yu, Z., Palmtag, J., and Kuhry, P.: Estimated stocks of circumpolar permafrost carbon with quantified uncertainty ranges and identified data gaps, Biogeosciences, 11, 6573-6593, 2014.

Jorgenson, M.T., Harden, J., Kanevskiy, M., O'Donnell, J., Wickland, K., Ewing, S., Manies, K., Zhuang, Q., Shur, Y., Striegl, R., and Koch, J.: Reorganization of Vegetation, Hydrology and Soil Carbon after Permafrost Degradation across Heterogeneous Boreal Landscapes, Environmental Research Letters, 8, 035017, 2013.

Kanevskiy, M., Shur, Y., Jorgenson, M.T., and Stephani, E.: Cryostratigraphy of late Pleistocene syngenetic permafrost (yedoma) in northern Alaska, Itkillik River exposure, Quaternary Research, 75, 584-596, 2011.

Kankaala, P., Huotari, J., Peltomaa, E., Saloranta, T., and Ojala, A.: Methanotrophic activity in relation to methane efflux and total heterotrophic bacterial production in a stratified, humic, boreal lake, Limnology and Oceanography, 51, 1195-1204, 2006.

Kessler, M.A., Plug, L.J., and Walter Anthony, K.M.: Simulating the decadal- to millennial-scale dynamics of morphology and sequestered carbon mineralization of two thermokarst lakes in NW Alaska, Journal of Geophysical Research, 117, G00M06, 2012.

Kholodov, A.L., Rivkina, E.M., Gilichinsky, D.A., Fyodorov-Davydov, D.G., Gubin, S.V., Sorokovikov, V.A., Ostroumov, V.E., and Maksimovich, S.V.: Estimation of the organic carbon input into Arctic ocean due to erosion of the East-Siberian seashore, Kriosphera Zemli, 7, 3-12, 2003.

Kling, G.W., and Kipphut, G.W.: Arctic lakes and streams as gas conduits to the atmosphere: Implications for tundra carbon budgets, Science, 251, 298-301, 1991.

Knoblauch, C., Beer, C., Sosnin, A., Wagner, D., and Preiffer, E.: Predicting long-term carbon mineralization and trace gas production from thawing permafrost of Northeast Siberia, Global Change Biology, 19, 1160-1172, 2013.

Lee, H., Schuur, E.A.G., Inglett, K.S., Lavoie, M., and Chanton, J.P.: The Rate of Permafrost Carbon Release under Aerobic and Anaerobic Conditions and Its Potential Effects on Climate, Global Change Biology, 18, 515-527, 2012.

Lofton, D.D., Whalen, S.C., and Hershey, A.E.: Effect of temperature on methane dynamics and evaluation of methane oxidation kinetics in shallow Arctic Alaskan lakes, Hydrobiologia, 721, 209-222, 2014.

McGuire, A.D., Anderson, L.G., Christensen, T.R., Dallimore, S.R., Guo, L., Hayes, D.J., Heimann, M., Loreson, T.D., MacDonald, R.B., and Roulet, N.: Sensitivity of the carbon cycle in the Arctic to climate change, Ecological Monographs, 79, 523-555, 2009.

Meyer, H., Yoshikawa, K., Schirrmeister, L., and Andreev, A.: The Vault Creek Tunnel (Fairbanks Region, Alaska): A Late Quaternary Palaeoenvironmental Permafrost Record, Ninth International Conference on Permafrost, 1191-1196, 2008.

Murton, J.B.: Thermokarst-lake-basin sediments, Tuktoyaktuk Coastlands, western arctic Canada, Sedimentology, 43, 737-760, 1996.

Myhre, G., Shindell, D., Breon, F.M., Collins, W., Fuglestvedt, J., Huang, J., Koch, D., Lamarque, J.F., Lee, D., Mendoza, B., Nakajima, T., Robock, A., Stephens, G., Takemura, T., and Zhang, H.: Anthropogenic and Natural Radiative Forcing. In: Climate Change 2013: The Physical Science Basis. Contribution of Working Group I to the Fifth Assessment Report of the Intergovernmental Panel on Climate Change, Intergovernmental Panel on Climate Change, New York, USA, 2013.

Pewe, T.L.: Quaternary geology of Alaska, USGS Numbered Series, Professional Paper 835, 1975.

Pienitz, R., Doran, P.T., and Lamoureux, S.F.: Origin and geomorphology of lakes in the polar regions, in: Polar Lakes and Rivers, edited by: Vincent, W., Oxford University Press, Oxford, 2008.

Plug, L.J., and West, J.J.: Thaw lake expansion in a two-dimensional coupled model of heat transfer, thaw subsidence, and mass movement, Journal of Geophysical Research, 114, F01002, 2009.

Reimer, P., Bard, E., Bayliss, A., Beck, J.W., Blackwell, P.G., Ramsey, C.B., Buck, C.E., Cheng, H., Edwards, R.L., Friedrich, M., Grootes, P.M., Guilderson, T.P., Haflidason, H., Hajdas, I., Hatté, C., and Heaton, T.J.: IntCal13 and Marine13 Radiocarbon Age Calibration Curves 0–50,000 Years cal BP, Radiocarbon, 55, 2013.

Rivkina, E., Gilichinsky, D., Wagener, S., Tiedje, J., and McGrath, J.: Biogeochemical activity of anaerobic microorganisms from buried permafrost sediments, Geomicrobiology Journal, 15, 187-193, 1998.

Romanovsky, V., Smith, S., and Christiansen, H.: Permafrost thermal state in the polar Northern Hemisphere during the International Polar Year 2007-2009: a synthesis, Permafrost and Periglacial Processes, 11, 137-152, 2010.

Schädel, C., Schuur, E.A.G., Bracho, R., Elberling, B., Knoblauch, C., Lee, H., Luo, Y., Shaver, G.R., and Turetsky, M.R.: Circumpolar assessment of permafrost C quality and its vulnerability over time using long-term incubation data, Global Change Biology, 20, 641-652, 2014.

Schaefer, K., Lantuit, H., Romanovsky, V.E., Schuur, E.A.G., and Witt, R.: The impact of the permafrost carbon feedback on global climate, Environmental Research Letters, 2014.

Schirrmeister, L., Grosse, G., Wetterich, S., Overduin, P.P., Strauss, J., Schuur, E.A.G., and Hubberten, H.: Fossil organic matter characteristics in permafrost deposits of the northeast Siberian Arctic Journal of Geophysical Research, 116, G00M02, 2011.

Schulz, S., Matsuyama, H., and Conrad, R.: Temperature dependence of methane production from different precursors in a profundal sediment (Lake Constance), FEMS Microbiology Ecology, 22, 207-213, 1997.

Schuur, E.A.G., and Abbott, B.: High risk of permafrost thaw, Nature, 480, 32-33, 2011.

Schuur, E.A.G., Abbott, B.W., Bowden, W.B., Brovkin, V., Camill, P., Canadell, J.G., Chanton, J.P., Chapin III, F.S., Christensen, T.R., Ciais, P., Crosby, B.T., Czimczik, C.I., Grosse, G., Harden, J., Hayes, D.J., Hugelius, G., Jastrow, J.D., Jones, J.B., Kleinen, T., Koven, C.D., Krinner, G., Kuhry, P., Lawrence, D.M., McGuire, A.D., Natali, S.M., O'Donnell, J.A., Ping, C.-L., Riley, W.J., Rinke, A., Romanovsky, V.E., Sannel, A.B.K., Schädel, C., Schaefer, K., Sky, J., Subin, Z.M., Tarnocai, C., Turetsky, M.R., Waldrop, M.P., Walter Anthony, K.M., Wickland, K.P., Wilson, C.J., and Zimov, S.A.: Expert assessment of vulnerability of permafrost carbon to climate change, Climatic Change, 119, 359-374, 2013.

Sepulveda-Jauregui, A., Walter Anthony, K.M., Martinez-Cruz, K., Greene, S., and Thalasso, F.: Methane and carbon dioxide emissions from 40 lakes along a north–south latitudinal transect in Alaska, Biogeosciences Discussions, 11, 13251–13307, 2014.

Shaver, G.R., Giblin, A.E., Nadelhoffer, K.J., Thieler, K.K., Downs, M.R., Launder, J.A., and Rastetter, E.B.: Carbon turnover in Alaskan tundra soils: effects of organic matter quality, temperature, moisture and fertilizer, Journal of Ecology, 94, 740-753, 2006.

Smemo, K., and Yavitt, J.: Evidence for Anaerobic CH$_4$ Oxidation in Freshwater Peatlands Geomicrobiology Journal, 24, 583-597, 2007.

Smol, J.P.: Pollution of Lakes and Rivers: a Paleoenvironmental Perspective, 2 ed., Blackwell Publishing, Oxford, United Kingdom, 2008.

Soloviev, P.A.: Thermokarst phenomena and landforms due to frostheaving in central Yakutia, Biuletyn Peryglacjalny, 135-155, 1973.

Steven, B., Léveillé, R., Pollard, W., and Whyte, L.: Microbial ecology and biodiversity in permafrost, Extremophiles, 10, 259-267, 2006.

Strauss, J., Schirrmeister, L., Grosse, G., Wetterich, S., Ulrich, M., Herzschuh, U., and Hubberten, H.: The deep permafrost carbon pool of the Yedoma region in Siberia and Alaska Geophysical Research Letters, 40, 6165-6170, 2013.

Tranvik, L., Downing, J., and Cotner, J.: Lakes and reservoirs as regulators of carbon cycling and climate, Limnology and Oceanography, 54, 2298-2314, 2009.

Valentine, D.: Biogeochemistry and microbial ecology of methane oxidation in anoxic environments: a review, Antonie van Leeuwenhoek, 81, 271-282, 2002.

Valentine, D., Holland, E.A., and Schimel, D.S.: Ecosystem and physiological controls over methane production in northern wetlands, Journal of Geophysical Research-Atmospheres, 99, 1563-1571, 1994.

Wagner, D., Gattinger, A., Embacher, A., Pfeiffer, E.M., Schloter, M., and Lipskis, A.: Methanogenic Activity and Biomass in Holocene Permafrost Deposits of the Lena Delta, Siberian Arctic and Its Implication for the Global Methane Budget, Global Change Biology, 13, 1089-1099, 2007.

Waldrop, M.P., Wickland, K.P., White III, R., Berhe, A.A., Harden, J.W., and Romanovsky, V.E.: Molecular investigations into a globally important carbon pool: permafrost-protected carbon in Alaskan soils, Global Change Biology, 16, 2543-2554, 2010.

Wallmann, K., Aloisi, G., Haeckel, M., Obzhirov, A., Pavlova, G., and Tishchenko, P.: Kinetics of organic matter degradation, microbial methane generation, and gas hydrate formation in anoxic marine sediments, Geochimica et Cosmochimica Acta, 70, 3905-3927, 2006.

Walter Anthony, K.M., and Anthony, P.: Constraining spatial variability of methane ebullition seeps in thermokarst lakes using point process models, Journal of Geophysical Research: Biogeosciences, 118, 1015-1034, 2013.

Walter, K.M., Chanton, J.P., Chapin, F.S., Schuur, E.A.G., and Zimov, S.A.: Methane production and bubble emissions from arctic lakes: Isotopic implications for source pathways and ages, Journal of Geophysical Research, 113, G00A08, 2008.

Walter, K.M., Smith, L.C., and Chapin, F.S.: Methane bubbling from northern lakes: present and future contributions to the global methane budget, Philosophical Transactions of the Royal Society A-Mathematical Physical and Engineering Sciences, 365, 1657-1676, 2007.

Walter, K.M., Zimov, S.A., Chanton, J.P., Verbyla, D., and Chapin, I.F.S.: Methane bubbling from Siberian thaw lakes as a positive feedback to climate warming, Nature, 443, 71-75, 2006.

Walter Anthony, K.M., Zimov, S.A., Grosse, G., Jones, M.C., Anthony, P.M., Chapin III, F.S., Finlay, J.C., Mack, M.C., Davydov, S., Frenzel, P., and Frolking, S.: A shift of thermokarst lakes from carbon sources to sinks during the Holocene epoch, Nature, 511, 452-456, 2014.

Westermann, P.: Temperature Regulation of Methanogenesis in Wetlands, Chemosphere, 26, 321-328, 1993.

Wetzel, R.G.: Limnology: Lake and River Ecosystems, 3rd Editon, Elsevier Academic Press, San Diego, CA, 2001.

Williams, P.J., and Smith, M.W.: The Frozen Earth: Fundamentals of Geocryology, Cambridge University Press, 1989.

Wright, E.L., Black, C.R., Cheesman, A.W., Drage, T., Large, D., Turner, B.L., and Sjögersten, S.: Contribution of subsurface peat to CO$_2$ and CH$_4$ fluxes in a neotropical peatland, Global Change Biology, 17, 2867-2881, 2011.

Yavitt, J.B., Williams, C.J., and Wieder, R.K.: Controls on Microbial Production of Methane and Carbon Dioxide in Three Sphagnum-Dominated Peatland Ecosystems as Revealed by a Reciprocal Field Peat Transplant Experiment, Geomicrobiology Journal, 17, 61-88, 2000.

Yavitt, J.B., Williams, C.J., and Wieder, R.K.: Soil chemistry versus environmental controls on production of CH$_4$ and CO$_2$ in northern peatlands, European Journal of Soil Science, 56, 169-178, 2005.

Yvon-Durocher, G.A., Bastviken, A.P., Conrad, D., Gudasz, R., St-Pierre, C., Thanh-Duc, A., Giorgio, N., and Paul A.: Methane fluxes show consistent temperature dependence across microbial to ecosystem scales, Nature, 507, 488-491, 2014.

Zimov, S.A., Voropaev, Y.V., Semiletov, I.P., Davidov, S.P., Prosiannikov, S.F., Chapin, F.S., Chapin, M.C., Trumbore, S., and Tyler, S.: North Siberian lakes: A methane source fueled by Pleistocene carbon, Science, 277, 800-802, 1997.

Zimov, S.A., Schuur, E.A.G., and Chapin, F.S.: Permafrost and the global carbon budget, Science, 312, 1612-1613, 2006.

Appendix 1.A: Supplement of Thermokarst-lake methanogenesis along a complete talik profile[2]

Table 1.A-1. Macrofossil samples observed in the Vault Lake core.

	Sample ID	VAULT13-14A-1G-1-W 8-10 cm	VAULT13-14A-1G-1-W 8-10 cm	VAULT13-14A-1G-1-W 48-50 cm	VAULT13-14A-3N-1-W 10.5-12.5 cm
	Depth in Core (cm)	3	3	45	62
Dry upland mosses	Detritus (%)	90	0	40	65
	Herbaceous Detritus (%)			40	
	Equisetum (%)				
	Total other mosses	5			
	Sphagnum	*		2	
	Polytrichum spp.			3	1*
	A. palustre	*		5	10
	T. nitens				
	Hylocomium stems				
Wet fen to aquatic mosses	S. scorpiodes	*			3*
	Drepanocladus spp.				
	Fine Ericaceous rootlets			10	10
	Ericaceous leaf fragment				2*
	Vaccinium leaf fragment			1	1*
	Betula nana leaf fragment				
	Ledum leaf fragment				
	Betula papyrifera seed				1*
	Picea needle			2*	3*
	wood fragments				10
	Bark				1*
	charred wood	2*			
	Charcoal	3*			2*
	Daphnia ephippia			3*	

* indicates presence
* with a number indicates a count
Numbers only indicate percent of total sieved fraction

[2] Supplement of: Heslop, J. K., Walter Anthony, K. M., Sepulveda-Jauregui, A., Martinez-Cruz, K., Bondurant, A., Grosse, G., and Jones, M. C.: Thermokarst lake methanogenesis along a complete talik profile, Biogeosciences, 12, 4317-4331, doi: doi:10.5194/bg-12-4317-2015-supplement, 2015.

Table 1.A-1 continued. Macrofossil samples observed in the Vault Lake core.

	Sample ID	VAULT13-14A-3N-1-W 20.5-22.5 cm	VAULT13-14A-3N-1-W 20.5-22.5 cm	VAULT13-14A-4N-1-W 8-10 cm	VAULT13-14A-4N-1-W 38-40 cm
	Depth in Core (cm)	72	72	144	174
Dry upland mosses	Detritus (%)	30	0	0	0
	Herbaceous Detritus (%)				
	Equisetum (%)				
	Total other mosses				
	Sphagnum	1			
	Polytrichum spp.	5			
	A. palustre	10			
	T. nitens	5			
Wet fen to aquatic mosses	Hylocomium stems				
	S. scorpiodes	3			
	Drepanocladus spp.	1			
	Fine Ericaceous rootlets	40			
	Ericaceous leaf fragment	1*			
	Vaccinium leaf fragment				
	Betula nana leaf fragment				
	Ledum leaf fragment				
	Betula papyrifera seed				
	Picea needle				
	wood fragments				
	Bark				
	charred wood				
	Charcoal	2*			
	Daphnia ephippia				

* indicates presence
* with a number indicates a count
Numbers only indicate percent of total sieved fraction

Table 1.A-1 continued. Macrofossil samples observed in the Vault Lake core.

	Sample ID	VAULT13-14A-6N-1-W 1-3 cm	14A-7N-Baggie 10 cm +125	14A-7N-Baggie 20 cm +125	VAULT13-14A-8N-1-W 41-43 cm
	Depth in Core (cm)	214	325	335	385
Dry upland mosses	Detritus (%)	55	0	0	0
	Herbaceous Detritus (%)	10			
	Equisetum (%)	1*			
	Total other mosses	5			
	Sphagnum	2			
	Polytrichum spp.				
	A. palustre	2			
	T. nitens	2			
Wet fen to aquatic mosses	Hylocomium stems				
	S. scorpiodes				
	Drepanocladus spp.				
	Fine Ericaceous rootlets	20			
	Ericaceous leaf fragment				
	Vaccinium leaf fragment	3*			
	Betula nana leaf fragment				
	Ledum leaf fragment				
	Betula papyrifera seed				
	Picea needle				
	wood fragments				
	Bark	4			
	charred wood				
	Charcoal				
	Daphnia ephippia	2*			

* indicates presence
* with a number indicates a count
Numbers only indicate percent of total sieved fraction

Table 1.A-1 continued. Macrofossil samples observed in the Vault Lake core.

	Sample ID	VAULT13-14A-10N-1-W 17-19 cm	VAULT13-14A-11N-1-W 19-21 cm	VAULT13-14A-11N-2-W 2-4 cm	VAULT13-14A-11N-2-W 27-28 cm
	Depth in Core (cm)	482	551	557	582
Dry upland mosses	Detritus (%)	0	10	99	10
	Herbaceous Detritus (%)		85		90
	Equisetum (%)			1	
	Total other mosses				
	Sphagnum				
	Polytrichum spp.				1*
	A. palustre		*		
	T. nitens				
	Hylocomium stems		1*		
Wet fen to aquatic mosses	S. scorpiodes				
	Drepanocladus spp.				
	Fine Ericaceous rootlets				
	Ericaceous leaf fragment				
	Vaccinium leaf fragment				
	Betula nana leaf fragment				1*
	Ledum leaf fragment				1*
	Betula papyrifera seed				
	Picea needle				
	wood fragments		3*		
	Bark				
	charred wood				
	Charcoal				
	Daphnia ephippia				

* indicates presence
* with a number indicates a count
Numbers only indicate percent of total sieved fraction

Chapter 2: Utilizing pyrolysis GC-MS to characterize organic matter quality in relation to methane production in a thermokarst lake sediment core[1]

Abstract

Thermokarst (thaw) lakes are an important source of atmospheric methane (CH_4); however, few studies have examined the composition and biodegradability of their sediment organic matter (OM). We quantified (i) the composition of bulk sediment OM (bulk SOM) using pyrolysis GC-MS and (ii) the statistical relationships between bulk SOM properties and anaerobic incubation CH_4 production rates at 3 °C in sediment core samples collected from a thermokarst lake system. Our lake sediment study core extended through the full vertically-thawed profile (0-550 cm) of Vault Lake, a small thermokarst lake near Fairbanks, Alaska, USA, and into the permafrost thawing beneath the lake (551-590 cm). Compared with the underlying mineral-dominated sediments (153-590 cm depth in core), the surface organic-rich sediment horizon (0-152 cm) had higher CH_4 production rates, greater substrate availability indicated by percent organic carbon and total nitrogen, and greater proportions of terrestrially-associated bulk SOM compounds (alkanes, alkenes, lignin products, and phenols and phenolic precursors). Correlation and principal component analyses indicated that CH_4 production potentials measured in the Vault Lake core were positively associated with initial substrate availability and terrestrially-derived OM compounds. We observed positive correlation ($p \leq 0.05$) between CH_4

---

[1] Heslop, J.K. Walter Anthony, K. M., Zhang, M.: Utilizing pyrolysis GC-MS to characterize organic matter quality in relation to methane production in a thermokarst lake sediment core, Organic Geochemistry, 103, 43-50, doi:10.1016/j.orggeochem.2016.10.013, 2017.

production and bulk SOM compounds classified as phenols and phenolic precursors, a pattern different from previously observed relationships in natural aquatic anaerobic environments.

2.1. Introduction

Many thermokarst (thaw) lakes formed in permafrost-dominated landscapes have exceptionally high rates of carbon dioxide (CO_2) and methane (CH_4) emission (Walter et al., 2007; Sepulveda-Jauregui et al., 2015; Wik et al., 2016). In rare cases, CH_4 emission from these lakes originates from ancient geologic sources (Walter Anthony et al., 2012). More commonly, CH_4 emissions are the result of modern microbial carbon (C) mineralization. The C utilized in the microbial production of CH_4 originates in terrestrial sources such as watershed soils (Kling and Kipphut, 1991), the mobilization of recently-thawed organic carbon (OC) from permafrost thaw beneath and surrounding the lakes (Walter et al., 2008; Brosius et al., 2012; Kessler et al., 2012), and decomposition of contemporary allocthonous and authochtonous organic matter (OM) in the lakes (Grosse et al., 2013; Walter Anthony et al., 2014; Heslop et al., 2015).

Several recent studies have begun to increase our understanding of sediment OM composition and mineralization in permafrost environments; however, most have been limited to examining permafrost C from shallow (< 1 m) soils in terrestrial environments (e.g. White et al., 2002, 2004; Dutta et al., 2006; Treat et al., 2014). Relatively few studies have examined OM biodegradability in the anaerobic incubation of deep (> 5 m) permafrost sediments (Wagner et al., 2007; Knoblauch et al, 2013; Ewing et al., 2015) and, to our knowledge, no studies have been conducted relating OM quality to anaerobic C mineralization in thermokarst lake sediments and deeper underlying taliks (thaw bulbs).

Anaerobic C mineralization rates depend on many factors, including substrate availability and quality, pH, moisture, temperature, oxidation-reduction potential, and microbial community

composition and abundance (Davidson and Janssens, 2006; Waldrop et al., 2010; Grosse et al., 2011; Olefeldt et al., 2013; Treat et al., 2014; Lawrence et al., 2015; Ping et al., 2015). In thermokarst lake sediments, studies suggest the majority of CH_4 production is concentrated in certain regions. In the lake center, surface sediments, which contain contemporary allocthonous and authochtonous OM as well as ancient thawed permafrost OM (Walter Anthony et al., 2014; Farquharson et al., 2016), contribute substantially to total thermokarst lake CH_4 production (Kessler et al., 2012; Heslop et al., 2015). The permafrost thaw boundary at the outer extent of a lake's talik, where ancient OM is supplied from thawing permafrost soil to fuel methanogenesis, has also been identified as a region of high CH_4 production (Kessler et al., 2012; Walter Anthony et al., 2016). High rates of CH_4 production in sediment zones receiving OM inputs from lacustrine deposition and thawing permafrost suggest that substrate availability has a large effect on CH_4 production potential in thermokarst lakes. However, few studies have characterized substrate availability in these systems.

Past studies using laboratory incubations and/or mass-balance approaches to compare sediment C stocks before and after permafrost thaw have shown that the labile fraction of recently-thawed permafrost OM is in limited supply. These studies suggest only 5-30% of C in mineral permafrost soils is bioavailable over a 100 yr period following thaw under both aerobic and anaerobic decomposition regimes (Shaver et al., 2006; Schädel et al., 2014; Walter Anthony et al., 2014). As the labile fraction of permafrost OC is utilized, CH_4 production rates in thawed permafrost sediments diminish over time (Kessler et al., 2012; Heslop et al., 2015). In anaerobic talik environments of Siberian thermokarst lakes, the labile fraction of the permafrost OC pool (28 ±12%) was estimated based on OM mass loss comparisons between undisturbed yedoma permafrost soils and taberites (the in situ thawed permafrost soil beneath lakes which are

refrozen after the lakes drain); however, there were large regional differences in the size of the labile fraction of permafrost OM based on this method (20- 36% labile fraction; Walter Anthony et al., 2014). Jones et al. (2016) also observed a ~30 ±20% loss of OC from mineral permafrost soils upon thaw in collapse-scar bogs in Alaska, but the amount of time it took to lose this C remained poorly constrained.

It has been well documented that permafrost C mineralization rate is positively related to sediment C concentration (e.g. Waldrop et al., 2010; Lee et al., 2012; Knoblauch et al., 2013). Improving our knowledge of the quality of the permafrost OC pool will further reduce uncertainty in estimating how thawed permafrost OC would behave in the global C cycle (Hugelius et al., 2012; Strauss et al., 2013; Schädel et al., 2014). Several studies have measured permafrost sediment OC quality using laboratory incubations (e.g. Lee et al., 2012; Knoblauch et al., 2013; Schädel et al., 2014). However, incubation periods can last weeks, months, or years and this labor-intensive method is not well-suited to determining OC quality for a large number of samples. It has been suggested that alternative OM quality indicators such as molecular characterization of OM composition, which can be measured in a relatively short period of time and at significantly lower cost than incubation, can be utilized to model C bioavailability and improve estimates of potential C emissions from thawing permafrost soils (e.g. Dai et al., 2002; White et al., 2002, 2004; Andersen and White, 2006; Paré and Bedard-Haughn, 2013; Treat et al., 2014). Models developed using molecular information from pyrolysis GC-MS (py-GC-MS) analyses have shown potential for estimating permafrost C mineralization rates (e.g. Dai et al., 2002; White et al., 2002, 2004; Andersen and White, 2006; Treat et al., 2014), but to our knowledge no study has characterized OM composition in relation to anaerobic C mineralization in thermokarst lake sediments and the underlying talik.

Vault Lake (65.0293 °N, 147.6987 °W) is a first generation thermokarst lake (3,200 m^2; 3.7 m average depth, ≤ 8.8 m talik depth below the sediment-water interface) estimated to have formed within the last 400 yr (Heslop et al., 2015). Heslop et al. (2015) quantified CH_4 production potential rates in a Vault L. sediment core representing the full talik profile in the lake center. In this study, we use the same core to examine sediment OM quality in a boreal zone thermokarst lake environment with the objectives of: (i) characterizing deep lake sediment OM using py-GC-MS analysis and (ii) identifying the strongest predictors of anaerobic permafrost OC biodegradability.

2.2. Material and methods

2.2.1. Sample collection and preparation

The collection of a 590 cm core from the center of Vault L., Alaska during March 2013 was described by Heslop et al. (2015). While Heslop et al. (2015) classified a larger set of sedimentary facies in the core, here we simplified the categorization by recognizing two general horizons: surface organic-rich sediments (0-152 cm) and underlying mineral sediments (153-590 cm). After retrieval of the core, the thawed segments were stored in the laboratory at 3 °C until further analysis; the frozen transitional permafrost core sediments from beneath the talik (551-590 cm) were stored in the laboratory at -10 °C (holding time 61 days until incubation for both thawed and frozen sediments). Sediment slurries (mean ±SD 269 ±253 g dw sediment/l water) were prepared for 22 depths along the core and CH_4 production potential rates in the slurries, measured at five monthly time steps for up to 175 days, were quantified by Heslop et al. (2015).

Two subsamples of slurry from each sampling depth were analyzed for OM characterization. We oven-dried (105 °C, 48 h) subsamples of the slurry sediments, homogenized the dried sediments using a mortar and pestle, and stored them in pre-ashed (450 °C for 3 h)

sealed glass vials at room temperature. We filtered a second set of slurry subsamples through a sterile 0.45 μm polyethersulfone membrane filter device (Whatman Puradisc PES) to remove particulate OM and stored the resulting solution in sealed, pre-ashed (450 °C, 3 h) glass vials in the dark at 3 °C until further analysis.

2.2.2. Water-extractable organic matter quantification

Dissolved organic carbon (DOC) concentrations of the filtered solution were determined using a total organic carbon analyzer (Aurora 1030; detection limit 2 μg/l) at the University of Alaska Fairbanks. DOC concentration (mg/l) was divided by the mass of dry sediment per unit volume in the corresponding slurry (g dw/l) to determine soil water-extractable organic carbon (WEOC) content (mg C/g dw). We refer to the dissolved OC fractions as WEOC, as opposed to DOC, for clarity. The term DOC typically refers to fractions of OC dissolved in situ within soil pore water or in aquatic systems, whereas WEOC specifically refers to fractions of sediment OC dissolved during a laboratory water extraction (Zsolnay, 1996; Corvasce et al., 2006).

2.2.3. Bulk SOM characterization

Sediment organic carbon (C_{org}), inorganic carbon ($C_{inorganic}$), total nitrogen (N_{tot}), C_{org}:N_{tot}, and C_{org} ($\delta^{13}C_{org}$) and N_{tot} ($\delta^{15}N_{tot}$) stable isotope ratio values were measured by Heslop et al. (2015) on the homogenized oven-dried slurry sediments. In this study, we used pyrolysis-gas chromatography-mass spectrometry [py-GC-MS; HP 6890 (Agilent Technologies) - HP 5973 (Agilent Technologies)] at the University of Alaska Palmer Research Center, Palmer, Alaska, to characterize bulk SOM composition of the same slurry sediment subsamples for 18 depths along the core. The pyrolyzer temperature was 600 °C. The GC carrier gas was run at 10 psi and constant 30 ml/min air flow. The GC program was: 35 °C (3 min) to 310 °C (held 5 min)

at 15 °C/min. We conducted duplicate runs and ran a methanol (CH_3OH) blank following every other sample.

Following White et al. (2004), the 30 most prevalent pyrolysis product compounds in the py-GC-MS dataset were identified using a spectral library (Wiley 275 library; Figs. 2.A-1, 2.A-2). The relative abundance of each of the identified compounds in every sample was calculated as follows:

$$A_i = \left(\frac{X_i}{\sum X_{ij}}\right) 100$$

where A_i is the relative abundance of compound i (%), X_i is the spectral peak area of compound i, and $\sum X_{ij}$ is the sum of all spectral peak areas in the sample (Vancampenhout et al., 2009). Standard deviation in compound relative abundance between duplicate runs ranged from 0.12-6.29% (mean = 0.85%). Identified compounds were classified into nine classes based on their origin: alkanes, alkenes, aromatics and polyaromatics, carboxylic acids, lignin products, lipids, N compounds, phenols and phenolic precursors, and primary and secondary polysaccharides (Table 2.1), as defined by White et al. (2002), White et al. (2004), Dai et al. (2002), Vancampenhout et al. (2009), Xu et al. (2009), Yassir and Buurman (2012), and Carr et al. (2013). We then summed the relative abundances of the compounds in each class to obtain the relative proportion (%) of each compound class in the detected pyrolysis products. In an independent Fourier transform infrared spectroscopy (FTIR) analysis, we confirmed the presence of functional groups that corresponded to the compounds assigned using py-GC-MS (data not shown).

It is important to note that py-GC-MS quantitatively characterizes individual pyrolysis product molecules thermally extracted from the bulk SOM. Since an unknown fraction of SOM

is undetected by py-GC-MS, we were not able to determine the absolute concentrations of individual compounds in the bulk SOM or the qualitative characteristics of the average bulk SOM structure (Wang et al., 2011). Therefore, consistent with similar past studies using py-GC-MS to characterize terrestrial soils and OM (e.g. Carr et al., 2013; Vancampenhout et al., 2009; Yassir and Burrman, 2012), we report results as the relative abundance of the most prominent pyrolysis product compounds derived from each bulk SOM class to create a "fingerprint" of the SOM. This method characterizes OM in a way which provides a proxy for bulk SOM composition, distinguishes our sediment samples from one another, and allows for SOM compounds to be quantified and statistically analyzed (White et al., 2004; Wang et al., 2011). The 30 compounds we identified represent 28-40% of total pyrolysis product compounds detected in the py-GC-MS analyses, but we acknowledge that additional unidentified or undetected compounds could alter the true proportions of each compound class throughout the core.

2.2.4. Statistical analyses

MATLAB (R2016a) software was used for statistical analysis. All measured parameters were tested for normal distribution using the Jarque-Bera test. WEOC concentration, all the bulk SOM compound classes measured via py-GC-MS, and CH_4 production potential rates expressed as μgC CH_4/g dw/d were not consistent with a normal distribution at the $\alpha = 0.05$ level; therefore, differences between core horizons were determined using nonparametric Wilcoxon rank sum tests. We determined relationships between sediment OM parameters and CH_4 production potential rates using nonparametric Spearman's rank correlation coefficients. Differences and correlations were considered statistically significant when $p \leq 0.05$ ($\alpha = 0.05$) or $p \leq 0.10$ ($\alpha = 0.10$); the level of significance is reported individually for all results.

We utilized principal component analyses (PCAs) using MATLAB (2016a) software to examine connections and relationships between the different SOM parameters measured in the Vault L. core. Prior to our PCAs, all variables were standardized using z-scores so all transformed variables were centered around 0 with a standard deviation of 1. Two principal component analyses (PCA-I and PCA-II) were run for the standardized geochemical data and the SOM compound class data, respectively.

2.3. Results

2.3.1. Bulk SOM compound classes

Statistical analyses of py-GC-MS data (Wilcoxon rank sum tests) revealed that the organic-rich sediments horizon contained greater proportions of alkanes ($p = 0.006$; Table 2.A-1; Figs. 2.1, 2.A-3), alkenes ($p = 0.006$), lignin products ($p = 0.002$), and phenols and phenolic precursors ($p = 0.002$) than the mineral sediments. All other compound classes did not have statistically significant differences between the organic-rich and mineral sediment horizons. Generally, carboxylic acids, N compounds, and primary and secondary polysaccharides represented the largest proportions of the pyrolysis product compounds. Alkanes, alkenes, lignin products, and phenols and phenolic precursors represented the smallest proportions of the pyrolysis product compounds.

2.3.2. Effect of bulk SOM properties and WEOC concentration on CH_4 production

Among the geochemical properties, CH_4 production potential rates in the whole core exhibited statistically significant correlation with C_{org} ($p \leq 0.05$), $C_{inorganic}$ ($p \leq 0.10$), WEOC ($p \leq 0.10$), N_{tot} ($p \leq 0.05$), C_{org}:N_{tot} ($p \leq 0.10$) and $\delta^{13}C_{org}$ ($p \leq 0.05$; Table 2.A-2; Figs. 2.2, 2.A-4). Relationships between CH_4 production potential and C_{org}, $C_{inorganic}$, WEOC, N_{tot} and C_{org}:N_{tot}

were positive and the relationship with $\delta^{13}C_{org}$ was negative. We did not observe statistically significant relationships between CH_4 production potential rates and WEOC:C_{org} ratios or $\delta^{15}N_{tot}$.

The proportions of alkanes ($p \leq 0.05$), alkenes ($p \leq 0.05$), lignin products ($p \leq 0.05$), phenolic and phenolic precursors ($p \leq 0.05$), and primary and secondary polysaccharides ($p \leq 0.10$) in the bulk SOM all positively correlated with CH_4 production potentials in our study (Fig. 2.A-5). None of the other pyrolysis product classes exhibited statistically significant relationships with CH_4 production potentials measured in the Vault L. sediment core.

2.3.3. Principal component analyses

Our results for the two principal component analyses [PCA-I (sediment geochemistry) and PCA-II (bulk SOM composition)], showed that the first three principal components (PCs) accounted for 81% (PCA-I: PC1 53%, PC2 16%, PC3 12%; Table 2.A-3; Fig. 2.3a) and 88% (PCA-II: PC1 44%, PC2 29%, PC3 15%; Fig. 2.3b) of the variability in the sediment geochemistry and SOM composition, respectively. According to PCA-I, a little over half the variability was accounted for in PC1, which positively correlated with substrate availability (C_{org}, N_{tot}) and the degree of OM decomposition ($\delta^{13}C_{org}$). PC2, which accounted for 16% of the variability in PCA-I, corresponded to proportions of algal and land-plant OM ($\delta^{15}N_{tot}$), the degree of OM decomposition (C_{org}:N_{tot}), and WEOC concentrations; PC3, which accounted for 12% of the total variability in PCA-I, was positively associated with WEOC concentration. In PCA-II, 44% of the variability was accounted for in PC1, which positively correlated with terrestrially-associated compounds representing the smallest proportions of the bulk SOM in our study (alkanes, alkenes, lignin products, and phenols and phenolic precursors). PC2, accounting for 29% of the bulk SOM composition variability in PCA-II, positively correlated with the more abundant bulk SOM compounds in our study (carboxylic acids, lipids, and N compounds).

Aromatics and polyaromatics and lipids were positively correlated with PC3, which accounted for 15% of the variability.

In PCA-I, CH_4 production potential rates had the strongest correlation with PC1, indicating CH_4 production had the greatest association with substrate availability as characterized primarily by C_{org} and N_{tot} concentrations. CH_4 production also had the strongest correlation with PC1 in PCA-II, indicating CH_4 production in our study also positively associated with terrestrially-associated compounds (alkanes, alkenes, lignin products, and phenols and phenolic precursors). Each of these bulk SOM compound classes also positively correlated ($p \leq 0.05$) with CH_4 production rates in our Spearman's rank analyses.

In both PCA-I and PCA-II, when we plotted the PC1 and PC2 component scores for each sample depth (Fig. 2.3), we observed separation between samples from the organic-rich sediments horizon (0-152 cm depth) and samples from the underlying mineral sediments horizon (153-590 cm depth). The surface organic-rich sediments were characterized by greater substrate availability (higher PC1 scores in PCA-I) and greater proportions of terrestrial bulk SOM compound classes positively associated with CH_4 production in our study (higher PC1 scores PCA-II) compared to the mineral sediments.

2.4. Discussion

2.4.1. Bulk SOM composition explained by sediment depositional history

Different depositional and processing environments in each horizon likely explain why the OM in the organic-rich sediment horizon was characterized by higher initial substrate levels (C_{org}, $C_{inorganic}$, and N_{tot}); less decomposed OM (indicated by lighter $\delta^{13}C_{org}$ and higher C_{org}:N_{tot} ratios; Meyers, 2003; Gundelwein et al., 2007; Schirrmeister et al., 2011); and greater proportions of biolabile SOM compounds (alkanes, alkenes, lignin products, and phenols and

phenolic precursors) with relatively short (months to years) residence times (Lorenz et al., 2007; Fenner and Freeman, 2011) compared to the underlying mineral sediment horizon. The organic-rich horizon consisted of allochthonous and autochthonous sediments and OM which were exposed to the lake water column, settled on the anoxic lake bottom, and were subsequently buried over time. Such surface sediment facies have been described for other thermokarst lakes in Canada (Murton, 1996), Siberia (Walter Anthony et al., 2014), and Alaska (Farquharson et al., 2016). At Vault L., radiocarbon dating of macrofossils from the organic-rich horizon suggest rapid sediment accumulation (152 cm in the lake center over ~400 yr) and burial in the anoxic lake bottom environment (Heslop et al., 2015). This, in turn, suggests minimal OM processing and a higher likelihood of preserving higher proportions of biolabile OM fractions.

In contrast, the Vault L. mineral horizon largely consisted of thawed yedoma sediments which were originally deposited in a non-lake environment over tens of thousands of years during the late Pleistocene. These yedoma sediments experienced significant deformation from post-depositional slope processes (e.g. landslides) prior to burial during syngenetic permafrost accumulation (Meyer et al., 2008; Schirrmeister et al., 2016). Based on high abundances of low molecular weight DOC compounds found in deep yedoma permafrost cores collected from a nearby location in central Alaska (Ewing et al., 2015), it is possible the silt-rich yedoma permafrost sediments surrounding Vault L. fostered long-term anaerobic OM processing prior to thaw. Therefore, the most biolabile OM fractions in these sediments may have been previously processed in aerobic and/or anaerobic conditions prior to being warmed and thawed beneath the thermokarst lake (Heslop et al., 2015).

2.4.2. Relationships between CH_4 production and bulk SOM

While relationships between sediment geochemical properties (C_{org}, $C_{inorganic}$, N_{tot}, and C_{org}:N_{tot}) and CH_4 production potentials are well-documented in prior aerobic and anaerobic permafrost incubation studies (e.g. Lee et al., 2012; Knoblauch et al., 2013; Treat et al., 2014, 2015) and have previously been reported for the Vault L. core (Heslop et al., 2015), here we report for the first time observations of statistically significant positive correlation between CH_4 production potential rates and bulk SOM composition of thermokarst lake sediments, specifically: alkanes, alkenes, lignin products, phenols and phenolic precursors, and primary and secondary polysaccharides. Polysaccharides are known to be rapidly degraded by microbes and have been previously shown to positively correlate with C mineralization in both aerobic and anaerobic environments (Andersen and White, 2006; White et al., 2002, 2004; Yavitt et al., 2005; Harrysson Drotz et al., 2010; Treat et al., 2014). The remaining bulk SOM compounds which positively correlated with CH_4 production in our study are typically more abundant in terrestrial environments (Lorenz et al., 2007; Ward et al., 2013) and were also more abundant ($p \leq 0.05$) in the surface organic-rich sediment horizon of the lake core. We note the terrestrially-derived compound classes which positively correlated with CH_4 production (alkanes, alkenes, lignin products, and phenols and phenolic precursors) also positively correlated ($p \leq 0.05$) with each other (Table 2.A-2). Therefore, CH_4 production in our study may be driven by terrestrially-derived compounds as a unit rather than the individual pyrolysis product compound classes.

Our study focused on a single lake center core; however, we may expect high variability in the relationships between CH_4 production rates and substrate availability and composition across lake basins. Studies of other thermokarst lakes in Alaska and Siberia have found substantial variability in the thickness of the surface organic-rich horizon across lake basins

(Walter Anthony et al., 2014; Farquharson et al., 2016). Closer to the lake margin, the thickness of this horizon decreases and the surface sediments are more heavily influenced by terrestrial vegetation inputs (Farquharson et al., 2016). The relative contribution of recently-thawed yedoma OM to the vertical profile also increases adjacent to expanding thermokarst margins (Kessler et al., 2012). These spatial variations in OM depositional rates and terrestrial vegetation inputs may, in turn, influence in situ associations between molecular SOM composition and CH_4 production.

2.4.3. CH_4 production associated with phenolic compounds

In previously studied natural anaerobic ecosystems, phenolic compounds negatively correlated with or inhibited C mineralization (White et al., 2002; Fenner and Freeman, 2011). Here, the abundance of compounds classified as phenols and phenolic precursors positively correlated with CH_4 production. To our knowledge, this study is the first observation of the abundance of phenol and phenolic precursor compounds being positively associated with anaerobic C mineralization in a natural aquatic ecosystem.

Under aerobic conditions (e.g. rivers, dry periods in wetlands), the presence of O_2 has been found to cause the removal of phenolic compounds via phenol oxidase activity, subsequently removing a barrier to C mineralization and causing an increase in C mineralization rates (Fenner and Freeman, 2011; Ward et al., 2013; Mann et al., 2014). While anaerobic mineralization of phenolic compounds has not been previously observed in these natural aquatic ecosystems, anaerobic microbial processing of phenols into CO_2 and CH_4 has been documented in wastewater treatment studies (e.g. Dwyer et al., 1986; Young and Rivera, 1985; Fang and Zhou, 1999). Since methanogens do not directly metabolize phenolic compounds (Wolfe, 1971), anaerobic conversion of phenolic compounds to CH_4 requires a multistep process. Phenolic

compounds are initially converted into benzoate ($C_7H_5O_2^-$), which is subsequently converted into intermediate fatty acids, then acetate ($C_2H_3O_2^-$) and hydrogen (H_2), and finally CH_4 (Fang and Zhou, 1999). This process requires syntrophic associations between phenol-oxidizing bacteria, *Methanothrix*-like bacteria, and H_2-utilizing methanogens (Dwyer et al., 1986).

Prior to anaerobic conversion of phenols into CH_4, anoxic conditions must be sustained long enough for (i) the syntrophic microbial communities to acclimate and (ii) redox conditions to allow for phenolic compounds to be reduced without competing electron acceptors such as nitrate (NO_3^-), manganese dioxide (MnO_2), iron (Fe^{3+}), sulfate (SO_4^{2-}), and CO_2 (Young and Rivera, 1985; Dwyer et al., 1986; Fang and Zhou, 1999; Pezeshki and DeLaune, 2012). We suggest the positive association between phenol abundance and methanogenesis may not have been previously observed in natural systems such as rivers (Ward et al., 2013; Mann et al., 2014) and peatlands (Fenner and Freeman, 2011) because periodic drying and exposure to O_2 may prevent these conditions from being met. In contrast, sediments in a thermokarst-lake talik are typically exposed to stable, saturated, anaerobic conditions for hundreds to thousands of years (West and Plug, 2008; Kessler et al, 2012), potentially allowing for the acclimation of necessary microbial communities and low redox potentials necessary to convert phenolic compounds to CH_4. We pose this explanation as a hypothesis, because to our knowledge no lab experiments have been conducted to prove this and we did not measure redox potential in our lake sediment core.

2.4.4. Other factors affecting CH_4 production

While our study examined how OM composition affected anaerobic CH_4 production in laboratory incubations, it is also important to consider how various additional factors affect C bioavailability in the field. Given the right physical and/or chemical conditions, labile C can be

stabilized and made unavailable for C mineralization and, conversely, recalcitrant C can be mineralized (von Lützow et al., 2006; Marschner et al., 2008; Kleber, 2010). Furthermore, a fraction of sediment OM can be associated with soil minerals, making it unavailable for decomposition, although studies of permafrost soils suggest much of its soil OM is poorly associated with minerals (Diochon et al., 2013; Höfle et al., 2013). Our characterization of bulk SOM, which we used to determine relationships with CH_4 production, did not take these processes into account.

Additional studies have suggested that microbial biomass and diversity also play an important role in determining C mineralization rate from permafrost sediment (Schimel and Chapin, 2006; Waldrop et al., 2010; Čapek et al., 2015). Carbon mineralization rates of thawed permafrost sediments correlate with microbial biomass; sediments with low microbial biomass, such as deep permafrost sediments and cryoturbated materials, have lower rates of C mineralization upon thaw (Waldrop et al., 2010; Čapek et al., 2015). Microbial community composition is also known to play an important role in determining how thawed permafrost C is processed to greenhouse gasses (McCalley et al., 2014), but the influence of permafrost microbial community composition remains poorly understood.

Temperature is also an important control over C mineralization rates. Anaerobic CH_4 production and relationships with bulk SOM characteristics in our study were determined at an incubation temperature of 3 $^{\circ}$C. This value is near the mean annual temperature of shallow sediment depths measured at Vault L. (mean annual temperate 3.57 $^{\circ}$C; Heslop et al., 2015), but observed temperatures in two profiles in the Vault L. talik ranged from -0.40 to 14.00 $^{\circ}$C during May 2013 to December 2014 (Heslop et al., 2015). The temperature deviation from the annual

mean is indicative of deviation in actual C mineralization rate throughout the talik sediments compared with C mineralization rate in our 3 °C incubations. It is also possible that the relationships between anaerobic CH_4 production and SOM characteristics change as temperature varies. For example, Dai et al. (2002) found that polysaccharides were the most bioreactive compounds in aerobic incubations at 4 °C, but at 25 °C they exhibited weaker correlations with C mineralization rate and more recalcitrant fractions of OM such as lignin were consumed. Andersen and White (2006) also observed lignin utilization at higher temperatures (20 °C) in anaerobic conditions, but did not incubate samples at other temperatures for comparison. These differences may be due to compound-specific microbial decomposition activation energies, which are available in warmer temperatures but possibly inhibiting in colder temperatures (Knorr et al., 2005; Davidson and Janssens, 2006; Conant et al., 2008). It is also possible these changes in substrate consumption at different temperatures are due to changes in microbial metabolism and active microbial communities (Allen et al., 2005; Waldrop et al., 2010; Yvon-Durocher et al., 2012). For instance, Dai et al (2002) found that phenolic compounds positively correlated with aerobic C mineralization rate at 4 °C but negatively correlated with aerobic C mineralization rate at 25 °C, possibly indicative of different microbial communities utilizing different fractions of soil OM at different temperatures. Therefore, when using OM characteristics to predict C biolability in situ, it is important to consider how these relationships change with temperature and to take the changes into account.

2.5. Conclusions

Our results suggest CH_4 production potential rates in the Vault L. sediment core are positively associated with substrate availability (C_{org}, N_{tot}) and terrestrially-derived OM

compounds (alkanes, alkenes, lignin products, and phenols and phenolic precursors). Furthermore, we used PCAs to show sediments from the lake core could be characterized into two distinct horizons (surface organic-rich sediments and mineral sediments) based on their bulk SOM characterization and CH_4 production potential rates. Compared to the mineral sediments, the organic-rich sediments horizon had: a higher level initial substrate, indicated by higher levels of C_{tot}, C_{org}, and N_{tot}; less decomposed OM, indicated by higher C_{org}:N_{tot} values and lighter $\delta^{13}C_{org}$ values; greater influence of terrestrial OM, indicated by greater proportions of alkanes, alkenes, lignin products, and phenols and phenolic precursors in the bulk SOM, and higher CH_4 production rates.

Author Contributions

J.K.H. devised the study, collected and analyzed the data, and wrote the manuscript. K.W.A. and J.K.H. conducted field work. All authors performed lab work and commented on data analysis and manuscript composition.

Acknowledgements

We thank P. Anthony, S. Billings, A. Bondurant, J. Guerard, N. Haubenstock, T. Howe, L. Oliver, K. Martinez-Cruz, A. Sepulveda-Jauregui, M. Short, A. Soria, B. Van Veldhuizen, and M. Wooller for assistance in data collection and/or analysis and S. Skidmore for granting access to Vault Lake. We also thank the anonymous reviewers for their helpful feedback on both this version and an earlier version of this manuscript. Funding for J.K.H. and K.W.A. was provided by DOE DE-SC0006920, NSF OPP-1107892, and ARC-1304823; additional funding for J.K.H. was provided under STAR Fellowship Assistance agreement no. FP-91762901-0 awarded by the US Environmental Protection Agency (EPA). The publication has not been formally reviewed by

the EPA. The views expressed in this publication are solely those of the authors and the EPA does not endorse any products or commercial services mentioned.

Figures

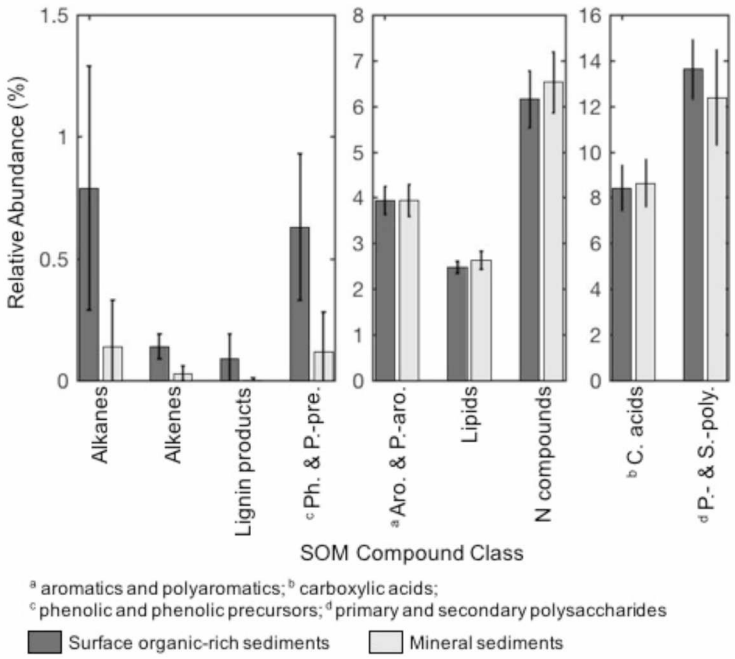

Figure 2.1. Relative abundance (mean ±SD) of each soil organic matter (SOM) compound class in total detected pyrolysis products. The organic-rich sediments contained greater proportions ($p \leq 0.05$) of alkanes, alkenes, lignin products, and phenols and phenolic precursors than the remainder of the core.

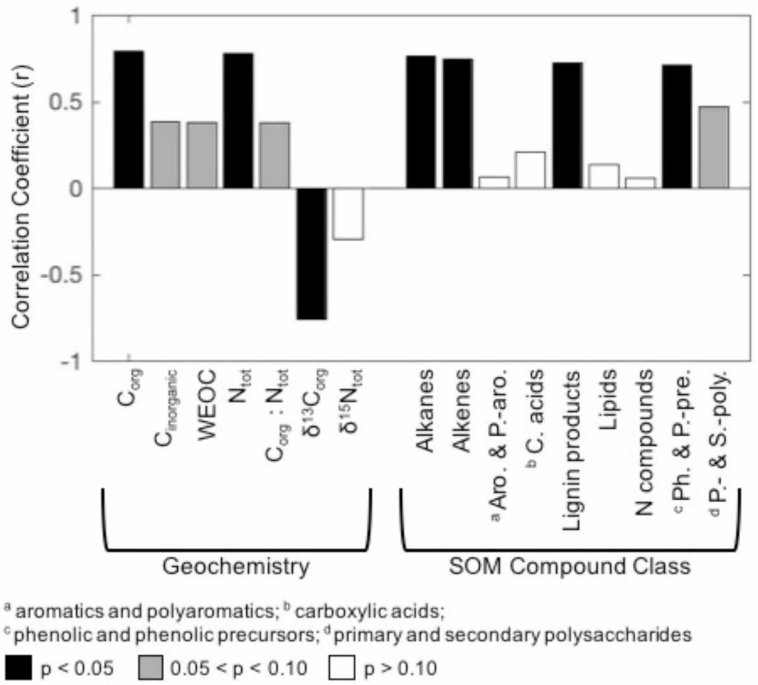

Figure 2.2. Correlation coefficients between CH_4 production potential rates at reference temperature of 3 ˚C and initial bulk SOM parameters. Correlations were determined using nonparametric Spearman's rank analyses. Statistically significant correlations ($p \leq 0.05$ and $p \leq 0.10$) are denoted by bar color.

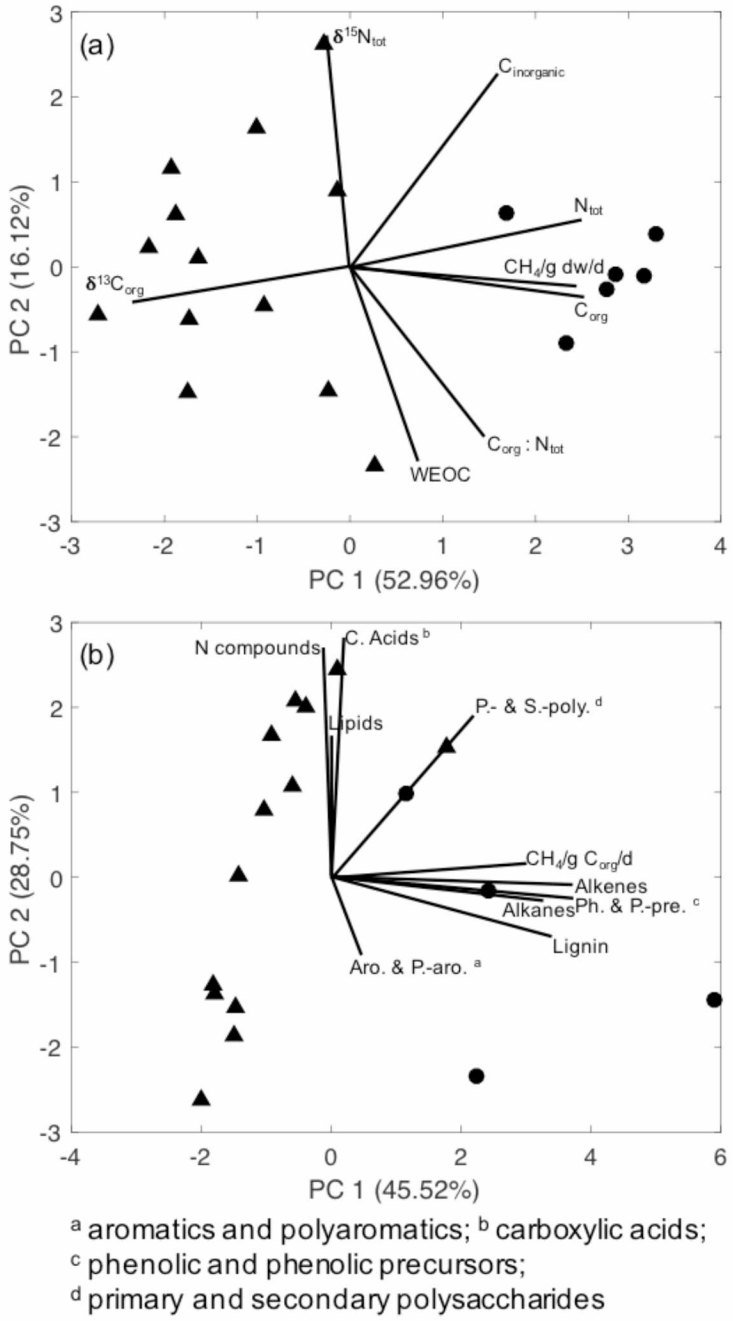

Figure 2.3. Ordination plots of the principal component analyses (PCA) results. Diagram (a) plots PCA-I results from the sediment geochemistry data; diagram (b) shows PCA-II results from the bulk SOM compound class data. In both diagrams, the first two principal components (PC) are plotted and we observe separation between the surface organic-rich sediments (circles; 0-152 cm depth in core) and the mineral sediments (triangles; 153-590 cm depth in core) Additional PCA results are presented in Table 2.A-3.

Tables

Table 2.1. The 30 most prevalent bulk SOM pyrolysis products identified using py-GC-MS, categorized into nine compound classes.

Class	Pyrolysis product
Alkanes	2-Trifloroacetoxypentadecane [a,b,c]
	3-Trifluoroacetoxytridecane [a,b,c]
	2,6,10-Trimethyltetradecane [a,b,c]
	Decane [a,b,c]
	Trifluoroactoxydodecane [a,b,c]
Alkenes	3-Undecene [*]
Aromatics and polyaromatics	2,3-Dimethylhylhydroquinone [*]
	Benzene, cyclobutyl- [d,e,f]
	Benzene, cyclopropylidenemethyl [d,e,f]
	Naphthalene [d,f]
	Toluene [a,b,c,d,f]
Carboxylic acids	1-Hydroxy-2-pentanone [a,b,c]
	2-Oxetanone, 4,4-dimethyl- [*]
	8.11-Octadecadiynois acid, methyl ester [e]
	Butanal, 3-hydroxy [*]
Lignin products	Phenol, 4-ethyl- [a,b,c]
Lipids	1-Eicosene [*]
	1-Tetradecene [a,b,c]
	3-Tetradecene, (Z)- [a,b,c]
	Heptanal [*]
N-compounds	N-ethyl-N'-nitroguanidine [*]
	Pyrrole [d,e,f]
Phenols and phenolic precursors	Phenol [a,b,c,f,g]
	Phenol, 2-methyl- [a,b,c,f]
	Phenol, 4-methyl- [a,b,c,f]
Primary and secondary polysaccharides	2-Butanmine [*]
	2-Furancarboxaldehyde, 5-methyl- [a,b,c,f]
	Acetic acid, 3,7,11,15-tetramethyl-hexadecyl ester [d,e,f]
	Benzofuran, 2,3-dihydro- [a,b,c,d]
	Furfural [a,b,c,f]

[a] White et al. (2002); [b] White et al. (2004); [c] Xu et al. (2009);
[*] classification uncertain; [d] Vancampenhout et al. (2009);
[e] Yassir and Buurman (2012); [f] Carr et al. (2013); [g] Dai et al. (2002).

References

Allen, A.P., Gillooly, J.F., Brown, J.H., 2005. Linking the global carbon cycle to individual metabolism. Functional Ecology 19, 202-213.

Andersen, S., White, D.M., 2006. Determining soil organic matter quality under anaerobic conditions in arctic and subarctic soils. Cold Regions Science and Technology 44, 149-158.

Brosius, L.S., Walter Anthony, K.M., Grosse, G., Chanton, J.P., Farquharson, L.M., Overduin, P.P., 2012. Using the deuterium isotope composition of permafrost meltwater to constrain thermokarst lake contributions to atmospheric CH_4 during the last deglaciation. Journal of Geophysical Research Biogeosciences 117, G01022.

Čapek, P., Diáková, K., Dickopp, J.-E., Bárta, J., Wild, B., Schnecker, J., Alves, R.J.E., Aiglsdorfer, S., Guggenberger, G., Gentsch, N., Hugelius, G., Lashchinsky, N., Gittel, A., Schleper, C., Mikutta, R., Palmtag, J., Shibistova, O., Urich, T., Richter, A., Šantrůčková, H., 2015. The effect of warming on the vulnerability of subducted organic carbon in arctic soils. Soil Biology and Biochemistry 90, 19-29.

Carr, A., Boom, A., Chase, B., Meadows, M., Roberts, Z., Britton, M., 2013. Biome-scale characterization and differentiation of semi-arid and arid zone soil organic matter compositions using pyrolysis–GC/MS analysis. Geoderma 200, 189-201.

Conant, R.T., Drijber, R.A., Haddix, M.L., 2008. Sensitivity of organic matter decomposition to warming varies with its quality. Global Change Biology 14, 868-877.

Corvasce, M., Zsolnay, A., D'Orazio, V., Lopez, R., Mioano, T.M., 2006. Characterization of water extractable organic matter in a deep soil profile. Chemosphere 62, 1583-1590.

Dai, X.Y., White, D.M., Ping, C.-L., 2002. Comparing bioavailability in five Arctic soils by pyrolysis-gas chromatography/mass spectrometry. Journal of Analytical and Applies Pyrolysis 62, 249-258.

Davidson, E.A., Janssens, I.A., 2006. Temperature sensitivity of soil carbon decomposition and feedbacks to climate change. Nature 440, 165-173.

Diochon, A., Gregorich, E.G., Tarnocai, C., 2013. Evaluating the quantity and biodegradability of soil organic matter in some Canadian Turbic Cryosols. Geoderma 202-203, 82-87.

Dutta, K., Schuur, E.A.G., Neff, J.C., Zimov, S.A., 2006. Potential carbon release from permafrost soils of Northeastern Siberia. Global Change Biology 12, 2336-2351.

Dwyer, D.F., Krumme, M., Boyd, S.A., Tiedje, J.M., 1986. Kinetics of phenol biodegradation by an immobilized methanogenic consortium. Applied and Environmental Microbiology 52, 345–351.

Ewing, S., O'Donnell, J., Aiken, G., Butler, K., Butman, D., Windham-Myers, L., Kanevskiy, M.Z., 2015. Long-term anoxia and release of ancient, labile carbon upon thaw of Pleistocene permafrost. Geophysical Research Letters 42, 10,730–10,738.

Fang, H., Zhou, G.M., 1999. Interactions of methanogens and denitrifiers in degradation of phenols. Journal of Environmental Engineering 125, 57-63.

Farquharson, L., Walter Anthony, K., Bigelow, N., Edwards, M., Grosse, G., 2016. Facies analysis of yedoma thermokarst lakes on the northern Seward Peninsula, Alaska. Sedimentary Geology 340, 25-37.

Fenner, N., Freeman, C., 2011. Drought-induced carbon loss in peatlands. Nature Geoscience 4, 895-900.

Grosse, G., Harden, J., Turetsky, M., 2011. Vulnerability of high-latitude soil organic carbon in North America to disturbance. Journal of Geophysical Research Biogeosciences 116, G00K06.

Grosse, G., Jones, B., Arp, C., 2013. Thermokarst lakes, drainage, and drained basins In: Shroder, J. F. (Ed.), Treatise on Geomorphology, Academic Press, San Diego, pp. 325-353.

Gundelwein, A., Müller-Lupp, T., Sommerkorn, M., Haupt, E.T.K., Pfeiffer, E.-M., Wiechmann, H., 2007. Carbon in tundra soils in the Lake Labaz region of arctic Siberia. European Journal of Soil Science 58, 1164-1174.

Harrysson Drotz, S., Sparrman, T., Nilsson, M.B., 2010. Both catabolic and anabolic heterotrophic microbial activity proceed in frozen soils. Proceedings of the National Academy of Sciences of the United States of America 107, 21046-21051.

Heslop, J.K., Walter Anthony, K.M., Sepulveda-Jauregui, A., Martinez-Cruz, K., Bondurant, A., Gross,e G., 2015. Thermokarst lake methanogenesis along a complete talik profile. Biogeosciences 12, 4317-4331.

Höfle, S., Rethemeyer, J., Mueller, C.W., John, S., 2013. Organic matter composition and stabilization in a polygonal tundra soil of the Lena Delta. Biogeosciences 10, 3145-3158.

Hugelius, G., Routh, J., Kuhry, P., Crill, P., 2012. Mapping the degree of decomposition and thaw remobilization potential of soil organic matter in discontinuous permafrost terrain. Journal of Geophysical Research Biogeosciences 117, G02030.

Jones, M., Harden, J., O'Donnell, J., Manies, K., Jorgenson, T., Treat, C., Ewing, S., 2016. Rapid carbon loss and slow recovery following permafrost thaw in boreal peatlands. Global Change Biology, doi: 10.1111/gcb.13403.

Kessler, M.A., Plug, L.J., Walter Anthony K.M., 2012. Simulating the decadal- to millennial-scale dynamics of morphology and sequestered carbon mobilization of two thermokarst lakes in NW Alaska. Journal of Geophysical Research Biogeosciences 117, G00M06.

Kleber, M., 2010. What is recalcitrant soil organic matter? Environmental Chemistry 7, 320-332.

Kling, G.W., Kipphut, G.W., 1991. Arctic lakes and streams as gas conduits to the atmosphere: implications for tundra carbon budgets. Science 251, 298-301.

Knoblauch, C., Beer, C., Sosnin, A., Wagner, D., Pfeiffer, E.-M., 2013. Predicting long-term carbon mineralization and trace gas production from thawing permafrost of Northeast Siberia. Global Change Biology 19, 1160-1172.

Knorr, W., Prentice, I.C., House, J.I., Holland, E.A., 2005. Long-term sensitivity of soil carbon turnover to warming. Nature 433, 298-301.

Lawrence, D.M., Koven, C.D., Swenson, S.C., Riley, W.J., Slater, A.G., 2015. Permafrost thaw and resulting soil moisture changes regulate projected high-latitude CO_2 and CH_4 emissions. Environmental Research Letters 10, 094011.

Lee, H., Schuur, E.A.G., Inglett, K., Lavoie, M., Chanton. J., 2012. The rate of permafrost carbon release under aerobic and anaerobic conditions and its potential effects on climate. Global Change Biology 18, 515-527.

Lorenz, K., Lal, R., Preston, C., Nierop, K., 2007. Strengthening the soil organic carbon pool by increasing contributions from recalcitrant aliphatic bio(macro)molecules. Geoderma 142, 1–10.

Mann, P., Sobczak, W., LaRue, M., Bulygina, E., Davydova, A., Vonk, J., 2014. Evidence for key enzymatic controls on metabolism of Arctic river organic matter. Global Change Biology 20, 1089–1100.

Marschner, B., Brodowski, S., Dreves, A., 2008. How relevant is recalcitrance for the stabilization of organic matter in soils? Journal of Plant Nutrition and Soil Sciences 171, 91-110.

McCalley, C.K., Woodcroft, B.J., Hodgkins, S.B., Wehr, R.A., 2014. Methane dynamics regulated by microbial community response to permafrost thaw. Nature 514, 478-481.

Meyer, H., Yoshikawa, K., Schirrmeister, L., Andreev, A., 2008. The Vault Creek Tunnel (Fairbanks Region, Alaska): A Late Quaternary Palaeoenvironmental Permafrost Record. Ninth International Conference on Permafrost, 1191–1196, University of Alaska Fairbanks, Fairbanks, Alaska, USA, 29 June to 03 July, 2008.

Meyers. P.A., 2003. Applications of organic geochemistry to paleolimnological reconstructions: a summary of examples from the Laurentian Great Lakes. Organic Geochemistry 34, 261-289.

Murton, J.B., 1996. Thermokarst-lake-basin sediments, Tuktoyaktuk Coastlands, western arctic Canada. Sedimentology 43, 737-760.

Olefeldt, D., Turetsky, M., Crill, P., McGuire, D., 2013. Environmental and physical controls on northern terrestrial methane emissions across permafrost zones. Global Change Biology 19, 589-603.

Paré, M.C., Bedard-Haughn, A., 2013. Soil organic matter quality influences mineralization and GHG emissions in cryosols: a field-based study of sub- to high Arctic. Global Change Biology 19, 1126-1140.

Pezeshki, S.R., DeLaune, R.D., 2012. Soil Oxidation-Reduction in Wetlands and Its Impact on Plant Functioning. Biology 1, 196–221.

Ping. C.-L., Jastrow, J.D., Jorgenson, M.T., Michaelson, G.J., Shur, Y.L., 2015. Permafrost soils and carbon cycling. Soil 1, 147-171.

Schädel, C., Schuur, E.A.G., Bracho, R., 2014. Circumpolar assessment of permafrost C quality and its vulnerability over time using long-term incubation data. Global Change Biology 20, 641-652.

Schimel, J.P., Chapin III, F.S., 2006. Microbial processes in the Alaskan boreal forest. In: Chapin, F. S., Oswood, M.W. (Eds.), Alaska's Changing Boreal Forest, Oxford University Press, New York, pp. 227-240.

Schirrmeister, L., Grosse, G., Wetterich, S., Overduin, P., Strauss, J., Schuur, E.A.G., 2011. Fossil organic matter characteristics in permafrost deposits of the northeast Siberian Arctic. Journal of Geophysical Research 116, G00M02.

Schirrmeister, L., Meyer, H., Andreev, A., Wetterich, S., Kienast, F., Bobrov, A., Fuchs, M., Sierralta, M., Herzschuh, U., 2016. Late Quaternary paleoenvironmental records from the Chatanika River valley near Fairbanks (Alaska). Quaternary Science Reviews, doi:10.1016/j.quascirev.2016.02.009.

Sepulveda-Jauregui, A., Walter Anthony, K.M., Martinez-Cruz, K., Greene, S., Thalasso, F., 2015. Methane and carbon dioxide emissions from 40 lakes along a north-south latitudinal transect in Alaska. Biogeosciences, 12, 3197-3223.

Shaver, G.R., Giblin, A.E., Nadelhoffer, K.J., Thieler, K.K., Downs, M.R., Laundre, J.A., Rastetter, E.B., 2006. Carbon turnover in Alaskan tundra soils: effects of organic matter quality, temperature, moisture and fertilizer. Journal of Ecology 94, 740-753.

Strauss, J., Schirrmeister, L., Grosse, G., Wetterich, S., Ulrich, M., Herzschuh, U., Hubberten, H.-W., 2013. The deep permafrost carbon pool of the Yedoma Region in Siberia and Alaska. Geophysical Research Letters 40, 6165-6170.

Treat, C.C., Wollheim, W.M., Varner, R.K., 2014. Temperature and peat type control CO_2 and CH_4 production in Alaskan permafrost peats. Global Change Biology 20, 2674-2686.

Treat, C.C., Natali, S.M., Ernakovich, J., Iversen, C.M., Lupascu, M., McGuire, A., 2015. A pan-Arctic synthesis of CH_4 and CO_2 production from anoxic soil incubations. Global Change Biology 21, 2787-2803.

Vancampenhout, K., Wouters, K., Vos, B., Buurman, P., Swennen, R., Deckers, J., 2009. Differences in chemical composition of soil organic matter in natural ecosystems from different climatic regions – A pyrolysis–GC/MS study. Soil Biology and Biochemistry 41, 568-579.

von Lützow, M., Kögel-Knabner, I., Ekschmitt, K., 2006. Stabilization of organic matter in temperate soils: mechanisms and their relevance under different soil conditions–a review. European Journal of Soil Science 57, 426-445.

Wagner, D., Gattinger, A., Embacher, A., 2007. Methanogenic activity and biomass in Holocene permafrost deposits of the Lena Delta, Siberian Arctic and its implication for the global methane budget. Global Change Biology 13, 1089-1099.

Waldrop, M.P., Wickland, K.P., White III, R., Berhe, A.A., Harden, J.W., Romanovsky, V.E., 2010. Molecular investigations into a globally important carbon pool: permafrost-protected carbon in Alaskan soils. Global Change Biology 16, 2543-2554.

Walter, K.M., Edwards, M., Grosse, G., Zimov, S.A., Chapin, F.S., 2007. Thermokarst lakes as a source of atmospheric CH_4 during the last deglaciation. Science 318, 633–636.

Walter, K.M., Chanton, J.P., Chapin, F.S., Schuur, E.A.G., Zimov, S.A., 2008. Methane production and bubble emissions from arctic lakes: Isotopic implications for source pathways and ages. Journal of Geophysical Research Biogeosciences 113, G00A08.

Walter Anthony, K., Anthony, P., Grosse, G., Chanton, J., 2012. Geologic methane seeps along boundaries of Arctic permafrost thaw and melting glaciers. Nature Geoscience 5, 419-426.

Walter Anthony, K.M., Zimov, S.A., Grosse, G., Jones, M.C., Anthony, P.M., Chapin III, F.S., 2014. A shift of thermokarst lakes from carbon sources to sinks during the Holocene epoch. Nature 511, 452-456.

Walter Anthony, K.M., Daanen, R., Anthony, P., Grosse, G., Ping, C.-L., 2016. Ancient methane emissions from permafrost thaw in arctic lakes c. 1950-2010. Nature Geosciences, in press.

Wang, J.J,, Dodla, S.K., He, Z., 2011. Application of analytical pyrolysis-mass spectrometry in characterization of animal manure. In: Z. He (Editor), Environmental Chemistry of Animal Manure. Nova Science Publishers, NY, pp. 3-24.

Ward, N.D., Keil, R.G., Medeiros, P.M., Brito, D.C., 2013. Degradation of terrestrially derived macromolecules in the Amazon River. Nature Geoscience 6, 530-533.

West, J.J., Plug, L.J., 2008. Time-dependent morphology of thaw lakes and taliks in deep and shallow ground ice. Journal of Geophysical Research 113, F01009.

White, D., Garland, D.S., Dai, X.Y., Ping, C.-L., 2002. Fingerprinting soil organic matter in the arctic to help predict CO_2 flux. Cold Regions Science and Technology 35, 185-194.

White, D.M., Garland, D.S., Ping, C.-L., Michaelson, G., 2004. Characterizing soil organic matter quality in arctic soil by cover type and depth. Cold Regions Science and Technology 38, 63-73.

Wik, M., Varner, R., Walter Anthony, K.M., MacIntyre, S., Bastviken, D., 2016. Climate-sensitive northern lakes and ponds are critical components of methane release. Nature Geoscience 9, 99-105.

Wolfe, R.S., 1971. Microbial formation of methane. Advanced Microbial Physiology, 6, 107-146.

Xu, C., Guo, L., Ping, C.-L., White, D., 2009. Chemical and isotopic characterization of size-fractionated organic matter from cryoturbated tundra soils, northern Alaska. Journal of Geophysical Research 114, G03002.

Yassir, I., Buurman, P., 2012. Soil organic matter chemistry changes upon secondary succession in Imperata Grasslands, Indonesia: A pyrolysis–GC/MS study. Geoderma 173, 94-103.

Yavitt, J.B., Williams, C., Wieder. R., 2005. Soil chemistry versus environmental controls on production of CH_4 and CO_2 in northern peatlands. European Journal of Soil Science 56, 169-178.

Young, L.Y., Rivera, M.D., 1985. Methanogenic degradation of four phenolic compounds. Water Research, 19, 1325-1332.

Yvon-Durocher, G., Caffrey, J.M., Cescatti, A., Dossena, M., 2012. Reconciling the temperature dependence of respiration across timescales and ecosystem types. Nature 487, 472-476.

Zsolnay, A., 1996. Dissolved humus in soil waters. In: Piccolo, A. (Ed.), Humic Substances in Terrestrial Ecosystem. Elsevier, Amsterdam, pp. 171–22

Appendix 2.A: Supplement of Utilizing pyrolysis GC-MS to characterize organic matter quality in relation to methane production in a thermokarst lake sediment core[2]

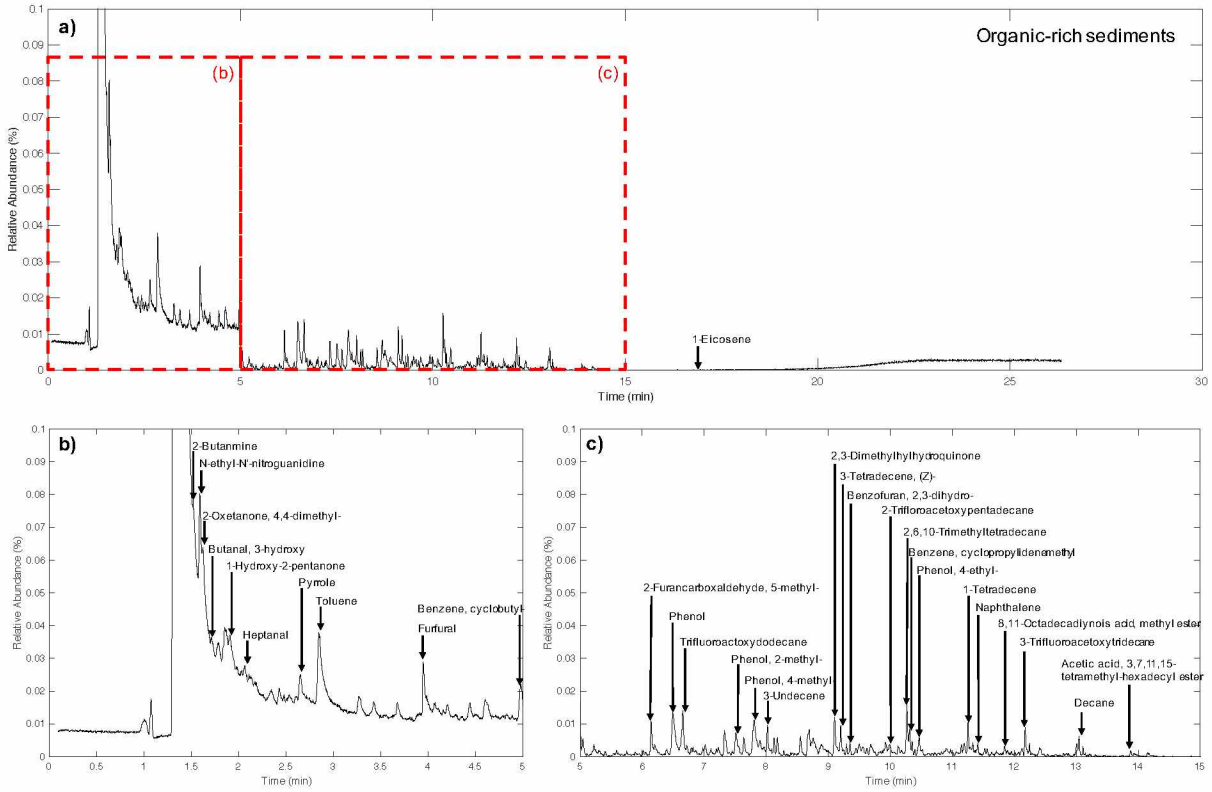

Figure 2.A-1. Representative py-GC-MS chromatogram from the Organic-rich sediments facies (a), with identified compound peak locations denoted. Chromatogram is from sample collected from 26 cm depth in the lake core. Panels b and c show the same chromatogram in greater detail from t=0-5 minutes and t=5-15 minutes, respectively. The unlabeled peak at t=1.5 minutes was identified as CO_2, a byproduct of pyrolysis, and was disregarded in our analyses.

[2] Supplement of: Heslop, J.K. Walter Anthony, K. M., Zhang, M.: Utilizing pyrolysis GC-MS to characterize organic matter quality in relation to methane production in a thermokarst lake sediment core, Organic Geochemistry, 103, 43-50, doi:10.1016/j.orggeochem.2016.10.013, 2017.

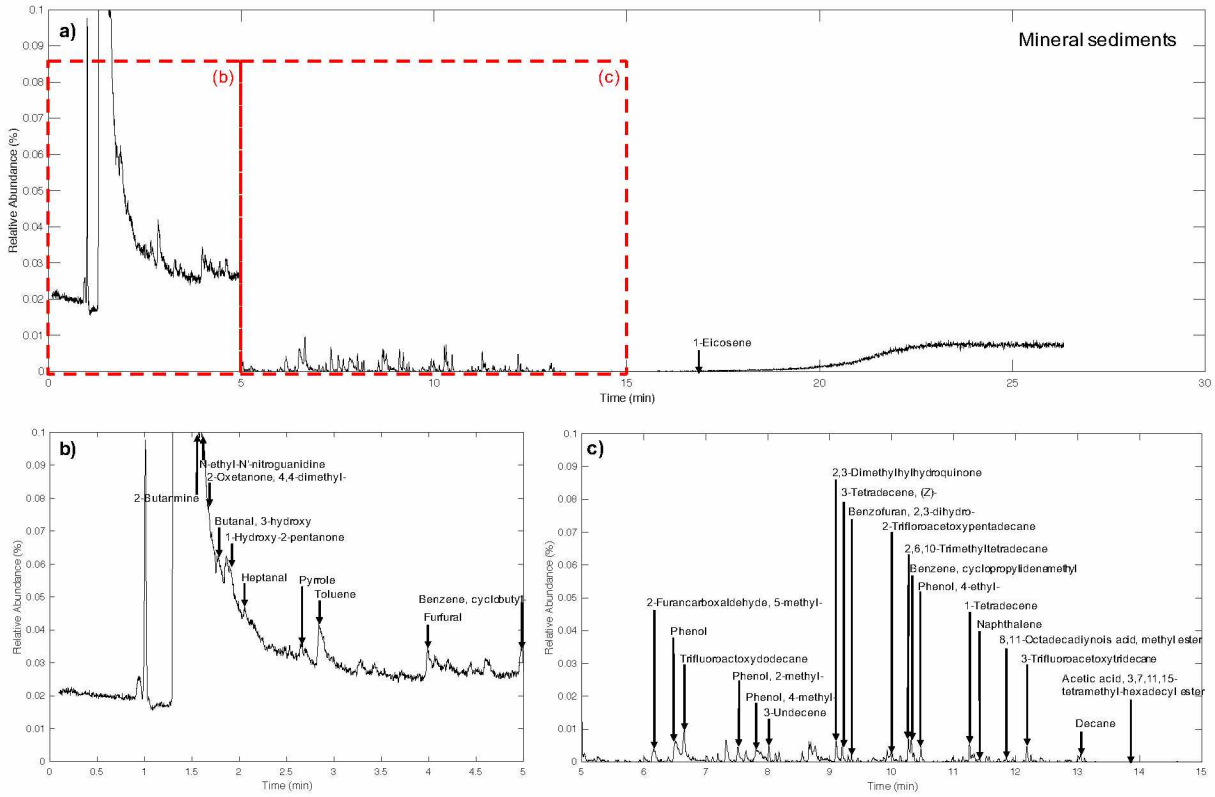

Figure 2.A-2. Representative py-GC-MS chromatogram from the Mineral sediments facies (a), with identified compound peak locations denoted. Chromatogram is from sample collected from 403 cm depth in the lake core. Panels b and c show the same chromatogram in greater detail from t=0-5 minutes and t=5-15 minutes, respectively. The unlabeled peak at t=1.5 minutes was identified as CO_2, a byproduct of pyrolysis, and was disregarded in our analyses.

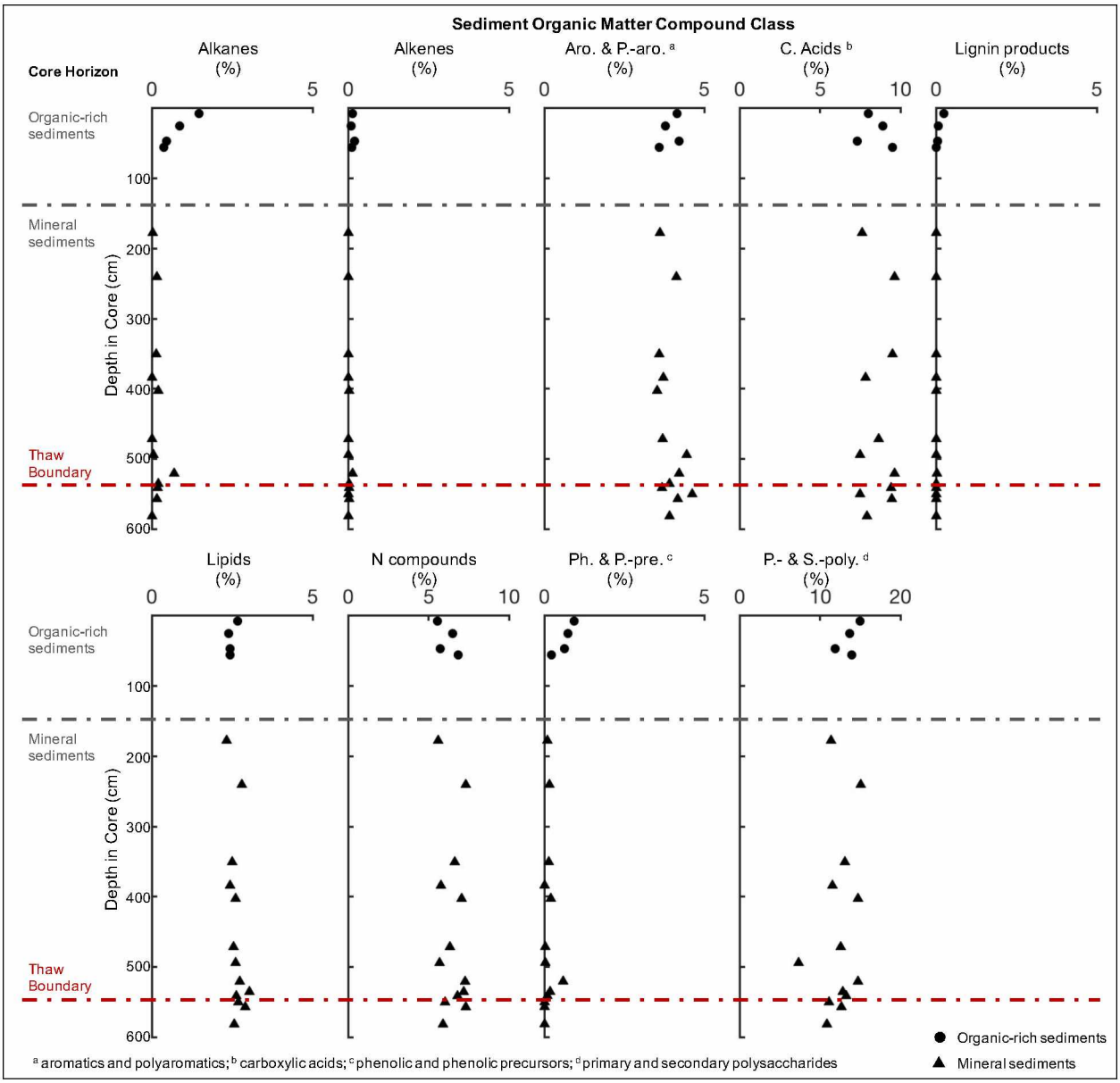

Figure 2.A-3. Proportions (%) of the 30 most prevalent compounds identified using pyrolysis-gas chromatography-mass spectrometry (py-GC-MS) analyses, categorized into nine SOM compound classes, relative to total pyrolysis products from the bulk SOM detected in the py-GC-MS analyses. Data are initial SOM composition measured on sediment samples from 18 depths in the Vault Lake sediment core. Note the different X-axis scale for carboxylic acids, N compounds, and primary and secondary polysaccharides.

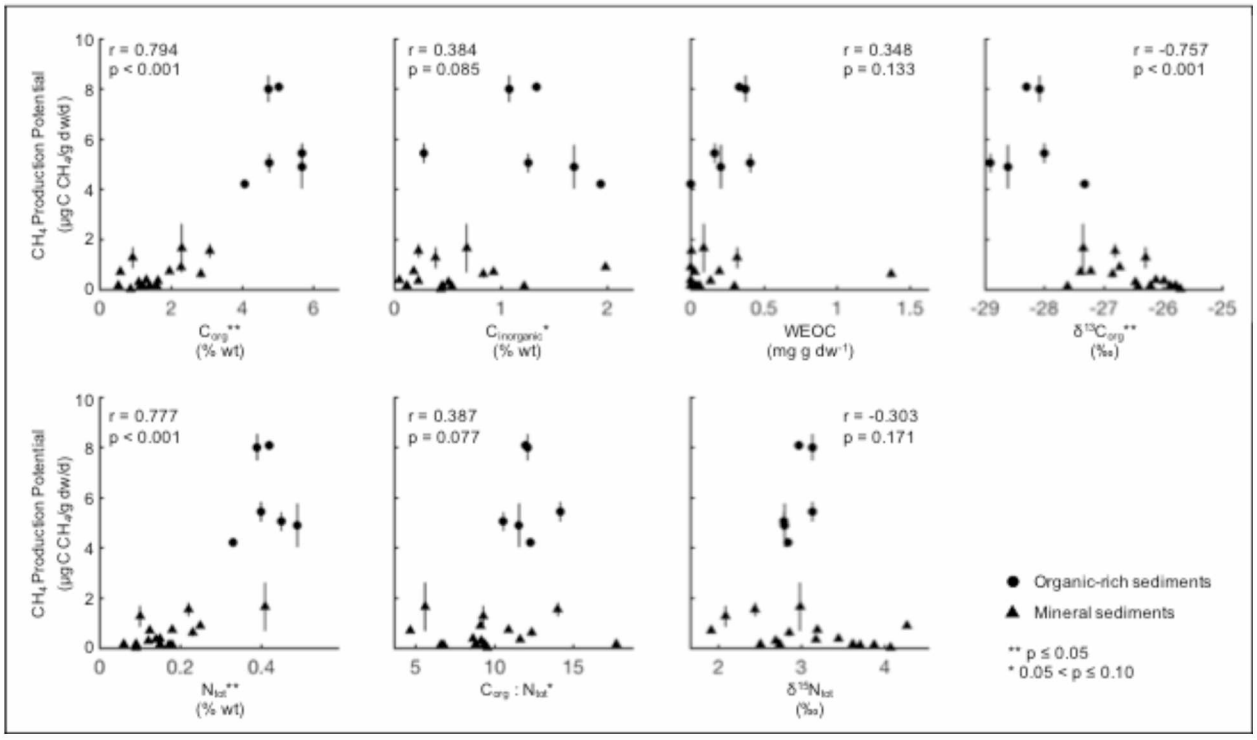

Figure 2.A-4. Relationships between anaerobic CH_4 production potentials at 3 ˚C and initial sediment core geochemical properties. Correlations were determined using nonparametric Spearman's rank testing. We observed statistically significant correlations between CH_4 production potentials and initial sediment: C_{org}, $C_{inorganic}$, $\delta^{13}C_{org}$, N_{tot}, and C_{org}:N_{tot}.

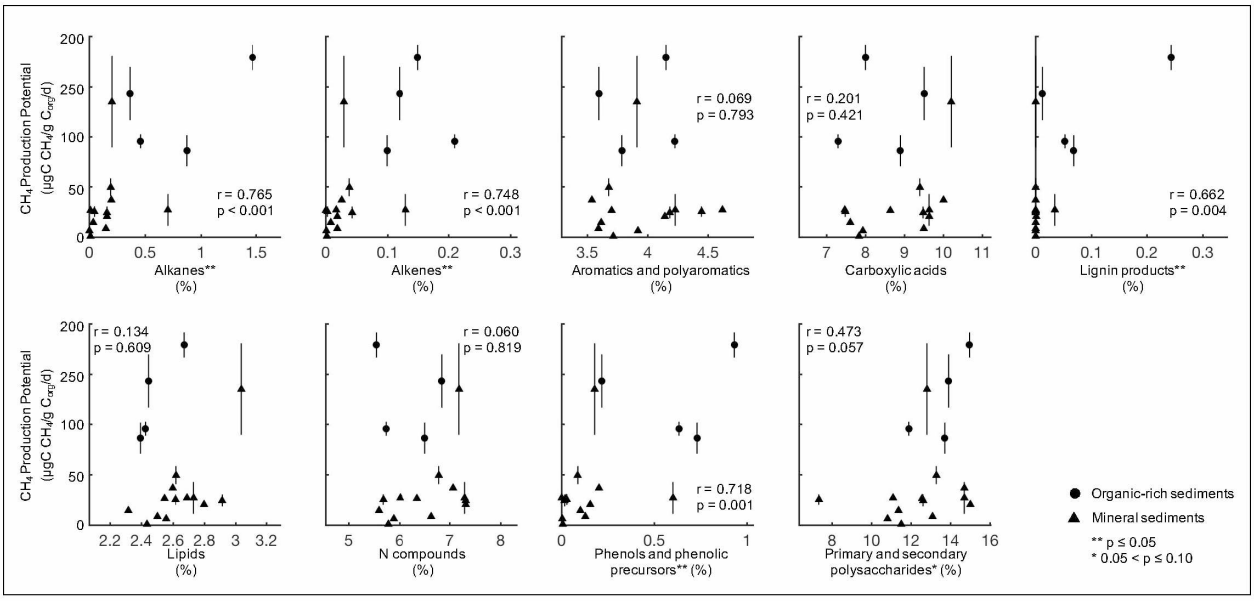

Figure 2.A-5. Relationships between anaerobic CH_4 production potentials at 3 ˚C and initial sediment core bulk sediment organic matter (bulk SOM) composition as determined via py-GC-MS analyses. Correlations were determined using nonparametric Spearman's rank testing. We observed statistically significant correlations between CH_4 production potentials and initial bulk SOM: alkanes, alkenes, lignin products, phenols and phenolic precursors, and primary and secondary polysaccharides.

Table 2.A-1. Mean (standard deviation) values of measured parameters in the Vault Lake sediment core.

Measured parameter	Organic-rich sediments (0-152 cm depth)	Mineral sediments (153-590 cm depth)
CH_4 Production Potential Rates (3°C)		
µgC CH_4/g dw/d [γ]	5.95 (1.67) [a]	0.56 (0.53) [b]
µgC CH_4/g C_{org}/d [γ]	125.89 (36.19) [a]	30.03 (31.92) [b]
Sediment Geochemistry		
C_{org} (% wt) [γ]	4.99 (0.62) [a]	1.55 (0.76) [b]
$C_{inorganic}$ (% wt) [γ]	1.27 (0.57) [a]	0.59 (0.51) [b]
WEOC (mg/g dw)	0.25 (0.15) [a]	0.19 (0.36) [a]
WEOC : C_{org} (%)	4.95 (3.29) [a]	10.82 (14.77) [a]
N_{tot} (% wt) [γ]	0.41 (0.05) [a]	0.17 (0.08) [b]
C_{org} : N_{tot} [γ]	12.1 (1.2) [a]	9.7 (3.3) [b]
$\delta^{13}C_{org}$ (‰) [γ]	-28.2 (0.6) [a]	-26.6 (0.6) [b]
$\delta^{15}N_{tot}$ (‰) [γ]	2.9 (0.2) [a]	3.1 (0.7) [a]
Bulk Sediment Organic Matter (bulk SOM) Compound Classes*		
Alkanes (%)	0.79 (0.50) [a]	0.14 (0.19) [b]
Alkenes (%)	0.14 (0.05) [a]	0.03 (0.03) [b]
Aromatics and polyaromatics (%)	3.94 (0.30) [a]	3.95 (0.35) [a]
Carboxylic acids (%)	8.43 (0.97) [a]	8.84 (1.03) [a]
Lignin products (%)	0.09 (0.10) [a]	0.00 (0.01) [b]
Lipids (%)	2.48 (0.13) [a]	2.64 (0.19) [a]
N compounds (%)	6.16 (0.62) [a]	6.53 (0.67) [a]
Phenols and phenolic precursors (%)	0.63 (0.30) [a]	0.12 (0.16) [b]
Primary and secondary polysaccharides (%)	13.64 (1.28) [a]	12.40 (2.06) [a]

[γ] Parameters previously measured by Heslop et al. (2015)

[a,b] Different letters indicate significant differences ($p \leq 0.05$) between mean values in horizons (Wilcoxon rank sum tests).

* Data show relative abundances of pyrolysis products from the bulk SOM

Table 2.A-2. Correlation coefficients between all measured parameters in our study. Correlations were determined using pairwise nonparametric Spearman's rank analyses. We note statistically significant correlations at the $p \leq 0.05$ (bold) and $0.05 < p \leq 0.10$ (italicized) levels.

	Depth	µgC CH_4/g dw/d	µgC CH_4/g C_{org}/d	C_{org}	$C_{inorganic}$	WEOC	WEOC : C_{org}	N_{tot}	C_{org} : N_{tot}	$\delta^{13}C_{org}$
Depth	--	**-0.50**	**-0.48**	**-0.66**	-0.31	-0.15	0.28	**-0.50**	**-0.50**	0.30
µgC CH_4/g dw/d		--	**0.93**	**0.79**	*0.38*	*0.38*	-0.05	**0.78**	*0.38*	**-0.76**
µgC CH_4/g C_{org}/d			--	**0.66**	0.33	*0.40*	0.05	**0.64**	0.33	**-0.68**
C_{org}				--	*0.41*	0.37	-0.18	**0.89**	0.64	**-0.68**
$C_{inorganic}$					--	0.24	-0.06	**0.59**	0.02	**-0.63**
WEOC						--	**0.81**	*0.38*	0.23	**-0.54**
WEOC : C_{org}								-0.12	-0.09	-0.16
N_{tot}								--	0.25	**-0.84**
C_{org} : N_{tot}									--	-0.10
$\delta^{13}C_{org}$										--
$\delta^{15}N_{tot}$										
Alkanes										
Alkenes										
Aro. & P.-aro [a]										
Carboxylic acids										
Lignin products										
Lipids										
N Compounds										
Ph. & P.-pre. [b]										
P.- & S.-poly. [c]										

Spearman's rank correlation coefficient significance: **$p \leq 0.05$** *$0.05 < p \leq 0.10$* $p > 0.10$

[a] aromatics and polyaromatics; [b] phenolic and phenolic precursors; [c] primary and secondary polysaccharides

Table 2.A-2 continued. Correlation coefficients between all measured parameters in our study. Correlations were determined using pairwise nonparametric Spearman's rank analyses. We note statistically significant correlations at the $p \leq 0.05$ (bold) and $0.05 < p \leq 0.10$ (italicized) levels.

	$\delta^{15}N_{tot}$	Alkanes	Alkenes	Aro. & P.-aro [a]	Carboxylic acids	Lignin products	Lipids	N Compounds	Ph. & P.-pre. [b]	P.- & S.-poly. [c]
Depth	-0.11	**-0.55**	-0.41	0.26	0.08	**-0.62**	**0.56**	0.33	**-0.73**	*-0.42*
µgC CH_4/g dw/d	-0.29	**0.88**	**0.90**	0.13	0.24	**0.84**	0.11	0.18	**0.79**	**0.55**
µgC CH_4/g C_{org}/d	-0.47	**0.76**	**0.75**	0.06	0.21	**0.72**	0.14	0.06	**0.71**	*0.47*
C_{org}	0.01	**0.78**	**0.86**	0.01	0.07	**0.80**	-0.17	0.08	**0.71**	**0.50**
$C_{inorganic}$	0.03	0.35	*0.44*	0.07	0.00	0.41	-0.13	0.01	0.26	0.20
WEOC	-0.15	0.42	*0.46*	0.13	0.20	0.41	0.26	0.19	0.27	0.26
WEOC : C_{org}	-0.15	-0.01	-0.04	-0.06	0.40	-0.02	**0.53**	0.38	-0.14	0.19
N_{tot}	0.11	**0.78**	**0.83**	0.13	0.14	**0.75**	-0.01	0.12	**0.66**	**0.50**
C_{org} : N_{tot}	-0.21	0.29	0.39	-0.33	-0.04	0.35	-0.32	0.01	0.27	0.22
$\delta^{13}C_{org}$	0.13	**-0.68**	**-0.75**	-0.15	-0.09	**-0.69**	0.00	-0.02	**-0.60**	-0.39
$\delta^{15}N_{tot}$	--	-0.18	-0.23	-0.02	-0.07	-0.19	-0.23	-0.05	-0.13	-0.10
Alkanes		--	**0.90**	0.00	0.40	**0.96**	0.06	0.21	**0.94**	**0.72**
Alkenes			--	0.15	0.24	**0.89**	0.12	0.21	**0.79**	**0.58**
Aro. & P.-aro [a]				--	-0.41	0.00	*0.46*	-0.12	-0.11	-0.28
Carboxylic acids					--	0.38	*0.46*	**0.84**	0.33	**0.73**
Lignin products						--	0.03	0.22	**0.95**	**0.76**
Lipids							--	**0.56**	-0.13	0.26
N Compounds								--	0.07	**0.54**
Ph. & P.-pre. [b]									--	**0.70**
P.- & S.-poly. [c]										--

Spearman's rank correlation coefficient significance: **$p \leq 0.05$** *$0.05 < p \leq 0.10$* $p > 0.10$

[a] aromatics and polyaromatics; [b] phenolic and phenolic precursors; [c] primary and secondary polysaccharides

Table 2.A-3. Correlations between measured parameters for the first three principal component (PC) axes for bulk SOM data collected from the Vault Lake sediment core. Prior to the principal component analyses, standardized data were divided into two groups: PCA-I sediment geochemistry (n = 19 depths in core) and PCA-II bulk SOM compound classes (n = 18 depths in core). The first three PCs explained approximately 81% and 88% of the total variance in PCA-I and PCA-II, respectively. Variables are listed in order of their contribution to the first PC.

	PCA-I: Sediment Geochemistry		
	PC 1	PC 2	PC 3
C_{org}	0.48	-0.08	-0.10
µgC CH_4/g dw/d	0.46	-0.05	-0.23
N_{tot}	0.45	0.12	-0.05
$C_{inorganic}$	0.31	0.51	0.33
C_{org} : N_{tot}	0.24	-0.39	-0.07
WEOC	0.13	-0.49	0.83
$\delta^{15}N_{tot}$	-0.04	0.57	0.35
$\delta^{13}C_{org}$	-0.42	-0.08	0.01
% Variance Explained	53	16	12
	PCA-II: Bulk Sediment Organic Matter (bulk SOM) Compound Classes		
	PC 1	PC 2	PC 3
Alkanes	0.47	-0.01	0.00
Ph. & P.-pre. [a]	0.46	-0.05	-0.03
Lignin products	0.43	-0.15	0.05
Alkenes	0.41	-0.06	0.01
µgC CH_4/g C_{org}/d	0.38	0.04	0.03
P.- & S.-poly. [b]	0.27	0.40	-0.21
Aro. & P.-aro [c]	0.05	-0.19	0.73
Carboxylic acids	0.03	0.58	-0.07
Lipids	0.00	0.34	0.63
N Compounds	-0.02	0.57	0.10
% Variance Explained	44	29	15

[a] phenolic and phenolic precursors; [b] primary and secondary polysaccharides; [c] aromatics and polyaromatics

Chapter 3: Century-scale time since permafrost thaw affects temperature sensitivity of methane production in thermokarst-lake sediments[1]

Abstract

Warming and thawing of permafrost soils removes a major barrier to soil organic carbon (SOC) mineralization, leading to microbial degradation of previously frozen SOC into the greenhouse gases carbon dioxide (CO_2) and methane (CH_4). Emission of these gases constitutes a positive feedback to climate warming. Two major uncertainties in estimating the strength of this permafrost C feedback are: (i) how mineralization rates of permafrost SOC thawed in saturated anaerobic conditions responds to changes in temperature and (ii) how temperature sensitivities of anaerobic SOC mineralization change over time since thaw. We anaerobically incubated sediments from a thermokarst-lake sediment core at four temperatures (0 °C, 3 °C, 10 °C, and 25 °C), largely bracketing those observed in the lake's thaw bulb (talik). We calculated temperature sensitivities (Q_{10}) of methanogenesis at different depths within the talik and at the different temperature intervals. Our results suggest that century-scale time since permafrost thaw affected temperature sensitivities of CH_4 production in taberite sediments, relatively homogenous sediments of Yedoma origin that thawed *in situ* beneath the lake. Freshly-thawed taberite sediments near the thaw boundary at the base of the talik were most sensitive to warming at the lower incubation temperatures (0 °C to 3 °C), while the overlying taberite sediments which had been thawed for longer periods of time (up to 400 yr based on radiocarbon dating) did not

---

[1] Heslop, J.K. Walter Anthony, K. M., Winkel, M., Grosse, G., Knoblauch, C., Liebner, S..: Century-scale time since permafrost thaw affects temperature sensitivity of methane production in thermokarst-lake sediments. In prep. for submission to Global Change Biology.

experience statistically significant ($p < 0.05$) increases in CH_4 production until higher incubation temperatures (10 °C to 25 °C). We propose these observed differences in temperature sensitivities are due to differences in SOM quality and/or functional microbial community composition, and suggest further research is necessary to better constrain the roles of these factors in determining temperature controls on anaerobic C mineralization.

3.1. Introduction

Permafrost contains an estimated 1330-1580 Pg of soil organic carbon (SOC), representing about one-third of total global SOC stocks (Hugelius et al., 2014; Schuur et al., 2015). Defined as ground at or below 0 °C for at least two consecutive years, permafrost covers about 24% of the Northern Hemisphere land surface (Schuur et al., 2015). Air temperature records suggest high latitudes (>60 °N) are warming twice as fast as the remainder of the Northern Hemisphere (Bekryaev et al., 2010; Schuur et al., 2015), and amplified Arctic warming is projected to continue into the coming century (IPCC, 2013). In this warming climate, warming and thawing of permafrost soils removes a major barrier to SOC mineralization, leading to the mobilization and microbial degradation of previously frozen, inactive permafrost SOC (Davidson and Janssens, 2006; Olefeldt et al., 2013; Schuur et al., 2015; Yang et al., 2016). Microbial degradation converts permafrost SOC into the greenhouse gases carbon dioxide (CO_2) and methane (CH_4), which, when released to the atmosphere, cause a positive feedback to climate warming (Schuur et al., 2015; Walter et al., 2006).

Permafrost thaw also changes local and regional hydrology, leading to fragmented wetting and drying of the landscape (Jorgenson et al., 2013). Landscape wetting and drying play an important role in controlling whether thawed SOC will be mineralized aerobically as CO_2 or anaerobically as CO_2 and CH_4. While it has been suggested that permafrost SOC mineralization

in aerobic conditions releases an average of 3.4 times more C than SOC mineralization in anaerobic conditions (Schädel et al., 2016), CH_4 production rates in anaerobic systems are more sensitive to variability in soil temperature than C mineralization in drier, aerobic ecosystems (Schädel et al., 2016; Olefeldt et al., 2013). In permafrost soils, previously observed anaerobic C mineralization Q_{10} values ranged from 1.2 to 22.0 (Capek et al., 2015; Chowdhury et al., 2015; Treat et al., 2015; Schädel et al., 2016), while in aerobic conditions, Q_{10} values ranged from 1.6 to 9.4 (Bracho et al., 2016; Capek et al., 2015; Mikan et al., 2002; Schädel et al., 2016). Given that CH_4 has a 34 times higher global warming potential than CO_2 over a century time scale (Myhre et al., 2013), and that northern soils are expected to warm during the next several decades and beyond (Guo and Wang, 2016), it is important to increase our understanding of CH_4 production response to temperature increases to fully estimate the potential strength of the permafrost C feedback.

SOC mobilization and mineralization from thawing permafrost are expected to be long-term, accelerating events, with over 60% of total C emissions expected to occur after 2100 (Grosse et al., 2016). Therefore, in addition to requiring a better understanding of how CH_4 production rates change with temperature, modeling the potential permafrost C feedback will require better estimates of how temperature sensitivities change over century-scale time since permafrost thaw. It is difficult to obtain this information from incubations and field warming experiments, which commonly capture temperature responses of labile SOC fractions with fast (days to years) turnover times (Bracho et al., 2016; Conant et al., 2011; Knoblauch et al., 2013). In permafrost soils, the size of this fast C pool is small (< 5%) and the majority (> 95%) of permafrost SOC has turnover times of decades to centuries (Schädel et al., 2014). Temperature sensitivities of these slower C pools are largely unknown (Conant et al., 2011).

Natural chronosequences where SOC has incubated *in situ* provide unique opportunities to examine how temperature sensitivity of SOC mineralization changes over time. Due to their formation and thaw histories, thermokarst-lake thaw bulbs (taliks) can provide a unique natural laboratory in which permafrost SOC thawed and incubated *in situ* under saturated anaerobic conditions for hundreds to thousands of years (West and Plug, 2008; Kessler et al, 2012). Thermokarst lakes are known to have high rates of CH_4 emission (Sepulveda-Jauregui et al., 2015; Walter et al., 2007), with the C primarily originating from permafrost SOC thawing both beneath and surrounding the lake (Brosius et al., 2012; Kling and Kipphut, 1991; Lenz et al., 2016; Walter Anthony and Anthony, 2013; Walter et al., 2008; Zimov et al., 1997) and the decomposition of deposited contemporary organic matter (OM) in the lakes (Walter Anthony et al., 2014). Once formed, thermokarst lakes strongly alter the local ground thermal balance by transferring heat from the water body to the underlying ground more effectively than other land cover types (Burn, 2005; Grosse et al., 2013; Jorgenson et al., 2013), which can subsequently trigger downward permafrost thaw and talik formation beneath the lake (Plug and West, 2009). After accounting for potential initial SOC heterogeneity in the vertical profile, the thawed permafrost soils beneath a thermokarst lake represent a natural chronosequence of time since thaw, with sediments closest to the thaw boundary at the base of the talik being the most recently thawed.

In this study, we anaerobically incubated sediments from a thermokarst lake core with the objective of examining temperature sensitivity of methanogenesis. Our work involved measuring temperature along two vertical profiles in the thermokarst lake talik, incubating sediments at four temperatures bracketing those found within the talik, and calculating temperature sensitivities (Q_{10}) at different depths within the talik and at the different temperature intervals. We show how

temperature sensitivity of CH_4 production changes with depth, as a proxy for increasing century-scale time since thaw in the taberite sequence, and with different depositional environments comparing the taberite sequence to overlying younger sediments.

3.2. Materials and methods

3.2.1. Vault Lake sediment core description

During March 2013, a 590-cm long sediment core was collected from the center of Vault Lake, Alaska, USA (65.0293 °N, 147.6987 °W) using methods described in detail in Heslop et al. (2015). Based on ^{14}C-dating of macrofossils picked from the sediment core, Vault Lake was estimated to have formed ca. 400 cal. years BP (Heslop et al., 2015). Heslop et al. (2015) classified and described in detail the lake profile subdivided into five sediment facies: (1) surface organic-rich mud, (2) lacustrine silt, (3) taberite, (4) recently-thawed taberite, and (5) frozen transitional permafrost. Briefly, the surface organic-rich mud facies (0-152 cm) represents deposited organic-rich sediments, which were exposed to the lake water column and settled at the bottom of the lake. The lacustrine silt (153-330 cm) facies represents material that sloughed off the thermokarst lake margin and was exposed to the lake water column during erosion and re-deposition. The lowest three facies comprise the Taberite sequence (T-I, T-II, T-III), consisting of Pleistocene-aged yedoma permafrost that either thawed in situ or is presently thawing and transitioning to taberite beneath the lake. The taberite facies (T-I, 331-550 cm) represents yedoma sediments, which thawed *in situ* beneath the lake during the past ~400 years since lake formation; the bottom section of the taberite (508-550 cm), which we estimate thawed within the past ~50 years based on talik growth functions of Kessler et al. (2012), was designated as the recently-thawed taberite facies (T-II). The frozen portion of the core beneath the talik that is currently thawing and transitioning to taberite was designated as the transitional permafrost

facies (T-III, 551-590 cm). Multivariate statistical analyses conducted by Heslop et al. (2017) on geochemical and sediment OM molecular composition data from the core indicate sediments from the surface organic-rich mud facies contained different SOM characteristic than the bottom four facies (lacustrine silt, taberite, recently-thawed taberite, frozen transitional permafrost), which contained statistically homogenous SOM. Due to the statistical homogeneity of their SOM (Heslop et al., 2017) and their history of thawing *in situ* beneath Vault Lake, we interpret the three lower facies (Taberite sequence T-I, T-II, and T-III) to represent a 400-year chronosequence of time since permafrost thaw.

3.2.2. Vertical temperature profile measurements

Temperature below the sediment-water interface at Vault Lake was measured in galvanized steel tubes placed in two boreholes [Borehole (BH) 10 and BH13] described in Heslop et al. (2015). At BH10, located 6.1 m from the actively expanding thermokarst margin in 2013, the talik thickness was 8.6 m and the lake water column was 1.4 m depth (Fig. 3.1). At BH13, located in the center of the lake ca. 40 m offshore from the expanding margins, the lake water column was deeper (4.0 m) and the talik was thinner (5.7 m). We installed temperature sensors (Onset TMCx-HD, accuracy ± 0.21˚C) at both sites at four depths below the sediment-water interface within the talik (BH10: 0.5 m, 1.0 m, 6.2 m, and 8.85 m; BH13: 0.5 m, 1.0 m, 5.7 m, and 6.2 m) and recorded temperatures hourly from May 2013-February 2016.

3.2.3. Anaerobic sediment incubations

We prepared and incubated sediment slurries [mean ±SD 262 ±121 g dry weight (dw) sediment L^{-1}; range 124-455 g dw sediment L^{-1}] from five depths in the core, representing one depth from each of the five facies described above (Table 3.1), using methods previously described in Heslop et al. (2015). For each core depth, we incubated sediment slurries in

triplicate at four temperatures (0 °C, 3 °C, 10 °C, and 25 °C) bracketing those found within thermokarst-lake environments and measured headspace CH_4 concentration in monthly timesteps using gas chromatography (Shimadzu GC-2014) until linear CH_4 production rates were achieved in all bottles, a period totaling 175 days. CH_4 production in each incubation bottle was quantified using two methods: CH_4 production potential rates and cumulative C-CH_4 production. CH_4 production potential rates were calculated as the linear slope of CH_4 concentration in the incubation vials over time and were normalized two ways: (i) by the mass of dry sediment in each bottle (μg C-CH_4 g dw^{-1} d^{-1}) and (ii) by the mass of SOC in each bottle (μg C-CH_4 g SOC^{-1} d^{-1}). Cumulative C-CH_4 production (mg C-CH_4 g $SOC_{initial}^{-1}$) was calculated as the total mass of C-CH_4 produced in each incubation vial during the 175-d incubation period. All CH_4 production values are presented as the mean ± standard deviation (SD) of the triplicate vials at each depth and incubation temperature.

3.2.4. Temperature sensitivity calculations

We utilized Q_{10} values as a measure of the temperature sensitivity of CH_4 production in our incubations. The Q_{10} value in our study is defined as the factor by which CH_4 production potential rates change with a 10 °C rise in temperature. In previous incubation experiments, dissimilarities in functional microbial diversities with respect to the temperature sensitivities of C mineralization increase as the incubation progresses (Bracho et al. 2016). To minimize this effect, we calculated Q_{10} values for each facies at each incubation temperature interval in our study using CH_4 production potential rates at the first time point with detectable CH_4 production in each incubation vial ($Q_{10\text{-}I}$). For each incubation vial, CH_4 production rates (R) were calculated as the mass of C-CH_4 produced in the incubation vial divided by the elapsed time (d)

since the previous headspace measurement. We then used the calculated CH_4 production rates to calculate $Q_{10\text{-}I}$ values (Equation 1):

$$Q_{10-I} = \left(\frac{R_c}{R_w}\right)^{\frac{10}{(T_w - T_c)}} \quad \text{Eq. 1}$$

where R_c is the initial C-CH_4 production rate at colder temperature T_c, and R_w is the initial C-CH_4 production rate at warmer temperature T_w (Liang et al., 2015). $Q_{10\text{-}I}$ values were calculated between T_1:T_2, T_1:T_3, T_2:T_3, and T_3:T_4.

3.2.5. Statistics

All statistical analyses were conducted using MATLAB R2016a software. Differences in CH_4 production and Q_{10} values were tested for statistical significance using two-sample t-tests. We considered differences between facies and incubation temperatures statistically significant when $p \leq 0.05$.

3.3. Results

3.3.1. Temperatures in the Vault Lake talik

In the profile adjacent to the thermokarst margin (BH10), with the exception of a data gap between 25 July 2014 and 11 November 2014, hourly temperatures recorded from May 2013 to February 2016 ranged from -0.40 to 14.00 ˚C (annual mean ± SD 2.35 ± 3.33 ˚C; Fig. 3.1). In the center of Vault Lake (BH13), observed temperatures in the vertical profile ranged from -0.40 to 4.51 ˚C (annual mean ± SD 1.08 ± 1.38 ˚C; Fig. 3.1). In both profiles, the shallow sediment depths (50-100 cm below the sediment-water interface) were warmer (0.14 to 14.00 ˚C) and showed clear seasonal variations compared to the deepest (5.70 m and 8.85 m) sediments near the thaw boundary (-0.40 to 2.37 ˚C), which showed less seasonal variation. Mean annual temperature was 3.26 ± 2.94 ˚C in the shallower sediments and 0.18 ± 0.59 ˚C near the thaw

boundary. In the temperature profile adjacent to the thermokarst margin (BH10), temperatures at the thaw boundary (8.85 m depth) increased from -0.10 °C during May 2013 to 0.16 °C during February 2016.

3.3.2. CH_4 production

Methane production increased with increasing incubation temperatures (Table 3.2; Fig. 3.2) in all samples except the T-III frozen transitional permafrost samples, in which CH_4 production was highest at incubation temperature T_2 (3 °C). Among the five facies, the surface organic-rich mud had the greatest CH_4 production rates per g dw sediment (5.04-262.4 μg C-CH_4 g dw^{-1} d^{-1}) at all four incubation temperatures. The surface organic-rich mud also produced the most CH_4 per g SOC at incubation temperatures T_1-T_3 (0-10 °C; 135.1-2,263 μg C-CH_4 g SOC^{-1} d^{-1}); however, CH_4 production per g SOC was higher in the T-I taberite facies at incubation temperature T_4 (25 °C; 14,464 ±376.0 μg C-CH_4 g SOC^{-1} d^{-1}). The T-II recently-thawed taberite (0.06-4.78 μg C-CH_4 g dw^{-1} d^{-1}; 5.29-434.9 μg C-CH_4 g SOC^{-1} d^{-1}) and T-III frozen transitional permafrost (0.00-0.13 μg C-CH_4 g dw^{-1} d^{-1}; 0.04-6.16 μg C-CH_4 g SOC^{-1} d^{-1}) had the lowest CH_4 production rates among the facies. Full CH_4 production results at all four incubation temperatures are presented in Table 3.2.

3.3.3. Q_{10} values

$Q_{10\text{-}I}$ values in our study ranged from 0.00 to $1x10^8$ (median ± SD 3.67 $\pm 2.4x10^7$). The T-II recently-thawed taberite facies had the highest mean $Q_{10\text{-}I}$ values among the facies (mean± SD $2.7x10^7$ $\pm 5.4x10^7$), followed by the T-III frozen transitional permafrost ($5.1x10^4$ $\pm 1.0x10^5$), lacustrine silt ($4.9x10^3$ $\pm 9.7x10^3$), T-I taberite ($3.7x10^3$ $\pm 7.3x10^3$), and the organic-rich mud (700 $\pm 1.4x10^3$) facies. Full Q_{10} value results are presented in Table 3.3.

3.4. Discussion

3.4.1. Understanding anomalously high Q_{10} values

We acknowledge that some of the Q_{10} values observed in our study are significantly higher than previously reported Q_{10} values for both permafrost soils and other anaerobic systems. A recent synthesis of 21 permafrost soil incubation studies found that a 10 °C increase in temperature (5 °C to 15 °C) resulted in net C release increasing by a factor of 2.0 (95% CI 1.8-2.2; Schädel et al., 2016). Here, we report Q_{10} values of CH_4 production for T_2:T_3 (3 °C to 10 °C) ranging from 0.02 to 5 $x10^3$. It is important to note that we did not measure anaerobic C-CO_2 production in this study, therefore our Q_{10} values reflect only changes in C-CH_4 production and not changes in net anaerobic C release. To our knowledge, separate Q_{10} values for CH_4 production have not been previously reported in permafrost literature. The high Q_{10} values of CH_4 production observed in this study are suggestive that the changes are not solely due to biological temperature responses of methanogens, and additional factors and interactions are contributing to the large Q_{10} values.

Both the chemical composition of SOM (SOC quality) and the microbial community composition are known to influence C mineralization rates in soils (Conant et al., 2008, 2011). By extension, each of these factors influence C mineralization temperature sensitivities, but the relative impact of each factor and the degree to which they influence each other remains poorly understood, particularly in permafrost environments (Bracho et al., 2016; Graham et al., 2012). While we did not measure SOC quality or microbial community composition in this study, the high Q_{10} values we observed may reflect temperature-dependent differences in these factors at our different incubation temperatures, as opposed to solely methanogen response to warming.

One possible contributing factor to the high Q_{10} values in our study could be that most OM in permafrost soils is poorly associated with minerals (Diochon et al., 2013; Höfle et al., 2013). When there is limited influence of the mineral soil matrix, SOC compounds with slower decomposition times may have a higher response to temperature increases (Conant et al., 2011). A more plausible explanation in our study could be that these high Q_{10} values in our study are due to functional microbial community dissimilarities with warming in our incubations, resulting in changes to microbial efficiency and $C\text{-}CO_2$:$C\text{-}CH_4$ ratios of mineralized SOC (Bracho et al., 2016; Conant et al., 2011). It has been suggested functional microbial groups in experimental warming studies become more dissimilar over different temperatures as the experiment progresses (Bracho et al., 2016). Furthermore, it has been suggested microbial community dissimilarities with warming observed in incubations are greater and more complete than dissimilarities observed in *in situ* field warming experiments (Bracho et al., 2016). While we attempted to minimize the effects of potentially dissimilar functional microbial communities in our $Q_{10\text{-}I}$ calculations by using CH_4 production rates at the first point of detectable CH_4 production, the high $Q_{10\text{-}I}$ values we observe at certain depths and temperature intervals in our incubation may indicate combined effects of differences in initial SOM quality and temperature-induced changes in microbial community composition within the incubation vials.

We suggest the roles of microbial community composition, SOC quality, and interactions between these factors are important to better understanding temperature sensitivity of C mineralization in thawing permafrost and should be further examined in future research. While the high Q_{10} values we observe in this study indicate one or more of these factors are influencing the observed changes in CH_4 production, the significant trends of Q_{10} values in relation to the sample facies and incubation temperature provide insights as to how temperature sensitivity of

CH_4 production changes over long (decades to centuries) time scales in thawed permafrost environments.

Given the paucity of data in this study to explain the anomalously high Q_{10} values, we base the rest of the discussion on the consistent trends among the Q_{10} values rather than on the absolute Q_{10} values.

3.4.2. Impacts of time since permafrost thaw on temperature sensitivity of CH_4 production

Time is known to be an important factor in determining temperature sensitivity of C mineralization (Gudasz et al., 2015), but it is almost unknown how temperature sensitivity changes over long (decades to centuries) time scales (Yvon-Durocher et al., 2012). Comparing CH_4 production along the time since thaw depth gradient in the Vault Lake core's Taberite sequence (T-I, thawed taberite; T-II, recently-thawed taberite; and T-III, transitional permafrost) provides a unique opportunity to examine how C mineralization changes in the decades to centuries following permafrost thaw under saturated anaerobic conditions. The T-III transitional permafrost facies, which was frozen when the sediment core was collected and thawed at the commencement of the incubation, had lower CH_4 production values than the T-II recently-thawed taberite, whose sediments we estimate thawed within the past 50 years (Heslop et al., 2015). We hypothesize this difference is due to sediments from the T-II recently-thawed taberite containing microbial communities acclimated to thawed conditions, which may not be present in sediments from the T-III frozen transitional permafrost. In turn, the T-I taberite facies, which represents permafrost which has been thawed for longer periods of time (up to 400 years based on estimated lake age; Heslop et al., 2015), had lower CH_4 production values than the T-II recently-thawed taberite facies. We hypothesize this difference in CH_4 production between permafrost thawed decades (T-II recently-thawed taberite) to centuries (T-III taberite) ago could

be due to sediments from the T-II recently-thawed taberite facies containing greater proportions of fresher, more labile SOC compared to the T-I taberite facies.

Freshly-thawed sediments from the T-III transitional permafrost facies experienced statistically significant ($p \leq 0.05$) increases in CH_4 production between both T_1 and T_2 (0 to 3 ˚C), but no significant increases in CH_4 production values at the higher incubation temperatures. In the sediment sample from the T-II recently-thawed taberite facies, we observed statistically significant increases in CH_4 production between both T_1 and T_2 (0 to 3 ˚C) and T_3 and T_4 (10 to 25 ˚C); however, the sediment sample from the T-I taberite facies only experienced a statistically significant increase in CH_4 production between T_3 and T_4. This suggests that, in the talik beneath a thermokarst lake, recently-thawed sediments are most sensitive to temperature changes at lower (< 5 ˚C) temperatures. As time since permafrost thaw increases from decades to centuries, the sediments shift to being more sensitive to changes at higher (< 10 ˚C) temperatures. This is consistent with findings from long-term field temperature sensitivity studies conducted in aerobic, non-permafrost systems, which suggest initial increases in SOC mineralization rates upon the first several years of warming do not persist (Conant et al., 2011). We further discuss potential mechanisms for these apparent shifts in temperature sensitivity of anaerobic CH_4 production over time since permafrost thaw observed in this study in the following sections.

3.4.3. Sensitivity of thawed permafrost to low-temperature warming

Our results suggest that the frozen and recently-thawed (decadal time scales) sediments at the base of the talik are much more sensitive to small temperature increases at lower temperatures than sediments which have been thawed for longer periods of time (centuries time scales) or were deposited after lake formation (surface organic rich much and lacustrine silt facies). The R_1:R_2 Q_{10} (0 °C to 3 °C) values in our incubation study are representative of

temperature increases as permafrost thaws and warms, and are consistent with *in situ* temperatures observed in the temperature profiles at the base of the talik below Vault Lake. In the Taberite sequence of the Vault Lake core, sediments from the T-II recently-thawed taberite and the T-III frozen transitional permafrost facies had statistically significant ($p \leq 0.05$) increases in CH_4 production potential rates between T_1 (0 °C) and T_2 (3 °C), coupled with the largest R_1:R_2 $Q_{10\text{-}I}$ values in our study (1×10^8 and 2×10^5, respectively). These $Q_{10\text{-}I}$ values were orders of magnitude higher than the T_1:T_2 $Q_{10\text{-}I}$ values of the T-I taberite facies and the overlying deposited sediments (surface organic rich much and lacustrine silt facies) in the remainder of the core. The large values of the R_1:R_2 $Q_{10\text{-}I}$ values in the T-II and T-III samples indicate that additional factors, such as initial methanogen biomass, may be playing significant roles in determining CH_4 production potential rates observed in our incubations; however, we suggest the significant difference in R_1:R_2 $Q_{10\text{-}I}$ values in these samples compared to the other facies in the core are also largely influenced by initial SOM quality.

In thermokarst lake environments, the permafrost thaw boundary at the outer extent of the lake's talik has been previously identified as a region of high CH_4 production (Kessler et al., 2012; Walter Anthony et al., 2016). The high R_1:R_2 $Q_{10\text{-}I}$ values for CH_4 production that we observed in the T-II recently-thawed taberite and T-III frozen transitional permafrost facies, which are respectively located above and below the permafrost thaw boundary, suggest temperature-dependent factors cause large increases in CH_4 production with permafrost thaw and warming, contributing to the high CH_4 production levels found in this region. We hypothesize the high R_1:R_2 Q_{10} values we observed in these facies may be the result of initial rapid C mineralization of biolabile permafrost SOC compounds due to the input of heat energy upon thaw. Both the T-II recently-thawed taberite and T-III frozen transitional permafrost facies

contain sediments and SOC that had been recently frozen. In frozen environments, there is some microbial SOC decomposition (Michaelson and Ping, 2003; Mikan et al., 2002), but rates are extremely low due to a lack of activation energy to initiate the chemical reactions involved in C mineralization (Conant et al., 2011; Davidson and Janssens, 2006), which serves to preserve most biolabile OC compounds. In yedoma-type permafrost sediments, such as those surrounding Vault Lake, it has been suggested that long-term anaerobic conditions within buried permafrost lead to a buildup of low molecular weight organic compounds (Ewing et al., 2015), which are especially biolabile upon permafrost thaw (Drake et al., 2015; Spencer et al., 2015). Thus, warming and thawing permafrost removes a major physical barrier to C mineralization, leading to rapid initial permafrost SOC mineralization upon thaw that has been linked to preferential mineralization of the most biolabile SOM compounds (Davidson and Janssens, 2006; Drake et al, 2015; Yang et al., 2016).

3.4.4. Impact of time since thaw on activation energies for methanogenesis

In contrast to sediments from the T-II recently-thawed taberites and T-III transitional permafrost, sediments from the lacustrine silt facies, deposited at the lake bottom, and the T-I taberite facies, which we estimate began thawing beneath the lake following lake formation ca. 400 ya, experienced statistically significant ($p \leq 0.05$) increases in CH_4 production between T_3 (10 ˚C) and T_4 (25 ˚C) but no statistically significant increases in CH_4 production at the colder incubation temperatures. We hypothesize this shift from recently-thawed sediments responding to warming at colder incubation temperatures to sediments which have been thawed for longer periods of time responding to warming at higher incubation temperatures is due to changes in SOC quality and *in situ* microbial community composition over time. SOM is composed of a continuum of compounds with increasing molecular complexity and, consequently, increasing

activation energies required for microbial decomposition (Bracho et al., 2016; Conant et al., 2011; Davidson and Janssens, 2006; Schädel et al., 2014). Generally, activation energies for more complex molecules are higher due to a higher number or enzymatic steps being needed for biological processing; therefore, per kinetic theory, complex (lower quality) OC should have greater temperature sensitivity than simpler (higher quality) OC (Conant et al., 2008; Conant et al., 2011; Craine et al., 2010; Gudasz et al., 2015). This also implies that, as temperatures increase, previously recalcitrant SOM fractions should become bioavailable due to increased ambient thermal energy and increased chemical reaction rates.

Temperature data collected from the BH-13 vertical profile at Vault Lake suggest that, as sediments from the lacustrine silt and T-I taberite facies historically incubated for centuries *in situ* beneath the lake center, they were exposed to temperatures below 10 °C (T_1 and T_2 in the incubations) but not temperatures as high as 10 °C and 25 °C (T_3 and T_4 in the incubations). Over time, we hypothesize simpler, higher quality OC compounds may have mineralized *in situ*, leaving behind more complex OC compounds that did not have sufficient activation energies to decompose at the temperatures present in the talik. Increasing temperatures to 25 °C in the incubations may have provided additional ambient energy to mineralize a fraction of the OC compounds that had not been previously mineralized *in situ*, explaining the increase in CH_4 production rates between incubation temperatures T_3 and T_4 in these samples. We attempted to run a C pool deconvolution model (Schädel et al., 2014) to estimate the relative sizes of initial SOC quality pools in each of our samples, but were unable to constrain the model parameters because most of our incubation samples did not experience exponential declines in CH_4 production rates during our incubation.

In this study, we used trends in Q_{10} values of CH_4 production to show that century-scale time since permafrost thaw affects temperature sensitivity of CH_4 production. Recently-thawed sediments collected from the T-II recently-thawed taberite and T-III transitional permafrost were most sensitive to warming at lower temperatures. Increased time since thaw in the T-I taberite and lacustrine silt lead to increased activation energies for CH_4 production. We believe that these changes are due to changes in SOC quality and *in situ* microbial community composition over time.

Figures

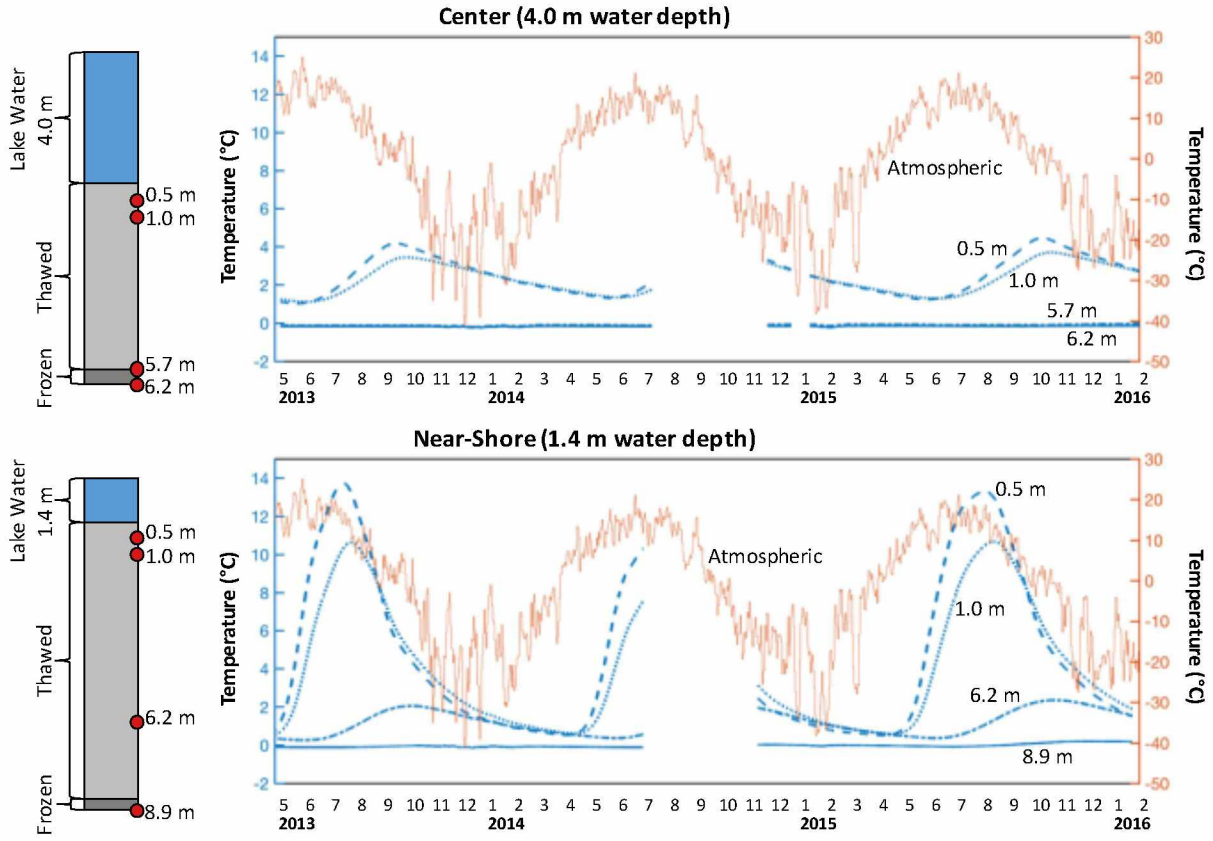

Figure 3.1. Atmospheric temperatures from Fairbanks, AK (ACIS Station Fairbanks AP #2) and talik temperatures from two profiles beneath Vault Lake. Temperature data at Vault Lake were recorded hourly from May 2013 through February 2016. Atmospheric temperature data are daily mean temperatures from the same time period.

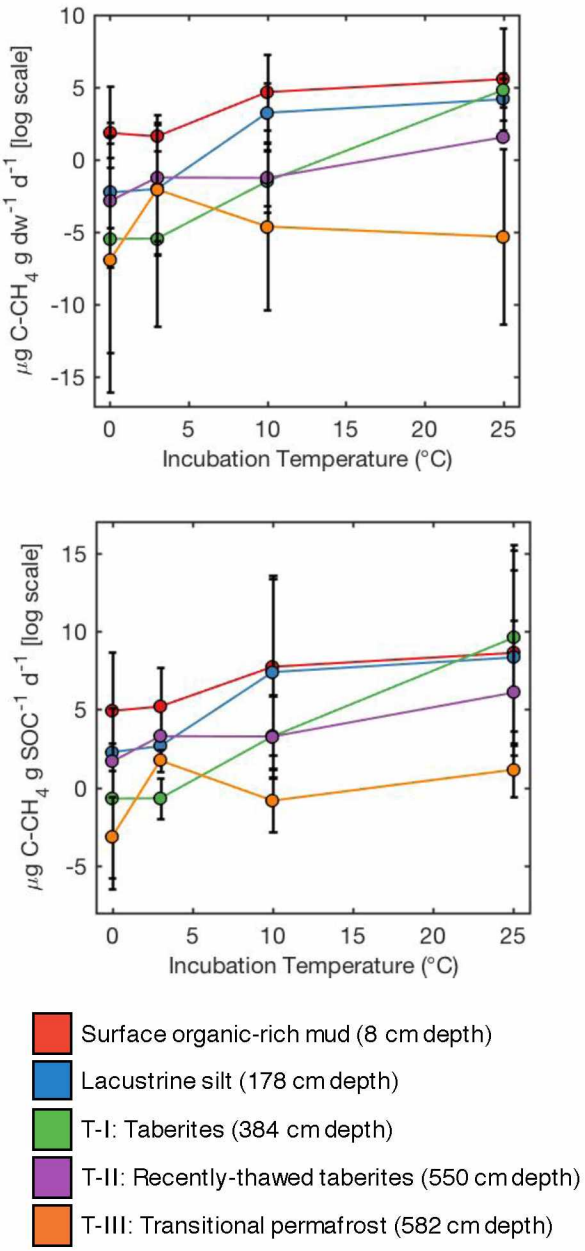

Figure 3.2. Methane (CH_4) production potential rates, normalized by both the mass of dry sediment in each incubation vial (g dw^{-1}; top) and the mass of soil organic carbon in each incubation vial (g SOC^{-1}; bottom) at four incubation temperatures. Production potential rates are shown in log scale.

Tables

Table 3.1. Initial characteristics of each sediment subsample, modified from Heslop et al. (2015).

Sample			Sediment Properties				
UAF lab ID	Facies	Depth in Core (cm)	SOC (% wt)	N (% wt)	C_{org}:N	$\delta^{13}C_{org}$ (‰)	$\delta^{15}N$ (‰)
1	Surface organic-rich mud	8	4.76*	0.45*	10.58	-28.91	2.79
2	Lacustrine silt	178	1.60	0.09	17.78	-25.79	2.50
3	T-I, Taberite	384	0.86	0.09	9.56	-25.70	4.07
4s	T-II, Recently-thawed taberite	550	1.10	0.12	9.17	-26.46	2.69
5	T-III, Frozen transitional permafrost	582	1.14	0.17	6.63	-27.61	3.87

* Statistically significant ($p \leq 0.05$) difference from other facies

Table 3.2. Methane (CH_4) production in the Vault lake core at four incubation temperatures (T; °C). CH_4 production potential rates are normalized by both the mass of dry sediment in each incubation vial (μg C-CH_4 g dw^{-1} d^{-1}) and the mass of initial soil organic carbon in each incubation vial (μg C-CH_4 g SOC^{-1} d^{-1}). Total C-CH_4 production through time (mg C-CH_4 g $SOC_{initial}^{-1}$) was calculated as the cumulative C-CH_4 production in each incubation bottle during the 175-d incubation period.

Sample Lab ID	Depth (cm)	C-CH_4 Production*	T_1 (0 °C)	T_2 (3 °C)	T_3 (10 °C)	T_4 (25 °C)
1	8	μg C-CH_4 g dw^{-1} d^{-1}	6.43 (2.11) [a]	5.04 (0.38) [a]	107.7 (13.4) [b]	262.4 (33.6) [c]
		μg C-CH_4 g SOC^{-1} d^{-1}	135.1 (44.2) [a]	178.9 (12.5) [a]	2,263 (282) [b]	5,512 (705.2) [c]
		mg C-CH_4 g $SOC_{initial}^{-1}$	23.6 (7.74) [a]	18.5 (1.41) [b]	396.1 (49.4) [c]	964.6 (123.4) [d]
2	178	μg C-CH_4 g dw^{-1} d^{-1}	0.16 (0.02) [a]	0.13 (0.01) [a]	25.9 (7.65) [a]	65.7 (4.33) [b]
		μg C-CH_4 g SOC^{-1} d^{-1}	9.69 (1.27) [a]	14.3 (1.07) [a]	1,616 (478) [a]	4,108 (270.7) [b]
		mg C-CH_4 g $SOC_{initial}^{-1}$	1.15 (0.97) [a]	1.47 (0.12) [a]	282.8 (83.7) [a]	718.8 (47.4) [b]
3	384	μg C-CH_4 g dw^{-1} d^{-1}	0.06 (0.09) [a]	0.00 (0.00) [a]	0.23 (0.12) [a]	124.4 (3.23) [b]
		μg C-CH_4 g SOC^{-1} d^{-1}	6.58 (10.5) [a]	0.51 (0.27) [a]	26.5 (14.1) [a]	14,464 (376.0) [b]
		mg C-CH_4 g $SOC_{initial}^{-1}$	0.09 (0.00) [a]	0.09 (0.05) [b]	4.65 (2.47) [b]	2,531(65.8) [c]
4s	550	μg C-CH_4 g dw^{-1} d^{-1}	0.06 (0.01) [a]	0.30 (0.01) [b]	0.29 (0.14) [b]	4.78 (1.10) [c]
		μg C-CH_4 g SOC^{-1} d^{-1}	5.29 (0.97) [a]	26.8 (1.18) [b]	26.2 (13.2) [b]	434.9 (99.8) [c]
		mg C-CH_4 g $SOC_{initial}^{-1}$	0.93 (0.17) [a]	4.70 (0.21) [b]	4.59 (2.30) [b]	76.1 (17.5) [c]
5	582	μg C-CH_4 g dw^{-1} d^{-1}	0.00 (0.00) [a]	0.13 (0.01) [b]	0.01 (0.00) [c]	0.00 (0.00) [c]
		μg C-CH_4 g SOC^{-1} d^{-1}	0.04 (0.07) [a]	6.16 (0.49) [b]	0.44 (0.14) [c]	0.29 (0.18) [c]
		mg C-CH_4 g $SOC_{initial}^{-1}$	0.02 (0.03) [a]	1.99 (0.17) [b]	0.15 (0.05) [c]	0.08 (0.04) [c]

* Mean (standard deviation)

[a,b,c,d] Statistically significant ($p \leq 0.05$) difference in CH_4 production with temperature increase

Table 3.3. Calculated temperature coefficients (Q_{10}) from methane (CH_4) production at each incubation temperature interval. Q_{10} values were calculated as temperature sensitivity at the start of detectable CH_4 production in our incubations ($Q_{10\text{-}I}$). T_1, T_2, T_3, and T_4 refer to incubation temperatures 0 ºC, 3 ºC, 10 ºC, and 25 ºC, respectively.

Sample		$Q_{10\text{-}I}$			
Lab ID	Depth (cm)	T_1:T_2	T_1:T_3	T_2:T_3	T_3:T_4
1	8	0.01	3.83	46.2	2×10^3
2	178	2.16	4.72	6.60	1×10^4
3	384	0.00	0.24	3.34	1×10^4
4s	550	1×10^8	101	0.26	0.00
5	582	2×10^5	3.52	0.03	0.05

References

Bekryaev R, Polyakov I, Alexeev V (2010) Role of Polar Amplification in Long-Term Surface Air Temperature Variations and Modern Arctic Warming. Journal of Climate, 23, 3888–3906.

Bracho R, Natali S, Pegoraro E et al. (2016) Temperature sensitivity of organic matter decomposition of permafrost-region soils during laboratory incubations. Soil Biology and Biochemistry.

Brosius L, Walter Anthony KM, Grosse G, et al. (2012) Using the deuterium isotope composition of permafrost meltwater to constrain thermokarst lake contributions to atmospheric CH_4 during the last deglaciation. Journal of Geophysical Research Biogeosciences 117, G01022.

Burn C (2005) Lake-bottom thermal regimes, western Arctic coast, Canada. Permafrost and Periglacial Processes, 16, 355–367.

Čapek P, Diáková K, Dickopp J-E et al. (2015) The effect of warming on the vulnerability of subducted organic carbon in arctic soils. Soil Biology and Biochemistry, 90, 19–29.

Chowdhury RT, Herndon EM, Phelps TJ (2015) Stoichiometry and temperature sensitivity of methanogenesis and CO_2 production from saturated polygonal tundra in Barrow, Alaska. Global change biology, 21, 722-737.

Conant RT, Drijber RA, Haddix ML (2008) Sensitivity of organic matter decomposition to warming varies with its quality. Global Change Biology, 14, 868-877.

Conant RT, Ryan MG, Ågren GI et al. (2011) Temperature and soil organic matter decomposition rates- synthesis of current knowledge and a way forward. Global Change Biology, 17, 3392–3404.

Craine J, Fierer N, McLauchlan K (2010) Widespread coupling between the rate and temperature sensitivity of organic matter decay. Nature Geoscience, 3, 854–857.

Davidson EA, Janssens IA (2006) Temperature sensitivity of soil carbon decomposition and feedbacks to climate change. Nature, 440, 165-173.

Diochon A, Gregorich EG, Tarnocai C (2013) Evaluating the quantity and biodegradability of soil organic matter in some Canadian Turbic Cryosols. Geoderma.

Drake T, Wickland K, Spencer R, McKnight D, Striegl R (2015) Ancient low–molecular-weight organic acids in permafrost fuel rapid carbon dioxide production upon thaw. Proceedings of the National Academy of Sciences, 112, 13946–13951.

Ewing S, O'Donnell J, Aiken G, Butler K, Butman D, Windham-Myers L, Kanevskiy M (2015) Long-term anoxia and release of ancient, labile carbon upon thaw of Pleistocene permafrost. Geophysical Research Letters, 42, 10,730–10,738.

Graham D, Wallenstein M, Vishnivetskaya T et al. (2012) Microbes in thawing permafrost: the unknown variable in the climate change equation. The ISME Journal, 6, 709–712.

Grosse G, Jones B, Arp C (2013) Thermokarst Lakes, Drainage, and Drained Basins, in: Treatise on Geomorphology, edited by: Shroder, J. F., Academic Press, San Diego, 325-353.

Grosse G, Goetz S, McGuire D, Romanovsky V, Schuur E (2016) Changing permafrost in a warming world and feedbacks to the Earth system. Environmental Research Letters, 11, 040201.

Gudasz C, Sobek S, Bastviken D (2015) Temperature sensitivity of organic carbon mineralization in contrasting lake sediments. Journal of Geophysical Research: Biogeosciemces, 120, 1215–1225.

Guo D, Wang H (2016) CMIP5 permafrost degradation projection: A comparison among different regions. Journal of Geophysical Research: Atmospheres, 121, 4499–4517.

Heslop JK, Walter Anthony WK, Sepulveda-Jauregui A, Martinez-Cruz K, Bondurant A, Grosse G, Jones MC (2015) Thermokarst lake methanogenesis along a complete talik profile. Biogeosciences, 12, 4317–4331.

Heslop JK, Walter Anthony K, Zhang M (2017) Utilizing pyrolysis GC-MS to characterize organic matter quality in relation to methane production in a thermokarst lake sediment core. Organic Geochemistry, 103, 43-50.

Höfle S, Rethemeyer J, Mueller CW, John S (2013) Organic matter composition and stabilization in a polygonal tundra soil of the Lena Delta. Biogeosciences.

Hugelius G, Strauss J, Zubrzycki S, et al. (2014) Estimated stocks of circumpolar permafrost carbon with quantified uncertainty ranges and identified data gaps. Biogeosciences, 11, 6573–6593.

IPCC in Climate Change 2013: The Physical Science Basis. Contribution of Working Group I to the Fifth Assessment Report of the Intergovernmental Panel on Climate Change. Eds Stocker, T. F. et al., 1535, Cambridge Univ. Press, 2013.

Jorgenson T, Harden J, Kanevskiy M et al. (2013) Reorganization of vegetation, hydrology and soil carbon after permafrost degradation across heterogeneous boreal landscapes. Environmental Research Letters, 8, 035017.

Kessler MA, Plug LJ, Walter Anthony KM (2012) Simulating the decadal- to millennial-scale dynamics of morphology and sequestered carbon mobilization of two thermokarst lakes in NW Alaska. Journal of Geophysical Research: Biogeosciences, 117.

Kling G, Kipphut G (1991) Arctic lakes and streams as gas conduits to the atmosphere: implications for tundra carbon budgets. Science, 251, 298-301.

Knoblauch C, Beer C, Sosnin A, Wagner D, Pfeiffer E-M (2013) Predicting long-term carbon mineralization and trace gas production from thawing permafrost of Northeast Siberia. Global Change Biology, 19, 1160–1172.

Lenz J, Jones B, Wetterich S et al. (2016) Impacts of shore expansion and catchment characteristics on lacustrine thermokarst records in permafrost lowlands, Alaska Arctic Coastal Plain. Arktos, 2:25.

Liang J, Li D, Shi Z et al. (2015) Methods for estimating temperature sensitivity of soil organic matter based on incubation data: A comparative evaluation. Soil Biology and Biochemistry, 80, 127–135.

Michaelson GJ, Ping CL (2003) Soil organic carbon and CO_2 respiration at subzero temperature in soils of Arctic Alaska. Journal of Geophysical Research, 108, 8164.

Mikan CJ, Schimel JP, Doyle AP (2002) Temperature controls of microbial respiration in arctic tundra soils above and below freezing. Soil Biology and Biochemistry, 34, 1785-1795.

Myhre G, Shindell D, Breon FM, et al. (2013) Anthropogenic and Natural Radiative Forcing. In: Climate Change 2013: The Physical Science Basis. Contribution of Working Group I to the Fifth Assessment Report of the Intergovernmental Panel on Climate Change. Intergovernmental Panel on Climate Change, New York, USA.

Olefeldt D, Turetsky M, Crill P, McGuire D (2013) Environmental and physical controls on northern terrestrial methane emissions across permafrost zones. Global Change Biology,19, 589–603.

Plug L, West J (2009) Thaw lake expansion in a two-dimensional coupled model of heat transfer, thaw subsidence, and mass movement. Journal of Geophysical Research, 114.

Schädel C, Schuur E, Bracho R et al. (2014) Circumpolar assessment of permafrost C quality and its vulnerability over time using long-term incubation data. Global Change Biology, 20, 641–652.

Schädel C, Bader M, Schuur E et al. (2016) Potential carbon emissions dominated by carbon dioxide from thawed permafrost soils. Nature Climate Change, advance online publication.

Schuur E, McGuire A, Schädel C, et al. (2015) Climate change and the permafrost carbon feedback. Nature, 520, 171–179.

Sepulveda-Jauregui A, Walter Anthony KM, Martinez-Cruz, Greene S, Thalasso F (2015) Methane and carbon dioxide emissions from 40 lakes along a north south latitudinal transect in Alaska. Biogeosciences, 12, 3197–3223.

Spencer R, Mann P, Dittmar T et al. (2015) Detecting the signature of permafrost thaw in Arctic rivers. Geophysical Research Letters, 42, 2830–2835.

Treat CC, Natali SM, Ernakovich J et al. (2015) A pan-Arctic synthesis of CH_4 and CO_2 production from anoxic soil incubations. Global Change Biology, 21, 2787–2803.

Walter K, Zimov S, Chanton J, Verbyla D, Chapin F (2006) Methane bubbling from Siberian thaw lakes as a positive feedback to climate warming. Nature, 443, 71–75.

Walter K, Edwards M, Grosse G, Zimov S, Chapin F (2007) Thermokarst Lakes as a Source of Atmospheric CH_4 During the Last Deglaciation. Science, 318, 633–636.

Walter K, Chanton J, Chapin F, Schuur E, Zimov S (2008) Methane production and bubble emissions from arctic lakes: Isotopic implications for source pathways and ages. Journal of Geophysical Research: Biogeosciences (2005–2012), 113.

Walter Anthony KM, Anthony P (2013) Constraining spatial variability of methane ebullition seeps in thermokarst lakes using point process models. Journal of Geophysical Research: Biogeosciences,118, 1015–1034.

Walter Anthony KM, Zimov SA, Grosse G et al. (2014) A shift of thermokarst lakes from carbon sources to sinks during the Holocene epoch. Nature, 511, 452–456.

Anthony K, Daanen R, Anthony P, von Deimling T, Ping C-L, Chanton J, Grosse G (2016) Methane emissions proportional to permafrost carbon thawed in Arctic lakes since the 1950s. Nature Geoscience, 9, 679-682.

Yang Z, Wullschleger S, Liang L, Graham D, Gu B (2016) Effects of warming on the degradation and production of low-molecular-weight labile organic carbon in an Arctic tundra soil. Soil Biology and Biochemistry, 95, 202–211.

Yvon-Durocher G, Caffrey J, Cescatti A et al. (2012) Reconciling the temperature dependence of respiration across timescales and ecosystem types. Nature, 487, 472–476.

Zimov SA, et al. (1997) North Siberian lakes: A methane source fueled by Pleistocene carbon. Science, 277, 800-802.

Appendix 3.A: Supplement of Century-scale time since permafrost thaw affects temperature sensitivity of methane production in thermokarst-lake sediments[2]

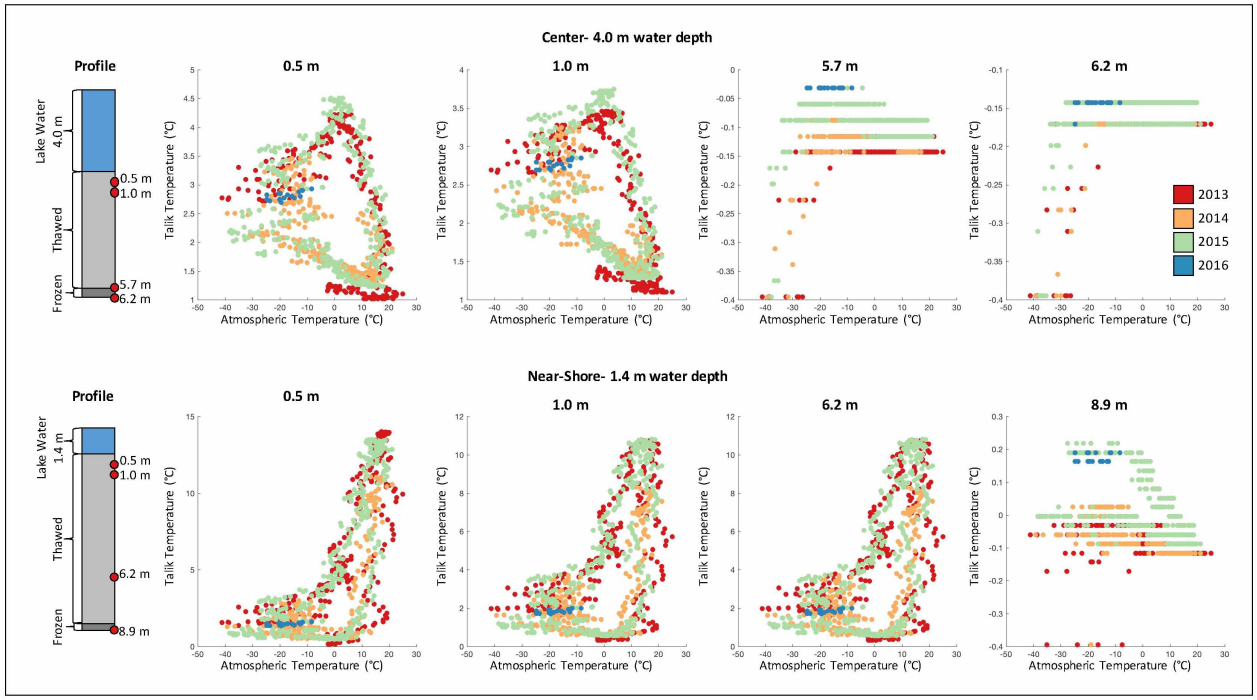

Figure 3.A-1. Atmospheric temperatures from Fairbanks, AK (ACIS Station Fairbanks AP #2) versus talik temperatures from two profiles beneath Vault Lake. Temperature data at Vault Lake were recorded hourly from May 2013 through February 2016 at four depths in each profile (Near-shore, BH10: 0.5 m, 1.0 m, 6.2 m, and 8.85 m; Center, BH13: 0.5 m, 1.0 m, 5.7 m, and 6.2 m). Atmospheric temperature data are daily mean temperatures from the same time period. Colors are representative of each year of collected data.

[2] Supplement of: Heslop, J.K. Walter Anthony, K. M., Winkel, M., Grosse, G., Knoblauch, C., Liebner, S..: Century-scale time since permafrost thaw affects temperature sensitivity of methane production in thermokarst-lake sediments. In prep. for submission to Global Change Biology.

Chapter 4: Organic carbon biolabilty increases with depth in a yedoma permafrost profile[1]

Permafrost warming and thaw subjects previously frozen, inactive organic carbon (OC) to microbial decomposition, generating the greenhouse gases carbon dioxide (CO_2) and methane (CH_4) and fueling a positive climate warming feedback[1]. Molecular structure and redox state are known to control biolability of thawed permafrost OC[2-4], but due to OC complexity the mechanisms are still poorly understood. A substantial portion (211 +160/-153 Gt) of global permafrost OC is stored in particularly deep, ice-rich permafrost deposits known as yedoma, which formed during the last Ice Age[5]. Here, we show yedoma OC biolability increases with depth using anaerobic incubations and ultrahigh-resolution mass spectrometry of water-extractable organic matter (WEOM) along a 12-m yedoma permafrost profile in central Alaska. Proportions of aliphatics and peptides (reduced, high H/C WEOM compounds), which are considered highly biolabile[2,4], increased with depth in the permafrost profile. These compounds positively correlated with anaerobic CO_2 and CH_4 production and corresponded to high proportions (53.3 ± 41.9%) of OC mineralization rates. Our results suggest that as yedoma permafrost thaws, OC biolability and greenhouse gas production potentials will increase with depth.

Permafrost, covering a quarter of the Northern Hemisphere, is considered a vulnerable carbon (C) pool[6]. As the global climate warms, temperatures in high latitudes are increasing at amplified rates and these increases are projected to continue into the coming century[7]. With

---

[1] Heslop, J.K. Walter Anthony, K.M., Spencer, R.G.M., Winkel, M., Knoblauch, C., Liebner, S., Podgorski, D., Zito, P., Kholodov, A..: Organic carbon biolabilty increases with depth in a yedoma permafrost profile. In prep. for submission to Nature Geoscience Letters.

rising temperatures, subsequent warming and thawing of permafrost soils removes a major barrier to OC mineralization, leading to the mobilization and microbial degradation of previously frozen, inactive permafrost OC[6]. However, many uncertainties remain concerning the magnitude, timing, and form of C mineralization from thawed permafrost OC.

A substantial portion (~16%) of the permafrost C pool is stored in yedoma-type permafrost soils[5]. Yedoma-type permafrost formed syngenetically due to sediment and peat accumulation in unglaciated regions of Siberia, Alaska and northwest Canada during the last Ice Age. Yedoma is characterized by high ice and OC contents relative to other mineral-type permafrost soils[8]. Incubation studies have shown that yedoma OC is particularly biolabile upon thaw, especially when compared with other permafrost types[4,9,10]. Of particular interest is the tendency of yedoma permafrost to form deep thermokarst lakes upon thaw, owing to its high volumetric ice content that extends tens of meters into the ground[11], resulting in deep ground surface subsidence when the ground ice melts. Thermokarst lake formation strongly alters the local thermal balance, triggering rapid permafrost thaw and talik (thaw bulb) formation. In turn, OC from deep yedoma deposits is mobilized for mineralization under anaerobic conditions[12]. Once formed, thermokarst lakes and their taliks provide a direct conduit for CH_4 produced from deep, old yedoma OC to be emitted directly into the atmosphere via bubbling[13]. Ancient yedoma OC from deep permafrost horizons can also be thawed and mineralized through riverbank and coastal erosion[10].

One major source of uncertainty in determining OC biodegradability upon thaw is its molecular composition. Studies of dissolved OC from yedoma permafrost have found that high proportions (17-62%)[4,9,10] of yedoma OC are bioavailable upon thaw. It has been suggested these high proportions of bioavailable OC in yedoma-type permafrost are due to the ancient OC

containing higher proportions of biolabile low molecular weight compounds[2-4]. Here, we examined molecular composition of WEOM from yedoma-type permafrost in central Alaska in conjunction with anaerobic C mineralization potentials of the thawed OC. We sought to determine how yedoma OC biodegradability, and by extension potentials for CO_2 and CH_4 emissions, change with depth in anaerobic conditions consistent with a thermokarst-lake environment.

We incubated soil samples from four depths in a 12-m yedoma profile under anaerobic conditions at two temperatures (3 °C and 13 °C; Methods). Samples were collected from the modern active layer horizon (AL, 0.7 m depth), the transitional permafrost horizon (TL, 1.3 m depth), and deeper yedoma soil samples (Y-9m and Y-12m, 9 m and 12 m depth, respectively). For each sample depth, CO_2 and CH_4 production were measured in monthly time steps during the 154-d incubation; net anaerobic C production (net C) was calculated as the sum of C-CO_2 and C-CH_4. We used Fourier transform ion cyclotron resonance mass spectrometry (FT-ICR-MS) to characterize molecular composition of WEOM at the beginning and end of the 154-d incubation period. Compounds identified through FT-ICR-MS were classified into six classes based on their elemental stoichiometries and a modified aromaticity index (Methods). Full results are available in the Supplement; here, we focus on results from three WEOM compound classes that are key indicators of permafrost OC biodegradation and biolability: condensed aromatic structures, aliphatics, and peptides.

Condensed aromatic structures have been previously associated with lignin degradation[14] and with polyphenols[15], which are closely linked with vascular plant biomarkers and are resistant to biodegradation. Initial proportions of condensed aromatic structures were higher in soils from the AL and TL horizons (13.9 ± 0.6%) than soils from the yedoma-type permafrost (8.9 ± 1.6%;

Fig. 4.1). This is suggestive of active and/or prior OC biodegradation in the AL and TL horizons. Soils in the AL currently experience seasonal freezing and thawing, and the TL horizon is comprised of yedoma soils which thawed ca. 5,000-7,000 years ago during the Holocene thermal optimum, subsequently refroze, and remained frozen until the present. The increased proportions of condensed aromatic structures in these horizons are evidence of prior OC degradation during thawed periods, resulting in accumulation of more recalcitrant, lower quality OC compounds.

In contrast, aliphatics and peptides (reduced, high H/C ratio compounds) have been previously identified as unique molecular signatures of permafrost-derived DOM in Arctic aquatic ecosystems[4]. Here, we observed higher initial proportions of aliphatics and peptides in soils from the deep yedoma permafrost (9.7±1.4% and 5.1±4.0% for aliphatics and peptides, respectively) compared to soils from the AL and TL horizons (4.5±1.2% and 0.4±0.3%; Fig. 4.1). The initial proportions of aliphatics and peptides in our samples positively correlated with anaerobic C mineralization ($C\text{-}CO_2$, $C\text{-}CH_4$, and net C) at both incubation temperatures during our 154-day incubation (Fig. 4.2). Degradation rates of these compounds were equivalent to 5.6% to 118% of OC mineralization rates (Fig. 4.3). This is consistent with prior findings in aerobic arctic streams and rivers, where aliphatic fractions of permafrost OC had rapid, high rates of degradation (83%) during 28-day aerobic incubation[4]. In the TL sample, degradation rates of aliphatics and peptides combined were 118% of OC mineralization rates. We hypothesize this is due to these compounds being preferentially utilized and but not directly processed into $C\text{-}CO_2$ or $C\text{-}CH_4$.

In the soil samples from the permafrost (TL, Y-9m, Y-12m), initial proportions of aliphatics and peptides increased with depth. The increasing proportions of these compounds may be the result of long-term reducing, anaerobic conditions in yedoma soil profiles[3]. The

syngenetic formation of yedoma permafrost sediments, coupled with the presence of unfrozen water[16], viable microbial communities[17], and millennia since permafrost formation, provides conditions favorable for potential long-term anaerobic fermentation of OC in yedoma permafrost[3]. We show WEOM in our profile contains increasing proportions of reduced, high H/C compounds (aliphatics and peptides) with depth in yedoma permafrost, which would be consistent with end products of anaerobic fermentation processes (e.g. acetate). The increasing proportion of these WEOM compounds with depth in the permafrost suggests increasing OC quality, and by extension that anaerobic C mineralization potentials per unit OC, increases with depth.

Our results suggest yedoma sediments will produce more greenhouse gas per unit OC as permafrost thaw depth increases. In the context of thawing yedoma permafrost, this finding is important for better understanding how the release of thawed ancient OC from deep yedoma permafrost in thermokarst lake and coastal erosional environments will impact global C cycling.

Methods

Soil sampling. We collected soil samples from four horizons at the Vault Creek (VC) permafrost tunnel (65°01'46.3" N, 147°42'22.4" W), located in the Chatanika River Valley 20 km north of Fairbanks, Alaska, USA. The entrance of the VC permafrost tunnel is secured by a steel tube, making the top 4 m of the vertical soil profile inaccessible from inside the tunnel. Therefore, we collected samples from the modern active layer horizon (AL; 0.7 m depth) and the transitional permafrost horizon (TL; 1.3 m depth) using a SIPRE drill (Jon Holmgren's Machine Shop, Fairbanks). The AL sample represents soils which currently experience seasonal freezing and thawing; the TL sample represents yedoma soils which thawed ca. 5,000-7,000 y.a. during the Holocene thermal optimum, subsequently refroze, and remained frozen until the present. Two deeper yedoma soil samples (Y-9m and Y-12m, 9 m and 12 m depth, respectively) were collected from the walls of the VC permafrost tunnel using an axe and hammer. These samples are representative of deep yedoma-type permafrost that formed during the last Ice Age and remained frozen until present[17]. All soil samples were kept frozen at -10 °C until further analyses.

Anaerobic incubations. We incubated soil samples under anaerobic conditions at two temperatures (3 °C and 13 °C) using previously described methods[19]. Briefly, we prepared sediment slurries under anaerobic conditions using homogenized sediment and O_2-free, sterilized DI water (mean ±SD 392 ±63 g dw sediment L^{-1}); two subsamples of slurry were reserved for geochemical and water-extractable organic matter (WEOM) analyses, and the remaining slurry was incubated in triplicate under anaerobic conditions. Headspace CO_2 and CH_4 concentrations in each incubation vial were measured in monthly time steps for 154 days using gas chromatography (Shimadzu GC-2014). Anaerobic C mineralization was normalized two ways:

(i) by the mass of dry sediment in each bottle (μg C g dw^{-1}) and (ii) by the mass of SOC in each bottle (μg C g SOC^{-1}). Net C mineralization in each incubation vial was calculated as the sum of CO_2 and CH_4 production. All C mineralization potential rates are presented as the mean ± standard deviation (SD) of the triplicate vials at each sample depth and incubation temperature. At the end of the 154-day incubation period, all incubation vials were destructively sampled and the sediment slurries were reserved for WEOM analyses, described below.

Geochemical analyses. One subsample of the initial slurry (collected prior to incubation) was oven-dried (105 °C for 48 hours), homogenized using a mortar and pestle, and analyzed for total C (C_{tot}) and nitrogen (N_{tot}), organic C (C_{org}), C_{org}:N_{tot} ratios, and stable isotope ratios ($\delta^{13}C_{org}$ and $\delta^{15}N_{tot}$) using a Finnigan DeltaPlus XP elemental analyzer (Thermo Scientific) coupled to a Costech ECS4010 elemental analyzer (Costech Scientific) at the University of Alaska Stable Isotope Facility.

Water-extractable organic matter (WEOM) analyses. Reserved initial and final slurry subsamples were filtered through a precombusted (450 °C for 4 hours) glass microfiber filter (0.7 μm, Whatman GF/F) to remove particulate organic matter. Filtered slurry was analyzed for dissolved organic carbon (DOC) content using a Shimadzu TOC-V at Florida State University, Tallahassee, FL, USA. Filtered slurry samples were prepared for Fourier transform ion cyclotron resonance mass spectrometry (FT-ICR-MS) analysis using the solid-phase DOM extraction method[20]. Filtered slurry sample volume used for solid phase extraction was adjusted based on the DOC concentration of each sample to obtain a 50 μg C mL^{-1} methanol eluate. Extracts were analyzed on a custom-built 9.4 Tesla FT-ICR mass spectrometer with a 22-cm diameter horizontal bore at the National High Magnetic Field Laboratory (NHMFL), Tallahassee, FL, USA. Negative ions were generated using direct infusion electrospray ionization at a rate of 500

nm min^{-1}; 100 time-domain acquisitions were co-added for each mass spectrum. Molecular formulas were assigned to each spectra using in-house software (EnviroOrg Software E 2.0) at the NHMFL based on published rules[20-21]. Molecular formulas with elemental combinations of $C_{1-45}H_{1-92}N_{0-4}O_{1-25}S_{0-2}$ were considered for assignment. Each formula was classified based on their elemental stoichiometries[22] and a modified aromaticity index (AI) calculated for each formula[23]. Based on the elemental stoichiometries and AI of each molecule, we classified identified compounds into six compound classes[14]: aromatic structures ($0.5 < AI < 0.67$), condensed aromatic structures ($AI > 0.67$), unsaturated low oxygen ($AI < 0.5$, $H/C < 1.5$, $O/C < 0.5$), unsaturated high oxygen ($AI < 0.5$, $H/C < 1.5$, $O/C > 0.5$), aliphatics ($1.5 < H/C < 2.0$, $O/C < 0.9$, $N = 0$), and peptides ($1.5 < H/C < 2.0$, $O/C < 0.9$, $N > 0$). WEOM compound class data are presented as relative proportions (%) of identified formulas.

Statistics. MATLAB (R2016a) software was used for all statistical analyses. All measured parameters were tested for normal distribution using the Jarque-Bera test. Due to multiple parameters not being consistent with a normal distribution, differences between sediment horizons were determined using nonparametric Wilcoxon rank sum tests. We determined relationships between WEOM composition and C mineralization using nonparametric Spearman's rank correlation coefficients. Differences and correlations were considered statistically significant when $p \leq 0.05$ ($\alpha = 0.05$).

References

1. Walter, K. M., Zimov, S. A., Chanton, J. P., Verbyla, D., Chapin, F. S. Methane bubbling from Siberian thaw lakes as a positive feedback to climate warming. *Nature* **443**, 71–75 (2006).
2. Drake, T., Wickland, K., Spencer, R., McKnight, D. & Striegl, R. Ancient low–molecular-weight organic acids in permafrost fuel rapid carbon dioxide production upon thaw. *Proceedings of the National Academy of Sciences* **112,**13946–13951 (2015).
3. Ewing, S., O'Donnell, J.A., Aiken, G.R., Butle, K., Butman, D., Windham-Myers, L., Kanevskiy, M.Z. Long-term anoxia and release of ancient, labile carbon upon thaw of Pleistocene permafrost. *Geophys Res Lett* **42,** 10,730–10,738 (2015).
4. Spencer, R. Mann, P.J., Dittmar, T., Eglinton, T.I., McIntyre, C., Holmes, M.R., Nikita Zimov, N., Stubbins, A. Detecting the signature of permafrost thaw in Arctic rivers. *Geophys Res Lett* **42,** 2830–2835 (2015).
5. Strauss, J., Schirrmeister, L., Grosse, G., Wetterich, S., Ulrich, M., Herzschuh, U., Hubberten H. -W. The deep permafrost carbon pool of the Yedoma region in Siberia and Alaska. *Geophysical Research Letters* **40,** 6165–6170 (2013).
6. Schuur, E.A.G., McGuire, A.D., Schädel, C., Grosse, G., Harden, J.W., Hayes, D.J., Hugelius, G., Koven, C.D., Kuhry, P., Lawrence, D.M., Natali, S.M., Olefeldt, D., Romanovsky, V.E., Schaefer, K., Turetsky, M.R., Treat, C.C., Vonk, J.E. Climate change and the permafrost carbon feedback. *Nature* **520,** 171–179 (2015).
7. IPCC in Climate Change 2013: The Physical Science Basis (eds Stocker, T. F. et al.) (Cambridge Univ. Press, 2013).

8. Zimov, S. A., Davydov, S. P., Zimova, G. M., Davydova, A. I., Schuur, E. A. G., Dutta, K., Chapin, F. S. I. Permafrost carbon: Stock and decomposability of a globally significant carbon pool. *Geophys. Res. Lett.* **33,** L20502 (2006).

9. Mann, P.J., Sobczak, W.V., LaRue, M.M., Bulygina, E., Davydova, A., Vonk, J.E., Schade, J., Davydov, S., Zimov, N., Holmes, R.M., Spencer, R.G.M. Evidence for key enzymatic controls on metabolism of Arctic river organic matter. *Global Change Biology* **20,** 1089–1100 (2014).

10. Vonk, J.E., Mann, P.J., Davydov, S., Davydova, A., Spencer, R.G.M., Schade, J., Sobczak, W.V., Zimov, N., Zimov, S., Bulygina, E., Eglinton, T.I., Holmes, R.M. High biolability of ancient permafrost carbon upon thaw. *Geophysical Research Letters* **40,** 2689–2693 (2013).

11. Ulrich, M, Grosse, G, Strauss, J, Schirrmeister, L. Quantifying Wedge-Ice Volumes in Yedoma and Thermokarst Basin Deposits. *Permafrost and Periglacial Processes*, **25**(3), 151-161 (2014).

12. Kessler, MA, Plug, LJ & Walter Anthony, KM. Simulating the decadal- to millennial-scale dynamics of morphology and sequestered carbon mobilization of two thermokarst lakes in NW Alaska. *Journal of Geophysical Research: Biogeosciences* **117,** G00M06 (2012).

13. Walter Anthony, K.M., Daanen, R., Anthony, P., von Deimling, T., Ping, C.-L., Chanton, J.P., Grosse, G. Methane emissions proportional to permafrost carbon thawed in Arctic lakes since the 1950s. *Nat Geosci* (2016). doi:10.1038/ngeo2795

14. Waggoner, D.C., Chen, H., Willoughby, A.S., Hatcher, P.G. Formation of black carbon-like and alicyclic aliphatic compounds by hydroxyl radical initiated degradation of lignin. *Org. Chem.* **82,** 69-76 (2015).

15. O'Donnell, J. Aiken, G.R., Butler, K.D., Guillemette, F., Podgorski, D.C., Spencer, R.G.M. DOM composition and transformation in boreal forest soils: the effects of temperature and organic-horizon decomposition state. *J Geophys Res Biogeosciences* (2016). doi:10.1002/2016JG003431

16. Romanovsky, V.E., Osterkamp, T.E. Effects of unfrozen water on heat and mass transport processes in the active layer and permafrost. *Permafrost Periglacial Processes* **11,** 219–239 (2000).

17. Rivkina, E.M., Friedmann, E.I., Mckay, C.P., Gilichinsky, D.A. Metabolic activity of permafrost bacteria below the freezing point, *Appl. Environ. Microbiol.* **66,** 3230–3233 (2000)

18. Schirrmeister, L., Meyer, H., Andreev, A., Wetterich, S., Kienast, F., Bobrov, A., Fuchs, M., Sierralta, M., Herzschuh, U. Late Quaternary paleoenvironmental records from the Chatanika River valley near Fairbanks (Alaska). *Quaternary Science Reviews* (2016). doi:10.1016/j.quascirev.2016.02.009

19. Heslop, J. K. *et al.* Thermokarst-lake methane production potentials along a full talik profile. *Biogeosciences* **12**, 4317–4331 (2015)

20. Dittmar, T., Koch, B., Hertkorn, N., Kattner, G. A simple and efficient method for the solid-phase extraction of dissolved organic matter (SPE-DOM) from seawater. *Limnol. Oceanogr.-Meth* **6,** 230-235 (2008)

21. Koch, B. P., Dittmar, T., Witt, M., Kattner, G. Fundamentals of molecular formula assignment to ultrahigh resolution mass data of natural organic matter. *Anal. Chem.* **79,** 1758-1763 (2007)

22. Stubbins, A., Spencer, R.G.M., Chen, H., Hatcher, P.G., Mopper, K., Hernes, P.J., Mwamva, V.L., Mangangu, A.M., Wabakanghanzi, J.N., Six J. Illuminated darkness: molecular signatures of Congo River dissolved organic matter and its photochemical alteration by ultrahigh precision mass spectrometry. *Limnol. Oceanogr.* **55,** 1467-1477 (2010)

23. Santi-Temkiv, T., Finster, K., Dittmar, T., Hansen, B.M., Thyrhaugt, R., Nielsen, N.W., Karlson, U.G. Hailstones: a window into the microbial and chemical inventory of a storm cloud. *PLOS One,* (2013) doi:10.1371/journal.pone.0053550.

Figures

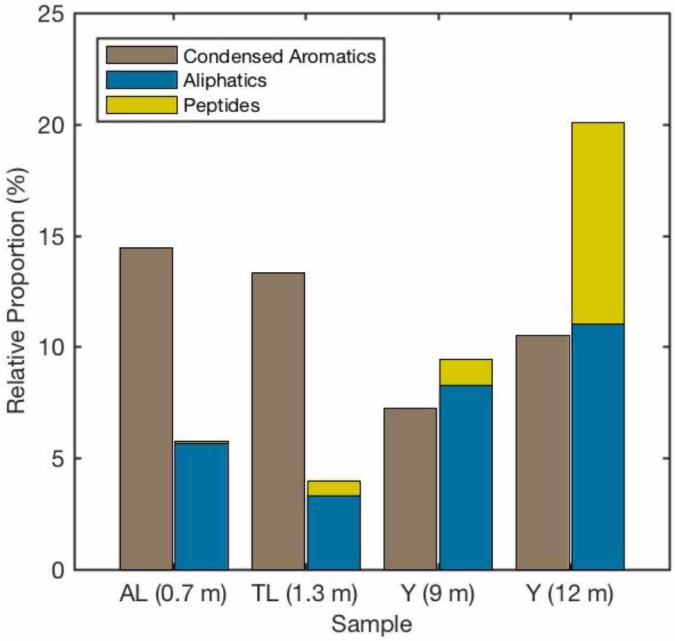

Figure 4.1. Initial proportions of selected WEOM compound classes. Initial proportions of condensed aromatics, aliphatics, and peptides in WEOM for each sample depth. AL represents the modern active layer horizon, TL represents the transitional permafrost horizon, and Y represents yedoma soil samples. Sample depths are in parentheses.

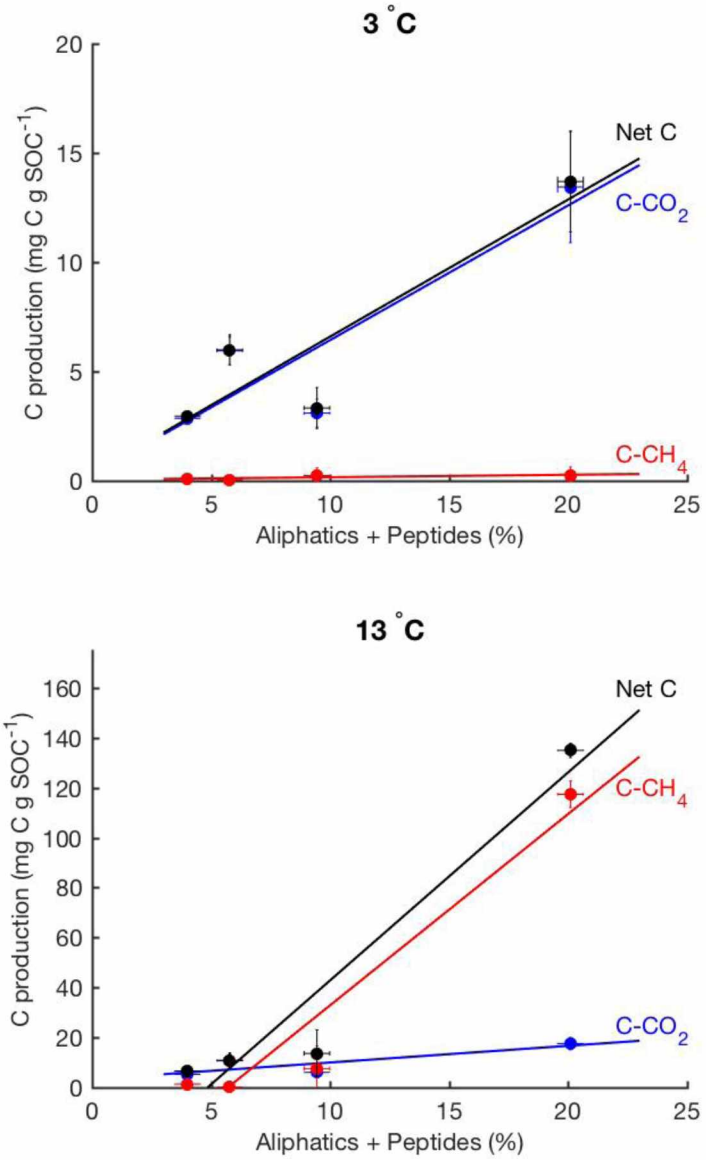

Figure 4.2. Relationships between initial aliphatics and peptides and anaerobic C mineralization. Relationships between initial proportions of aliphatics and peptides in WEOM and anaerobic C mineralization potentials (C-CO_2, C-CH_4, and net C) during a 154-day incubation at two incubation temperatures (3 °C and 13 °C).

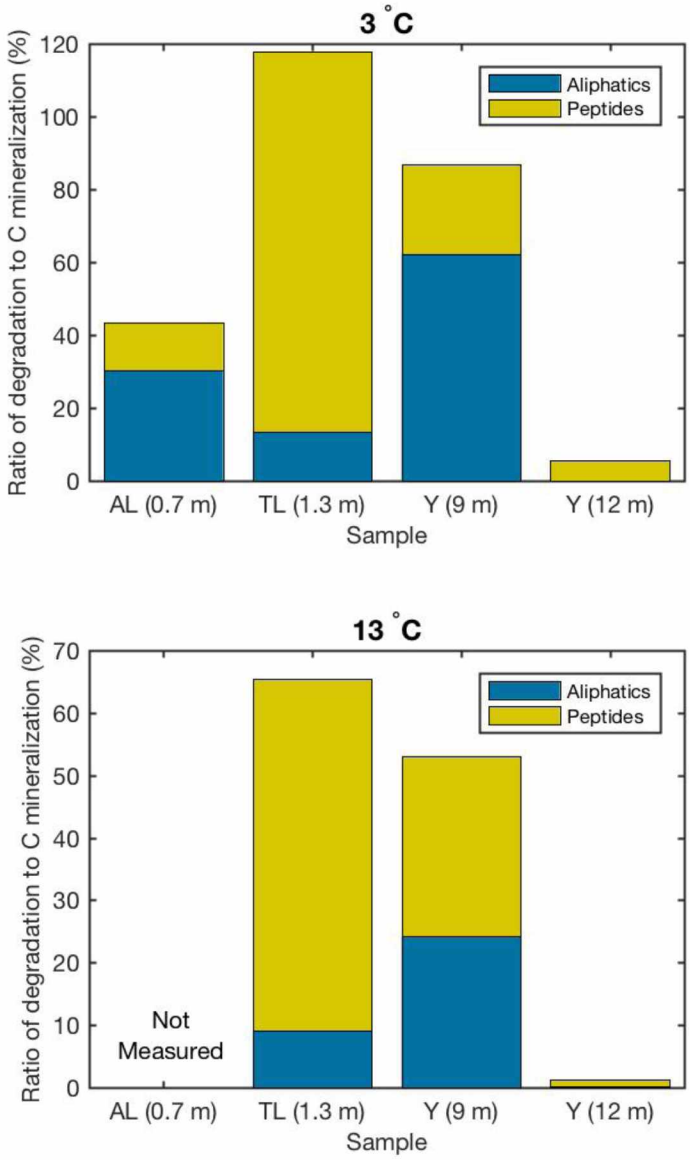

Figure 4.3. The relative contribution of aliphatics (blue) and peptides (yellow) to net anaerobic C mineralization. AL represents the modern active layer horizon, TL represents the transitional permafrost horizon, and Y represents yedoma soil samples. Sample depths are in parentheses.

Appendix 4.A: Supplement of Organic carbon biolabilty increases with depth in a yedoma permafrost profile[2]

Table 4.A-1. Initial geochemical properties for each sediment sample.

Sample ID	Depth (m)	Initial Sediment Properties OC (% wt)	N (% wt)	OC:N	WEOC (mg C g dw^{-1})	$\delta^{13}C_{org}$ (‰)	$\delta^{15}N$ (‰)
AL	0.7	0.44	0.05	8.2	14.0	-25.2	5.5
TL	1.3	1.58	0.16	9.6	85.0	-25.6	3.4
Y-9m	9.0	1.45	0.19	7.7	596.8	-25.0	4.0
Y-12m	12.0	2.26	0.33	6.8	1454.3	-26.5	1.8

[2] Prepared for submission to Nature Geoscience Letters

Table 4.A-2. Cumulative anaerobic C mineralization (mean ± SD) during the 154-day incubation period at two incubation temperatures (3 °C and 13 °C).

Sample ID	Depth (m)	Anaerobic C mineralization (mg C g SOC^{-1}; t = 154 d)					
		3 °C			13 °C		
		$C\text{-}CO_2$	$C\text{-}CH_4$	Net C	$C\text{-}CO_2$	$C\text{-}CH_4$	Net C
AL	0.7	5.94 ±0.63	0.04 ±0.08	5.99 ±0.69	10.67 ±2.73	0.19 ±0.24	10.85 ±2.97
TL	1.3	2.86 ±0.02	0.10 ±0.16	2.96 ±0.17	5.25 ±0.70	1.33 ±1.98	6.58 ±1.35
Y-9m	9.0	3.01 ±0.64	0.24 ±0.35	3.33 ±0.94	6.05 ±0.64	7.58 ±9.05	13.63 ±9.41
Y-12m	12.0	13.44 ±2.54	0.25 ±0.38	13.69 ±2.31	17.57 ±2.49	117.38 ±5.30	134.95 ±2.83

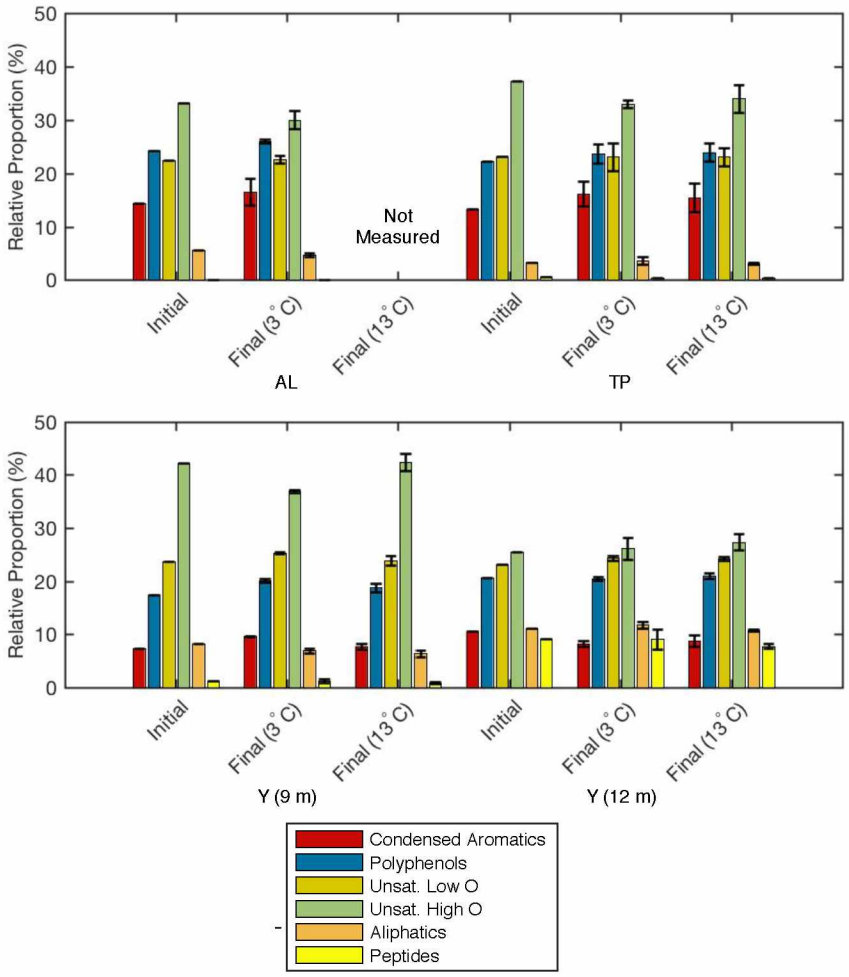

Figure 4.A-1. Initial and final proportions of WEOM compound classes in our incubations, measured using Fourier transform ion cyclotron resonance mass spectrometry (FT-ICR-MS; see Methods). AL represents the modern active layer horizon, TL represents the transitional permafrost horizon, and Y represents yedoma soil samples. Sample depths are in parentheses.

Conclusions

Thermokarst lakes and their taliks provide a direct conduit for carbon dioxide (CO_2) and methane (CH_4) produced from the decomposition of deep, old yedoma organic carbon (OC) to be emitted directly into the atmosphere (Walter Anthony et al., 2016). Once released to the atmosphere, these greenhouse gases cause a positive feedback to climate warming (Schuur et al., 2015; Walter et al., 2006). Large uncertainties remain about the magnitude, timing, and form of C loss to the atmosphere from thawing permafrost. In thermokarst (thaw) lake environments, specific knowledge gaps include: (i) the relative magnitude of CH_4 production in surface lake sediments vs. deeper thawed permafrost horizons, (ii) composition and biodegradability of their sediment organic matter (OM), and (iii) temperature sensitivity of methanogenesis in thermokarst-lake sediments.

My research examined OC composition and mineralization potentials at the Vault Creek (VC) permafrost tunnel and Vault Lake, located 20 km north of Fairbanks, Alaska, USA, to better constrain these uncertainties for anaerobic permafrost OC mineralization in thermokarst-lake environments. In Chapter 1 I showed that, in the center of Vault Lake, whole-column CH_4 production is dominated by methanogenesis in the Organic-rich mud facies; however, it is likely that other facies, such as deeper, rapidly thawing talik sediments, contribute significantly more to CH_4 production along laterally expanding thermokarst lake margins. CH_4 production data suggest labile fractions of OC were more absent in near-surface portions of the taberite, causing reduced CH_4 production rates compared to the underlying recently thawed taberite along the permafrost thaw boundary. Research presented in Chapter 2 supported the hypothesis OC quality may be a limiting factor in determining how thawing permafrost C is processed in a thermokarst-

lake environment. I found CH_4 production potential rates in the Vault Lake sediment core positively associated with substrate availability (C_{org} and N_{tot} concentrations) and the relative abundances of terrestrially-derived OM compounds (alkanes, alkenes, lignin products, and phenols and phenolic precursors). Furthermore, principal component analyses showed sediments from the lake core could be characterized into two distinct horizons (surface organic-rich sediments and mineral sediments) based on their OM characterization and CH_4 production potential rates. The knowledge as to where CH_4 originates and what OM compounds correlate with CH_4 production will aid in future research efforts to estimate and model C processing and release in thermokarst lakes.

Organic C mobilization and mineralization from thawing permafrost are expected to coincide with long-term, accelerating permafrost thaw, with over 60% of permafrost thaw and corresponding C emissions expected to occur after 2100 (Grosse et al., 2016). Two major uncertainties in estimating the long-term strength of the permafrost C feedback are: (i) how permafrost OC thawed and mineralized in saturated anaerobic conditions responds to changes in temperature and (ii) how temperature sensitivities change over century-scale time since thaw. Temperature sensitivity analyses conducted on a subset of sediment samples from the Vault Lake core, which I presented in Chapter 3, suggest century-scale time since permafrost thaw affects temperature sensitivities of CH_4 production. Freshly-thawed taberite sediments near the thaw boundary at the base of the talik were most sensitive to warming at lower incubation temperatures (0 °C to 3 °C), while the overlying taberite sediments which had been thawed for longer periods of time (up to 400 yr based on radiocarbon dating) did not experience statistically significant increases in CH_4 production until higher incubation temperatures that have not yet occurred in the lake center sediments (10 °C to 25 °C). I propose these observed differences in

temperature sensitivities are due to differences in OM quality and/or functional microbial community composition, and suggest further research is necessary to better constrain the roles of these factors in determining temperature controls on anaerobic C mineralization.

It has been previously suggested that OC from yedoma-type permafrost, which also surrounds Vault Lake, is more biolabile upon thaw than OC from other non-yedoma permafrost types because yedoma contains higher proportions of low molecular weight compounds (Drake et al., 2015; Ewing et al., 2015; Spencer et al., 2015). In Chapter 4, I showed yedoma OC biolability increased with depth using anaerobic incubations and ultrahigh-resolution mass spectrometry of water-extractable organic matter (WEOM) along a 12-m yedoma profile in the VC permafrost tunnel. Proportions of aliphatics and peptides (reduced, high H/C WEOM compounds), which have been previously identified as unique molecular signatures of permafrost-derived OM (Spencer et al., 2015), increased with depth in the VC permafrost tunnel samples. These compounds also positively correlated with anaerobic CO_2 and CH_4 production and corresponded to high proportions of OC mineralization rates. If the yedoma permafrost profile in the VC permafrost tunnel is representative of yedoma at larger regional scales, my results suggest, as yedoma permafrost thaws in anaerobic conditions beneath thermokarst lakes, greenhouse gas production potentials will increase with thaw depth, leading to an acceleration of the permafrost C feedback that has not yet been considered in any models.

References

Drake T, Wickland K, Spencer R, McKnight D, Striegl R (2015) Ancient low–molecular-weight organic acids in permafrost fuel rapid carbon dioxide production upon thaw. Proceedings of the National Academy of Sciences, 112, 13946–13951.

Ewing S, O'Donnell J, Aiken G, Butler K, Butman D, Windham-Myers L, Kanevskiy M (2015) Long-term anoxia and release of ancient, labile carbon upon thaw of Pleistocene permafrost. Geophysical Research Letters, 42, 10,730–10,738.

Grosse G, Goetz S, McGuire D, Romanovsky V, Schuur E (2016) Changing permafrost in a warming world and feedbacks to the Earth system. Environmental Research Letters, 11, 040201.

Schuur E, McGuire A, Schädel C, et al. (2015) Climate change and the permafrost carbon feedback. Nature, 520, 171–179.

Spencer R, Mann P, Dittmar T et al. (2015) Detecting the signature of permafrost thaw in Arctic rivers. Geophysical Research Letters, 42, 2830–2835.

Walter K, Zimov S, Chanton J, Verbyla D, Chapin F (2006) Methane bubbling from Siberian thaw lakes as a positive feedback to climate warming. Nature, 443, 71–75.

Walter Anthony K, Daanen R, Anthony P, von Deimling T, Ping C-L, Chanton J, Grosse G (2016) Methane emissions proportional to permafrost carbon thawed in Arctic lakes since the 1950s. Nature Geoscience, 9, 679-682.